Kamal Ghalan

Stability Assessment of the Underground Powerhouse for the Tamakoshi V Hydroelectric Project

Master's thesis in Hydropower Development
Supervisor: Krishna Kanta Panthi
Co-supervisor: Bikash Chaudhary

June 2022

Master's thesis

NTNU
Norwegian University of
Science and Technology

Kamal Ghalan

Stability Assessment of the Underground Powerhouse for the Tamakoshi V Hydroelectric Project

Master's thesis in Hydropower Development
Supervisor: Krishna Kanta Panthi
Co-supervisor: Bikash Chaudhary
June 2022

Norwegian University of Science and Technology
Faculty of Engineering
Department of Geoscience and Petroleum

NTNU
Norwegian University of
Science and Technology

Your ref.: MS/I22T66/IGP/KGKKP   Date: 01.02.2022

TGB4945 ENGINEERING GEOLOGY - MSc thesis
for
HPD student Kamal Ghalan

Stability assessment of the underground powerhouse for Tamakoshi V Hydropower Project

Background

Placement of an underground powerhouse cavern is very important in consideration with long-term stability and sustainability of any hydropower project. This is especially the case in Himalayan geological condition where rock mass is heavily influenced with period earthquake movement. Therefore, it is important that the underground cavern is located such a way that the selected location is optimum with respect to stability, accessibility, cost, and construction time efficiency. The planned underground powerhouse caver of Tamakoshi V Hydroelectric Project is located very near to the Main Central Thrust (MCT) of the Himalaya. The rock mass at the area is in general influenced by persistent tectonic movement.

MSc thesis task

This MSc thesis is to focus on the planning and design aspects of underground hydropower cavern of Tamakoshi V hydropower project. The candidate will focus on the following issues while working in MSc thesis.

- Review theory on the design of an underground powerhouse cavern, prevailing stability assessment methods.
- Briefly describe Tamakoshi V Hydroelectric Project. Present the extent of engineering geological investigations carried out for underground powerhouse cavern.
- Assess and estimate engineering geological and mechanical input parameters needed for stability assessment using empirical, analytical and numerical modelling methods.
- Critically evaluate existing location, orientation, and placement design of underground powerhouse cavern. Assess whether there exists possibility for alternative location.

- Carry out extensive assessment on the type of stability challenges that the underground powerhouse cavern may face during construction. Evaluate each of the challenges using prevailing rock engineering theory (empirical and analytical methods) discussed in the theory review chapter.
- Carry out stability assessment of underground powerhouse cavern using both 2D and 3D numerical modelling and optimize the rock support need.
- Make comprehensive assessment on the impact of earthquake load on the long-term stability of underground powerhouse cavern.
- Compare and discuss the stability condition of the cavern under both static and dynamic (earthquake) loading.

Relevant computer software packages

Candidate shall use *roc-science package* and other relevant computer software.

Background information for the study

- Relevant information such as reports, maps, information, and data given to the candidate by supervising professor.
- Scientific papers, reports and books related to mechanical properties of the rocks and rock mass collected by the candidate.
- Literatures in rock engineering, in-situ stress, rock mass quality and rock support principles.

Co-supervisor

PhD fellow Mr. Bikash Chaudhary will be the co-supervisor of this MSc thesis work.

The project work has started on 10th January 2022 and to be completed by 10th June 2022.

The Norwegian University of Science and Technology (NTNU)
Department of Geoscience and Petroleum

February 01, 2022

Krishna Panthi

Dr. Krishna K. Panthi
Professor of geological engineering, main supervisor

Note: This MSc task must be inserted in the MSc thesis after cover page

PREFACE

This master's thesis, entitled **"Stability Assessment of the Underground Powerhouse for the Tamakoshi V Hydroelectric Project,"** was submitted to the Department of Geosciences and Petroleum at the Norwegian University of Science and Technology (NTNU). This work was carried out for the requirements for partial fulfilment of the Master in Hydropower Development (2020-2022).

The main focus of the thesis is to evaluate the existing layout of the underground structures of the Tamakoshi V Hydropower Project and to estimate the input parameters for the analysis. The work also assesses the stability problems that the underground systems (powerhouse and transformer cavern) may face during excavation using the prevailing rock engineering theory, including empirical, analytical, and numerical modelling. In addition, this work also includes a comprehensive assessment of the impact of earthquakes on the long-term stability of the powerhouse cavern.

Professor Dr Krishna Kanta Panthi was the primary supervisor of the thesis, and PhD student Bikash Chaudhary was the co-supervisor. The information on the Tamakoshi V hydroelectric project was obtained by the immediate supervisor and provided by Tamakoshi Jal Vidhyut Company Limited.

Kamal Ghalan
NTNU, Trondheim, Norway
June, 2022

ACKNOWLEDGEMENT

ABSTRACT

Underground excavation presents several hazards and difficulties, especially when weak and schistose rock masses are involved. Excavated caverns in weak, deformable rock masses with thick rock cover are more prone to instability in the form of deformation. In weak rocks such as shales, schists, phyllites, Lesser Himalayan shales, and Siwalik, as well as in zones of weakness and faults, squeezing is quite common during subsurface outcrop (Panthi, 2006). In the Himalayas, rock masses are highly stressed and brittle due to active tectonic movements. They are unable to withstand high in-situ stress. These rocks are soft and plastic. Mostly, block/wedge fractures and plastic deformation are the cause of instability of these rock masses.

The Tamakoshi V Hydroelectric Project is a cascade system with an installed capacity of 99.8 MW under the 456 MW Upper Tamakoshi Hydroelectric Project. According to NEA (2019), the project is located on the right bank of the Tamakoshi River in Dolakha district, Nepal. Block/wedge failure and plastic deformation analyzes have been conducted to investigate the instabilities that may occur during construction and in the long term at this project. In addition, the power cavern close to the main central overthrust (MCT) of the Himalayas, which may be affected by ongoing tectonic movements, requires a comprehensive assessment of the effects of earthquakes.

This study aims to evaluate and interpret the various methods for assessing block/wedge failure, plastic deformation, and earthquake effects on long-term stability in the underground powerhouse and caverns and optimise support. Wedge failure was evaluated using UnWedge 5.0. Singh (1992), Goel (1995), and Q-system (1993) all used empirical approaches to study plastic deformation. (Hoek & Marinos, 2000), and (Panthi & Shrestha, 2018) used semi-empirical approaches. The analytical technique of (Carranza-Torres & Fairhurst, 2000), known as the convergence confinement method (CCM), was used for plastic deformation analysis and support pressure study. The work includes a numerical analysis using sophisticated 2D and 3D finite element software, namely RS2 and RS3, for both static and dynamic loading, which showed that the supports such as bolts and concrete lining (SFR) yielded to certain extent and kept the deformation to a minimum. The analysis was performed with a critically disturbed zone to determine the size of the failure. The resulting, deformations of up to 0.37 m were observed in the wall of the powerhouse and the transformer cavern.

Table of Contents

List of Figures

viii

List of Tables

1. INTRODUCTION
1.1. Background

Geologically diversified and enriched with nature and natural resources, Nepal is a small landlocked country with high variation in the altitude from 59 m above the sea level to 8848m above the sea level. This vast difference in the geological altitude and the steep topographic gradient make Nepal a suitable and potential country for hydroelectricity production.

Nepal could produce a considerable amount of energy, making it an energy-independent country and addon to the growth of the economic statutes and the country's overall development. Nonetheless, Nepal has not yet been able to do so due to political instability and financial restraints to do massive projects, thus making it very slow-paced and suffering from a power crisis (Basnet & Panthi, 2017). Nevertheless, the Government of Nepal has set forth a goal of achieving an installed capacity of 15000 MW by 2029 with collaboration between the private and governmental sectors.

The benefit of the geographical altitude and steep gradient also pose a considerable setback for the Himalayan region due to the ongoing tectonic activities. Young and weak rock masses of the Himalayas are subjected to intense deformation, causing faulting, shearing, folding and jointing due to the persistent compressive tectonic stress. These activities increase the uncertainties in the stability of the tunnels and the underground caverns (Panthi, 2006).

As part of the plan to achieve the target of installed capacity 15000 MW, Tamakoshi V Hydroelectric Project (99.8 MW) has been proposed by the Tamakoshi Jal Vidyut Company under NEA (2020/2021) as a tandem cascade project with Upper Tamakoshi Hydroelectric Project, 456 MW. The proper study and the analysis of the site, proper geological investigation and consideration of the design and construction of the project are crucial; moreover, in an active tectonic zone like Nepal. All the components of the Tamakoshi V HEP will be underground, which calls for even more careful study of the design and the stability issues that may arise during the construction and later at long-term stability. For this purpose, this thesis study has been done to evaluate, analyze and assess the potential stability issues related to the underground Powerhouse caverns due to the in-situ stress and the tectonic movement of the tectonic plates and support optimization using prevailing rock theories. Using numerical modelling, the Gorkha earthquake (2015) has been considered for the dynamic analysis at the powerhouse cavern location.

1.2. Objective and Scope

The scope of this thesis topic includes the followings tasks:

- Review theory on an underground powerhouse cavern design and prevailing stability assessment methods.
- Briefly describe Tamakoshi V Hydroelectric Project. Then, present the extent of engineering geological investigations for the underground powerhouse cavern.
- Assess and estimate engineering geological and mechanical input parameters needed for stability assessment using empirical, analytical, and numerical modelling methods.
- Critically evaluate the existing location, orientation, and underground powerhouse cavern placement design. Assess whether there exists a possibility for an alternative location.
- Carry out an extensive assessment of underground powerhouse caverns' stability challenges during construction. Then, evaluate each challenge using prevailing rock engineering theory (empirical and analytical methods) discussed in the chapter on the theory review.
- Carry out the stability assessment of underground powerhouse caverns using 2D and 3D numerical modelling and optimize the rock support need.
- Make a comprehensive assessment of the impact of earthquake load on the long-term stability of the underground powerhouse cavern.
- Compare and discuss the cavern's stability condition under static and dynamic (earthquake) loading.

1.3. Methodology

The entirety of the thesis uses the following methodology:

1.3.1.   Literature Review

Many essential theories and methods that have been well recognized and accepted by rock engineering and geological communities globally are used for the literature review. All the literature, scientific papers, journals, national and international reports about the rock, rock mass properties, design and planning of the underground powerhouse and caverns, stability issues and methods of assessments, Himalayan geology, and earthquake are found in different sources. Search engines such as Oria, Mendeley, ResearchGate, google scholar, and the university library database of the Norwegian University of Science and Technology (NTNU) helped narrow the search scope for relevant articles. Topics used for the literature review:

- Design consideration for large underground cavern
- Stability assessment methods for underground powerhouse
- 3D Numerical analysis of the underground cavern

- Impacts of the earthquake on underground structures
- Stability assessment against dynamic loading and more.

1.3.2. Study of Tamakoshi V Hydroelectric Project

- Study of the Detail reports and the development history of Tamakoshi V HEP, an overview of the layout of the powerhouse and transformer cavern.
- The detailed geological and geotechnical report by TRACEBEL Engineering GmbH. Photographs, lab test reports, and hydropower projects with the same geological area.
- Study geological engineering conditions and powerhouse and transformer cavern rock mass properties.
- Cavern placement and orientation

1.3.3. Input parameters for Stability Assessment

Several engineering and mechanical parameters needed to carry out the stability assessment of the powerhouse and transformer caverns have been studied and determined using the following approach:

  ➢ Empirical Methods: Q-System, RMR, GSI
  ➢ Numerical Method: numerical modelling with RS2 and RS3 (Rocscience Software) with both plastic and elastic material

1.3.4. Stability Assessment

Stability assessment by using different techniques or methods:

- Empirical methods: Singh (1992), Q-method (1993) and Goel's approach (1995)
- Semi-analytical method by (Hoek & Marinos, 2000), (Panthi & Shrestha, 2018)
- Analytical method: Convergence-Confinement method by (Carranza-Torres & Fairhurst, 2000)
- Wedge Failure through UnWedge (Rocscience software),
- 2D numerical modelling using RS2/Phase2 (Rocscience software),
- 3D numerical modelling using RS3 (Rocscience software),

1.3.5. Seismicity

- Seismic Analysis using Gorkha Earthquake (2015)
- Pseudo static Analysis in RS2
- Simple dynamic in RS2
- Full Dynamic Analysis RS2

1.4. Limitations

The study's main limitation was finding reliable input parameters for the analysis. No actual construction work has been done for the project besides exploratory tunnels in the vicinity of the powerhouse. Various analyses on the stability of the powerhouse and transformer cavern were performed based on the available data of the project and the assumption of a possible situation considering the problems at the nearby projects and the existing rock conditions. All information and understanding of the project complexity are based on a desk study of available reports provided by the Supervisor. There has not been any study of horizontal stress conditions around the project site was performed. Measurements of tectonic stresses were taken from the nearest hydropower plant with similar geological conditions, as no actual measurements were taken at the project. Limited testing and measurements were a significant limitation of the study. Due to lack of time, the dynamic analysis in RS3 was not performed in detail.

2. PROPERTIES OF ROCK MASS

Rocks are naturally occurring heterogeneous materials made up of one or more minerals that serve as structural elements; however, there is a crucial difference between a rock and a rock mass. These rocks have different properties, and distinct characteristics influencing their physical and mechanical properties such as density, porosity, heat transfer, expansion, and wave velocity depending on the mode of formation, degree of metamorphism, type of mineral composition, orientation, shape, and size, as well as the force between the minerals. On the other hand, the rock mass is constructional material composed of intact rock, joints, and discontinuities (Nilsen & Thidemann, 1993). (Panthi, 2006) states that rock mass is a heterogeneous medium, and its ability to tolerate stress and deformation depends on rock mass quality and mechanical process. Therefore, understanding the qualities of rock mass and, thus, the nature of the rock mass is critical, particularly when it comes to the stability of subsurface excavation and construction (Panthi, 2006; Shang et al., 2016). From a broader perspective, rock mass includes intact rock, joints, and discontinuities. Figure 2.1 shows the rock mass properties that should be assessed to understand the rock mass of interest.
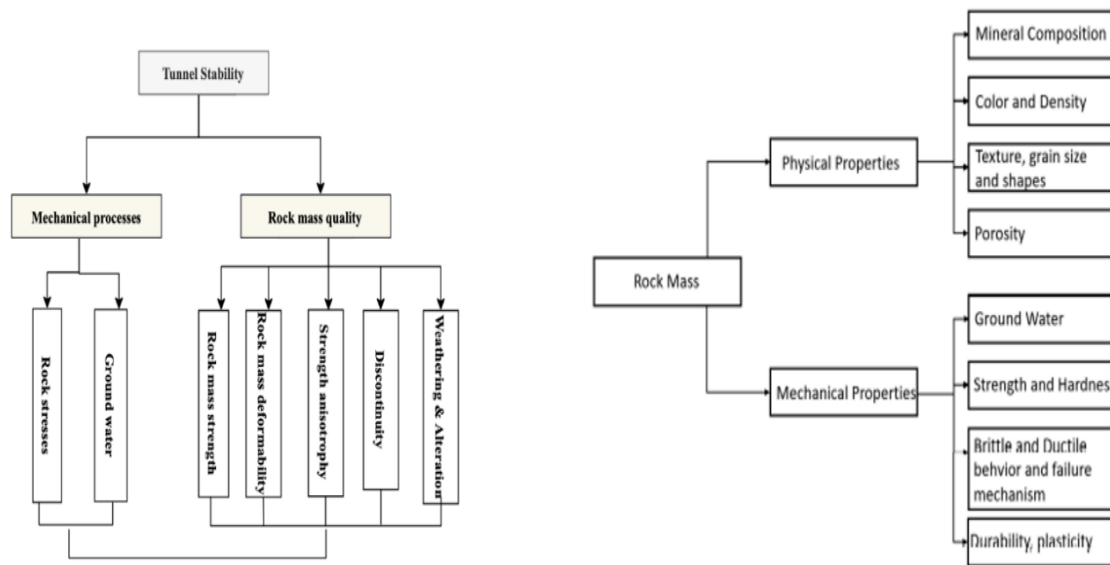
Figure 2.1: Factors influencing on tunnel stability (Panthi, 2006)(left) Rock Mass Properties Redrawn after (Singh and Goel, 2011)(right)

This chapter will provide a quick overview of some of the elements that influence rock mass quality and should be considered when assessing the stability of an underground excavation. The basic concepts of rock engineering for estimating and evaluating the quality of rock masses will be given. The following chapter will go into rock stresses and the mechanical processes that lead to failure.

2.1. Rock mass structure

As per the definition, rock mass structure is an in-situ material consisting of intact rocks, bedding planes, joints, discontinuities, faults, weakness zones, and dykes (Brady & Brown, 2007; Nilsen & Thidemann, 1993).

2.1.1. Discontinuity

Discontinuities are mechanical fractures that modify the rock mass's homogeneity, governing the rock's mechanical characteristics from a geological standpoint. Discontinuities arise due to stresses, most notably tectonic stress, which causes significant deformation and earthquakes when released. According to (Chandra et al., 2010), any mechanical discontinuity in a rock mass has little or no tensile strength. Discontinuity components such as joints, bedding planes, weakness zones, and fault zones, on the other hand, play an essential part in defining the characteristics and strength of the rock mass, as discussed below.

2.1.1.1. Bedding or foliation planes

Bedding or foliation planes is a discontinuity, a plane with lower strength and higher compressibility compared to rock mass. These planes are highly persistent and divide the rock into strata or layers in the sedimentary rock as bedding planes and in metamorphic rock as foliation planes. Anisotropic and elastic minerals such as mica, chlorite, amphiboles, and pyroxenes are often found in parallel orientation in sedimentary rock and regional metamorphic rocks, forming weak planes of brittle rocks of mica shists and often phyllites, thus influencing the anisotropic mechanical properties of the rock and rock construction. In addition, sheet materials such as serpentine, talc, and graphite reduce the strength of rocks, leading to failure in sliding along the cleavage surfaces (Henriksen & Selmer-Olsen, 1970).

2.1.1.2. Jointing of rock mass

Under a rock mass, joints are minor structures created in tension or compression but with no considerable shear in the plane of the joint. The strike, dip, and dip directions define the fundamental geometry of a joint. Although Joints are most found in earth's crust surfaces and are widely studied, they are still the most complex structures to analyze. Numbers of parallel joints are located in the joint sets. When these joint sets intersect are formed. The joint system formed may have distinct joint patterns and random joints without any specific patterns of the joints in a rock mass (Nilsen & Palmström, 2000) shown in Figure 2.2.
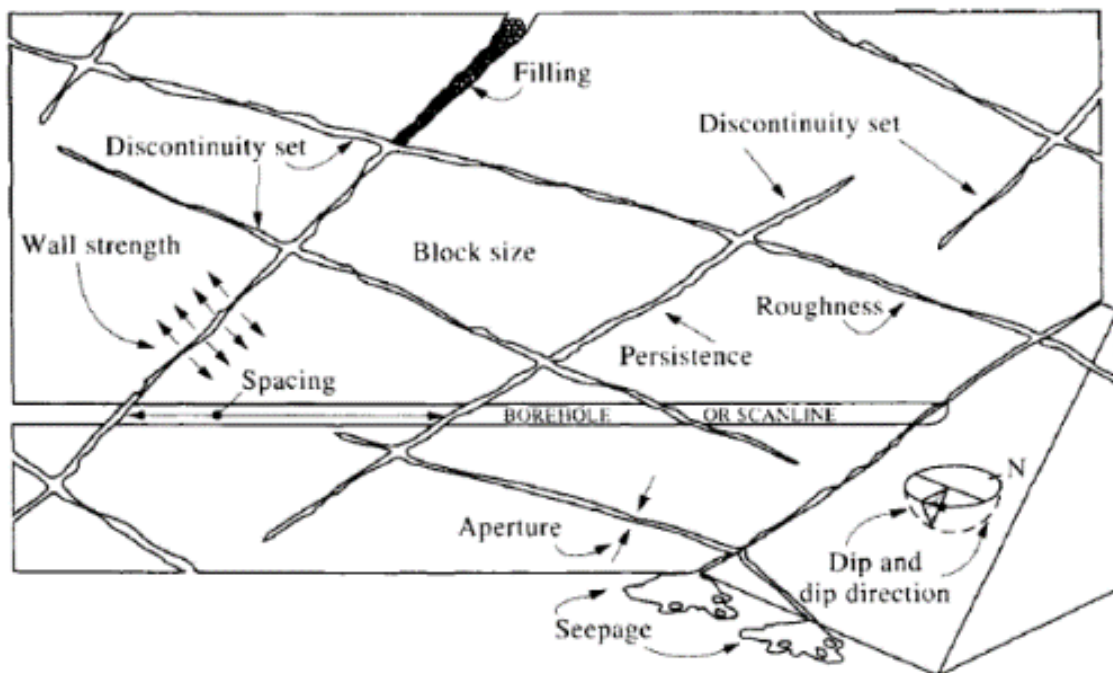
Figure 2.2: Joint Characteristics in a rock mass (Hudson and Harrison, 2000)

Joints are three-dimensional discontinuity consisting of two matching surfaces called joint walls, which may be open or closed. Moreover, joints have the specific parameterized characteristic that influences the shear strength of the joint and the volume of water flowing through it. The following characteristics are some essential features of joints:

- The roughness or planarity of joint wall
- Alteration or condition of coating of joint wall
- Presence of possible filling
- The length and continuity of the joint.

2.1.1.3.   **Weakness zones and faults**

Weakness zones or faults are rock mass properties formed in a rock mass due to the shearing of the rock mass, resulting in tectonic movements (Nilsen & Palmström, 2000). Thus, these weak zones may be layers or beds of soft minerals of sedimentary and metamorphic rocks like clay, mica, talc and graphite, resulting in a weak rock mass (Nilsen & Thidemann, 1993). Therefore, knowing the presence of these weak zones can be crucial in planning the location of the underground caverns. According to (Nilsen & Broch, 2009), weakness zones consist of tectonic faults and weak rock layers associated with squeezing and collapsing the roof and sidewall of the underground openings. This can cause severe stability issues in the cavern and during the excavation.

According to (Panthi, 2006), weakness zones are composed of the central core, which is highly fractured and consists of altered rock mass with clay filling, surrounded by a transition zone with decreased frequency of fractures. Due to the presence of filling materials between the weakness zones called *gauge materials,* like Smectite and montmorillonite, there may be intense pressure on the support installed as a result of an increase in volume when in contact with water. Figure 2.3 shows some types of weakness zones.
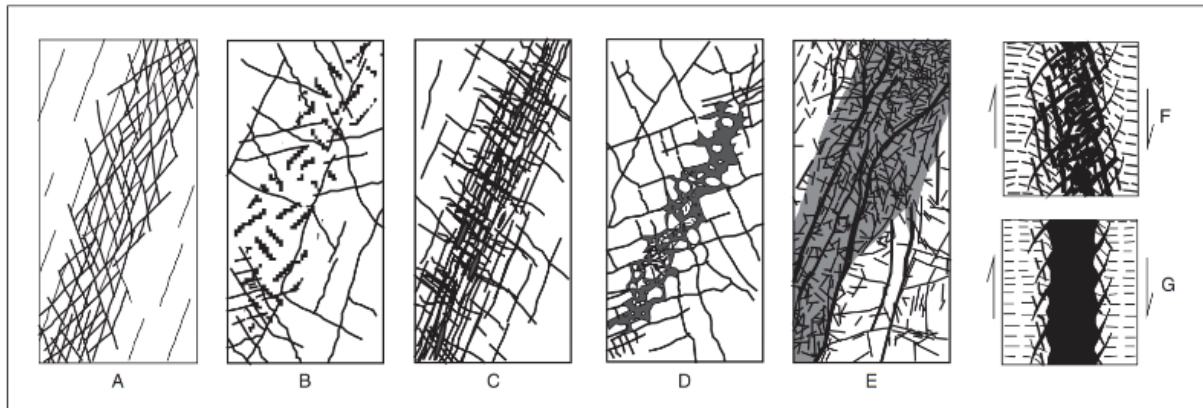
Figure 2.3: Some types of weakness zone, black areas indicate clay and shaded areas indicate altered rock (B-D) are reproduced from ISRM, 1978@Elsevier, F-G are reproduced from Selmer-Olsen, 1950)

2.1.2.   Ground Water

Groundwater moves through permeable discontinuities or open channels along them, below the groundwater table, in the rock mass, a jointed aquifer. Groundwater makes up a significant portion of subsurface water. Overall, rock masses at the surface are more jointed, and the joints are more open than those at higher depths. According to visual observations in ungrouted subsurface excavations, most water leakage occurs near the surface, contained in cracks, worn zones, and (Karlsrud & Kveldsvik, 2002; Nilsen & Thidemann, 1993). Groundwater that is free to move has the most significant impact on underground excavation conditions and long-term stability concerns (Palmstrom & Stille, 2010).

Groundwater travels large dist ances through rock masses as part of the hydrological cycle. As a result, it is critical to think about area geology and groundwater trends while analyzing potential water concerns or planning. In addition, groundwater reduces the strength of rock material and the shear strength of discontinuities to some amount, decreasing the excavations' stability. In expanding clays, the reduction in friction and strength will be substantial. Although failure due to joint water pressure is uncommon in underground excavations, it can contribute to instability,

especially in weak rock masses. As a result, when groundwater pressure is potentially considerable, it is critical to assess its influence (Nilsen & Palmström, 2000). Because there isn't much leakage in the exploratory drift for the subterranean powerhouse, and the piezometric line isn't established in reports, numerical modelling is done without groundwater modelling.

2.2. Rock Mass Quality
2.2.1.   Rock mass strength and estimation

The strength of the rock mass is a critical parameter in the design and stability analysis of numerical modelling of rock engineering issues as it determines how the rock mass behaves. As per (Panthi, 2006) Rock mass strength is the ability to withstand stress and deformation. Uniaxial compressive strength (σ_{ci}) of rock sample is frequently measured in situ or in the lab due to the impracticality and impracticability of laboratory testing of an in-situ rock mass (Hoek & Marinos, 2007a; Nilsen & Palmström, 2000). As a result, the rock mass strength (σ_{cm}) is determined approximately based on geological observation and empirical relationships as well as first-hand estimations (Palmstrom & Singh, 2001). Classification of the rock mass on the uniaxial compress strength is given in Table 2.1.

Table 2.1: Classification based on uniaxial compressive strength (ISRM 1978), modified by Nilsen and Palmström (2000)

Type	Classification	Uniaxial Compressive Strength, UCS (MPa)
Soil		<0.25
Rock	Extremely Low Strength	0.25 - 1
	Very low Strength	1.0 - 5.0
	Low Strength	5.0 - 25
	Medium Strength	25 - 50
	High Strength	50 - 100
	Very High Strength	100 - 250
	Extremely High Strength	> 250

The UCS test for determining uniaxial compressive strength is the most common, while triaxial strength, point load tests, Schmidt hammer tests, simple field hammer tests, and others can all be performed for intact rock strength testing (Nilsen & Palmström, 2000). However, designers of rock engineering encounter a significant challenge in estimating rock mass strength. In most cases, entire core samples from superior and stronger sections are robust and more stable than rock masses because they are

homogeneous and have minimal discontinuities. The strength of a rock mass, on the other hand, is not the same as the strength of intact rock. Because calculating rock mass strength directly is challenging, various empirical formulas for predicting rock mass strength have been given by various writers and researchers, as shown in Table 2.2.

Table 2.2: The Empirical formulas for the estimation of rock mass strength

Proposed By	Empirical Relationship	
Kalamaras et al. (1995)	$$\sigma_{cm} = 0.5 * \sigma_{ci} * \frac{RMR_{89} - 15}{85}$$	2.1
Hoek et al. (2002)	$$\sigma_{cm} = \sigma_{ci} * \frac{(m_b + 4s - a(m_b - 8s)) * (\frac{m_b}{4} + s)^{a-1}}{2(1+a)(2+a)}$$	2.2
Barton (2002)	$$\sigma_{cm} = 5\gamma * Qc^{\frac{1}{3}} = 5\gamma * \left[\frac{\sigma_{ci}}{100} * Q\right]^{\frac{1}{3}}$$ $$= 5\gamma * [\frac{\sigma_{ci}}{100} * 10^{\frac{RMR-50}{15}}]^{\frac{1}{3}}$$	2.3
Panthi (2006)	$$= \frac{\sigma_{ci}^{1.5}}{60}, for\ highly\ schistose\ and\ deformed\ rock\ mass$$	2.4
Panthi (2017)	$$\sigma_{cm} = \frac{\sigma_{ci}^{1.6}}{60}, for\ strong\ and\ brittle\ rock\ mass$$	2.5

In the above empirical relations, σ_{cm} is the unconfined compressive strength of the rock mass in MPa, γ is the density of rock in t/m^3, Q is the rock mass quality value, σ_{ci} is the uniaxial compressive strength of the intact rock in MPa, m_b is the reduced value of the material constant m_i. s and a are the material constant related to Hoek-Brown failure criteria, Q_c is the normalized rock mass quality rating, and RMR stands for Bieniawski's rock mass rating. The rock mass classification ratings are related as follows (Z. T. Bieniawski, 1989), (Barton, 2002):

$$RMR = 9 * ln\ Q + 44 \qquad 2.6$$
$$RMR = 15 * \log Q + 50 \qquad 2.7$$
$$GSI = RMR - 5 \qquad 2.8$$

When evaluating weak, fractured, and schistose rocks, the methods correlating both rock mass rating and intact rock strength have been determined to have a drawback. The reduced strength of discontinuous rocks will be taken into consideration twice: in the laboratory when calculating σ_{ci} and when calculating the rock mass rating (RMR, Q, or GSI) (Hoek & Marinos, 2000). (Panthi, 2006) relationship is solely dependent on one rock parameter, σ_{ci}. His relation is a best-fit empirical power function based on plots of intact rock strength vs predicted rock mass strength using the three other relations in (Panthi, 2006). (Panthi, 2006) claims that the relationship can be used to metamorphic and sedimentary rocks with low

compression strength that are strongly schistose, foliated, thinly bedded, and anisotropic.

2.2.1.1. **Factors affecting rock mass strength**
The effect of scale

The intact rock specimen is sturdy and uniform, with minimal fractures. As a result, the strength and deformability of this specimen do not reflect the strength and deformability of genuine rock mass. A considerable-scale impact exists. σ_{ci} reduces as the size of the specimen grows larger.

As a result, the strength of a uniaxial compressive strength test performed on a smaller specimen would be greater (Hoek & Marinos, 2007a) as shown in Figure 2.4. Metamorphism has an impact on the size effect. Unweathered crystalline rocks have a small impact, but heavily schistose foliated and weathered rock masses have a significant size effect (Panthi, 2006).

The effect of Strength anisotropy

Strength anisotropy in the rock mass is due to the orientation of mineral grains and directional stress history. In the sedimentary and metamorphic rocks anisotropy is found to be high due to the formation of parallel and weak layers of minerals indicating the schistosity and foliation (Nilsen & Palmström, 2000).
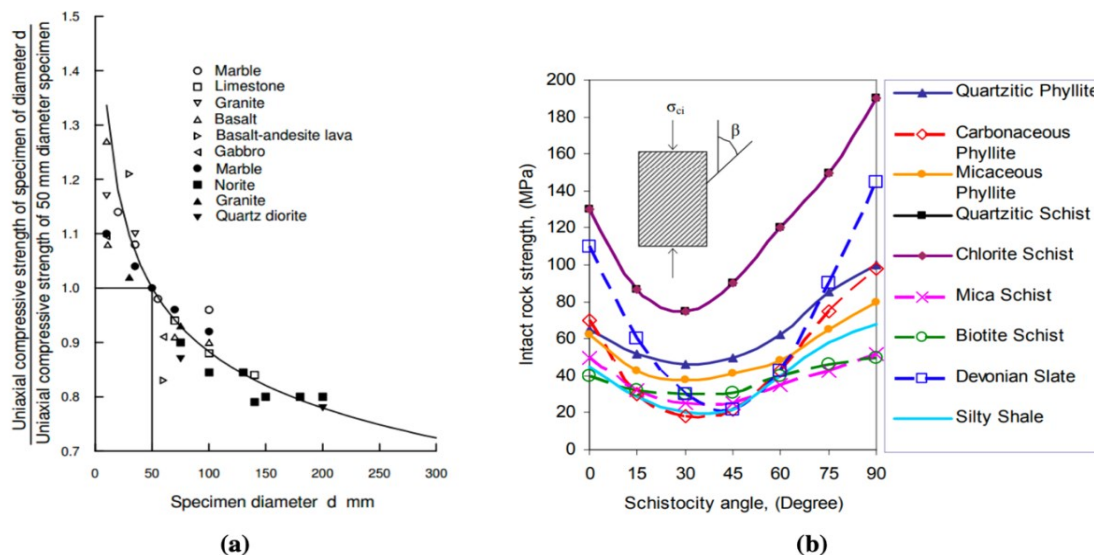
Figure 2.4: (a) Curve showing the influence of specimen size of rock core on uniaxial compressive strength of intact rock (Nilsen and Palmström, 2000), (b). Variation of uniaxial compressive strength of different rock types at different schistosity plane angles (Panthi, 2006)

(Panthi, 2006) found that when the schistosity plane is perpendicular to the direction of loading, the maximum strength of intact rock is observed while minimum strength is seen when the angle is close to 30º. The degree of

anisotropy is the ratio of the two strengths, measured through the point load test where the load is first applied perpendicular to foliation and then in parallel.

The effect of Weathering and alteration

Weathering of rock on the earth's surface is the physical disintegration and decomposition due to exposure to the atmosphere(rainfall) and the hydrosphere. At the same time, alteration is the changes in the composition of the rock due to hydrothermal solutions or chemical weathering. The physical weathering reduces the rock to its mineral constituents due to the rock's thermal expansion and contraction. Weathering action at the surface layers starts with an increased number of joints in which the rock's mineral composition is changed, reorganized, or redistributed in its mineral constituents and leaching or solution of calcite, anhydrite, and salt minerals (Nilsen & Palmström, 2000). Visual observations can assess the degree of weathering while precise characterization can be done through analysis in a microscope.
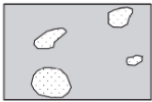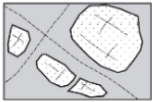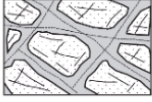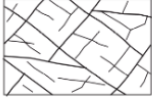
Grade		Rock characteristics	Ground type
Residual soil		Original rock texture completely destroyed Can be crumbled by hand and finger pressure into constituent grains	Soil
	W5 Completely decomposed	Original rock texture preserved Can be crumbled by hand and finger pressure into constituent grains Easily indented by the point of a geological pick Slakes when immersed in water Completely discoloured compared with fresh rock	Soil, probably with clay properties
	W4 Highly decomposed	Can be broken by hand into smaller pieces Makes a dull sound when struck by a geological pick Does not slake when immersed in water Completely discoloured compared with fresh rock	Mixed ground
	W3 Moderately decomposed	Cannot usually be broken by hand; easily broken by a geological hammer Makes a dull or slight ringing sound when struck by a geological hammer Completely stained throughout	
	W2 Slightly decomposed	Not broken easily by a geological hammer Makes a ringing sound when struck by a geological hammer Fresh rock colours generally retained but stained near joint surfaces	Rockmass
	W1 Fresh	Not broken easily by a geological hammer Makes a ringing sound when struck by a geological hammer No visible signs of decomposition (i.e. no discolouration)	

Figure 2.5: Summary of the main stages of weathering (adapted from Gurocak and Kilic, 2005)

Weathering in a rock mass begins at discontinuities and progresses to the rock mineral due to natural processes and the dynamic earth's response to changing environments. There is a wide diversity in the degree of

12

weathering of rock masses and weathering zones as such that in the Himalayas, weathering has a considerable impact on underground excavation stability. Thus it must be considered while evaluating rock mass quality and analyzing subterranean excavation stability (Panthi, 2006). Weathering grade categorization in a rock mass can be used to measure variations. Flaws and fault zones influence weathering. The weakness and fault zones generated by fracturing, shearing, and hydrothermal alteration, provide ideal conditions for increased weathering and serve as a conduit for groundwater flow. Weathering alters the attributes of the rock mass, such as its strength, deformability, frictional resistance, and slaking durability, while also increasing permeability.

2.2.2. Rock mass deformability and estimation

Rock mass deformability is yet another essential, integral parameter that is significantly important as rock mass strength not only for the design of underground opening and excavation but also for the stability analysis through numerical modelling of rock engineering problems for pre-and post-failure analysis and assessment of the effectiveness of the design. However, it is challenging to determine the rock mass deformation modulus in the field, and the result obtained may be questionable due to very complicated procedures.

Plate loading test (PLT), Plate Jacking test (PJT) and Radial Jacking test (Goodman jack test) are some in-situ measurement methods to estimate the rock mass deformability, although deformability tests are expensive, time-consuming and challenging to run (Palmstrom & Singh, 2001). Therefore, many researchers and designers prefer to estimate the rock mass deformation modulus rather than determining it in the field within situ techniques. According to (Palmstrom & Singh, 2001), discontinuities in the rock mass interpret the result values due to sensitivity toward the scale effect. This thesis uses some of the standard empirical relationships in Table 2.3.

Table 2.3: Empirical relationships for estimation of rock mass deformability (Panthi, 2006)

Proposed by	Empirical Relationship	
Hoek et al. (2002)	$$E_{rm} = \left[(1 - 0.5 * D) * \sqrt{\frac{\sigma_{ci}}{100}} * 10^{\left(\frac{GSI-10}{40}\right)} \right]$$	2.9
Barton (2002)	$$E_{rm} = 10 * Q_c^{\frac{1}{3}} = 10 * (\frac{\sigma_{ci}}{100} * Q)^{\frac{1}{3}}$$	2.10
Hoek and Diederichs (2006)	$$E_{rm} = E_{ci} * [0.02 + \frac{1 - \frac{D}{2}}{1 + e^{\frac{60+15D-GSI}{11}}}]$$	2.11

Panthi (2006)	$E_{rm} = E_{ci} * \dfrac{\sigma_{cm}}{\sigma_{ci}}$	2.12

Instead of using a subjective categorization method, (Panthi, 2006) uses elasticity modulus (E_{ci}) and intact rock strength(σ_{ci}). Furthermore, planning estimates may differ from actual ground conditions. (Panthi, 2006) can thus be used to calculate the deformation modulus of schistose, foliated, and bedded rock masses with low, though it has not been used in this thesis. The numerical modelling of RocData is based on (Hoek & Diederichs, 2006).

2.3. Failure Criterion

In rock engineering, several theories have been developed throughout the years to forecast the failure of rock masses. Some of the classic failure criteria used in Engineering geology include the Tresca, Mohr-Coulomb, Drucker-Prager, and Griffith. The Mohr-Coulomb criteria, based on maximum effective shear stress (J. A. Hudson & Harrison, 1997) is commonly acknowledged among these traditional criteria; nonetheless, the true nature of failure has not been identified through these criteria. As a result, the Generalized Hoek-Brown failure criteria, based on an experimental failure plot in the σ_1- σ_3 plane, are generally recognized and adopted (J. A. Hudson & Harrison, 1997)

2.3.1. Mohr-Coulomb Failure Criterion

A Mohr-Coulomb failure criterion is a classical approach of linear approximation which utilizes the relationship between the shear strength and the peak stresses with confining pressures. The method of failure criteria is suitable for the brittle materials like rock mass having one or two joints utilizing the two material constants viz. cohesion and Friction angle to represent the failure envelope. Cohesion and Friction angle varying with normal stress gives the shear strength of the rock material. The shear strength (τ) is given by equation 2.13.

$$\tau = c + \sigma_n tan\emptyset \qquad 2.13$$

where, c is the cohesion, σ_n the normal stress acting on the plane of failure and $\emptyset$ is the angle of friction (Zhao, 2000).

2.3.2. Generalized Hoek-Brown Failure Criterion

The Hoek-Brown failure criterion is one of the most often used failure criteria for determining the failure envelope and stability of underground excavations in the jointed rock mass. The original Hoek and Brown failure criterion for entire rock was given as follows by (Hoek & Brown, 1980):

$$\sigma_1 = \sigma_3 + \sigma_{ci}\sqrt{\frac{m\,\sigma_1}{\sigma_3} + s}$$

<div align="right">2.14</div>

Where, σ₁ and σ₃ are major and minor principal stress. σ_ci is the uniaxial compressive strength of intact rock, m and s being constants that depend on the rock mass properties.

The empirical connection provided by Hoek-Brown's fitting of parabolic curves from triaxial test data has undergone multiple modifications based on experiences and practical circumstances, according to (Nilsen & Thidemann, 1993) The new updated version of the equation has considered the impact of blast damage on the surface rock mass and includes a disturbance parameter D with a value ranging from 0 to 1 (Hoek et al., 2002). The following equation is thus adopted and also suggested by ISRM for jointed rock mass is:

$$\sigma'_1 = \sigma'_3 + \sigma_{ci}(m_b\frac{\sigma'_3}{\sigma_{ci}} + s)^a$$

<div align="right">2.15</div>

Where,
- σ'_1 and σ'_3 are the maximum and minimum effective principal stresses at failure.
- σ_{ci} is the uniaxial compressive strength of the intact rock sections;
- m_b is the value of the Hoek-Brown constant for the rock mass, depending on the Hoek-Brown constant of the intact rock (m_i), the Geological Strength Index (GSI) and the blast disturbance (D) determined by the following equation.

$$m_b = m_i exp\left(\frac{GSI - 100}{28 - 14D}\right)$$

<div align="right">2.16</div>

- S and a are the parameters depending on the rock mass characteristics:

$$s = exp\left(\frac{GSI - 100}{9 - 3D}\right)$$

<div align="right">2.17</div>

And,

$$a = \frac{1}{2} + \frac{1}{6}(e^{-GSI/15} - e^{-20/3})$$

<div align="right">2.18</div>

From the equation (eq by ISRM) given by Hoek-Brown, the ratio of the uniaxial compressive strength of the rock mass (σ_{cm}) to that of the intact rock (σ_{ci}) is:

$$\sigma_{cm}/\sigma_{ci} = s^a$$

<div align="right">2.19</div>

Where s and a can be calculated by the equation 2.17 and 2.18 respectively.

To analyse post peak behaviour of the rock mass, residual parameters must be conducted. (Cai et al., 2007) proposes a set of equations 2.20 to 2.23 to determine residual Hoek-Brown parameters from a residual GSI value (GSI_r). The equations are especially applicable for rock masses with GSI values between 40 and 80, which is suitable for the particular case in this thesis.

$$GSI_r = GSI\, e^{-0,0134 GSI} \qquad\qquad 2.20$$

$$m_r = m_i exp^{(\frac{GSIr-100}{28})} \qquad\qquad 2.21$$

$$s_r = exp^{(\frac{GSIr-100}{9})} \qquad\qquad 2.22$$

$$a_r = 0.5 + \frac{1}{6}\,(e^{-GSIr/15} - e^{-20/3}) \qquad\qquad 2.23$$

The Hoek-Brown criterion is developed through an extensive evaluation of laboratory test data covering a wide range of rock types. It also provides empirical means to estimate rock mass properties (Eberhardt, 2012).

The Hoek-Brown failure criteria are best suited for intact rock or rock masses with closely spaced joints with similar characteristics and isotropic behaviours. Furthermore, it may be used in rock masses with block sizes smaller than the structure being studied (Hoek, 2007) as shown in Figure 2.6.

(a) Schematic Diagram of failure envelope (Brown and Hoek, 1980)

(b) Condition for selecting Generalized Hoek and Brown Criterion (Hoek and Brown, 2019). Modified after (Brown and Hoek, 1980)
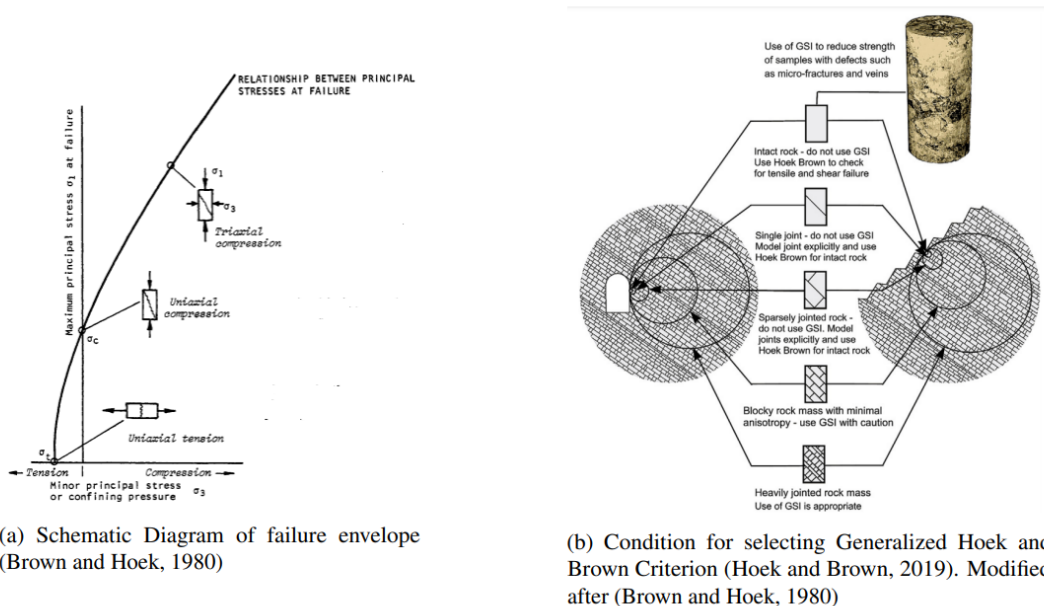
Figure 2.6: Failure Criteria by rock mass characterization. Modified after Hoek and Brown (1980a)

Many geotechnical software programs are still written in terms of Mohr-Coulomb, and it may therefore be necessary to determine equivalent angles of friction and cohesive strengths for a rock mass and the stress range

(Hoek, 2007). This is done by fitting an average linear relationship to the curve defined by the original Hoek-Brown criterion for a range of principal stress values $\sigma_t < \sigma_3 < \sigma'_{3max}$ (Figure 2.6). σ'_{3max} is the upper limit of confining stress for which the relationship between the Mohr-Coulomb and Hoek-Brown criteria is considered (Hoek, 2007).

2.3.3.   Post-Failure Characteristics

In order to predict the failure mode, it is critical to collect information on the elasticity of the rock mass. Stiff Rock is naturally brittle due to its high elastic modulus and thus resulting in brittle failure. Plastic deformation is more likely to occur when the elastic modulus is low, creating more deformation. For the advanced study of rock mass failure, estimating a post-failure behaviour is essential in numerical modelling. (Hoek & Brown, 1997) proposed a post-failure characteristic for a rock of varying quality while carrying out modelling for studying rock mass behaviour after failure, as shown in Figure 2.7

(a) Very good quality hard rock mass   (b) Average quality rock mass   (c) Very poor quality soft rock mass
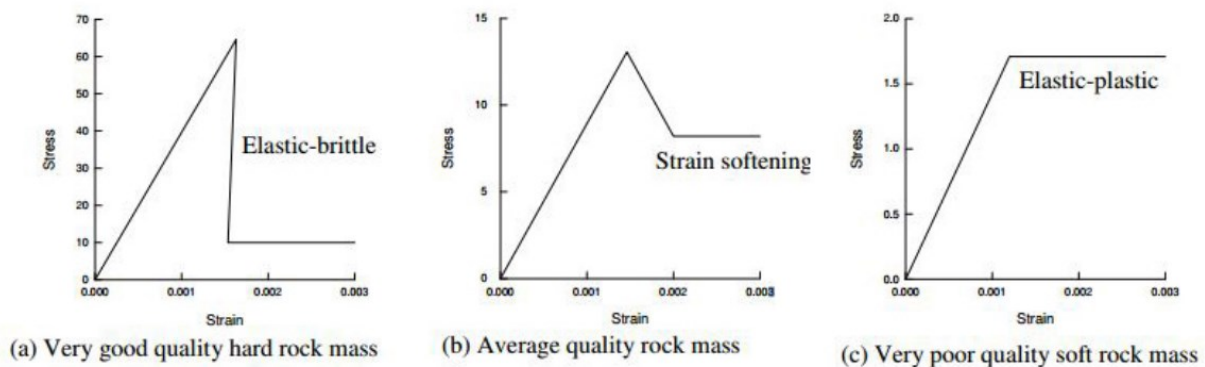
Figure 2.7: Post Failure Characteristics of rock based on quality (Hoek and Brown, 1997)

2.4. Rock Mass Classification

Potential stability problems are often difficult to quantify. Hence, the evaluation of stability and rock support is often based on more or less subjective judgement and practical experience. In such cases, classification systems can be a helpful tool. Classification systems help the user to relate decisions to experiences gained on other sites (Nilsen & Thidemann, 1993). Classification systems aim to identify features or parameters of importance to a project and the assessments to be performed. Such systems should also describe the properties of these parameters, giving values according to their structure, composition and properties (Palmstrom & Stille, 2010). In general, classification systems have the following aims:
- Identify zones of material of similar geomechanical characteristics
- Indicate the predicted stability for excavations of a given size
- Aid in the selection of an appropriate support strategy

- Provide an indication of in situ rock mass strength and deformability modulus (Palmstrom & Stille, 2010)

Over the years, several rock mass classification systems have been developed. However, the most relevant systems in the context of a stability assessment are those involving rock support estimates. Among these are the Terzaghi, RMR, RMi and Q classification system. In the following, the GSI, RMR and Q systems will be discussed further since these systems are widely used in rock engineering today

2.4.1.   Geological strength index (GSI)

The GSI system estimates the strength of jointed rock masses based upon an assessment of the interlocking of rock blocks and the condition of the surfaces between these blocks (Hoek & Marinos, 2000). GSI was introduced by (Hoek, 1994) and (Hoek et al., 1995) and provided a value that, when combined with intact rock properties, can be used for estimating the reduction in rock mass strength for different geological conditions (Hoek, 2007).

GSI chart proposed by (Hoek, 1994) did not represent thinly foliated, folded and sheared rock weak rock mass. (Hoek et al., 1998)updated the chart to include such rock mass category to eradicate this limitation. GSI chart is six by five matrix, where six structural rock categories are taken based on Terzaghi's classification (Intact or Massive, Blocky, Very Blocky, Blocky/folded, Crushed, Laminate/sheared) and five discontinuities classes (Excellent, Good, Fair, Poor and Very poor). While evaluating the GSI value of the rock mass, (Hoek et al., 1998) advise that a range should be taken rather than a single value of GSI for assessing rock mass. (Cai et al., 2004) quantified the GSI chart as shown in Appendix A.4. with undertaking the block volume (Vb) representing joint spacing and frequency and Joint Conditioning Factor (Jc) as given by Equation 2.24 and Equation 2.25. Furthermore, (Cai & Kaiser, 2006) formulated a relationship between GSI, Jc and Vb given by Equation 2.26.

$$V_b = \frac{s1 s2 s3\ 3}{\sqrt[3]{p1\ p2\ p3}\ sin\gamma 1 sin\gamma 2\ sin\gamma} \qquad 2.24$$

$$J_c = \frac{J_{ws}J_s}{JA} \qquad 2.25$$

$$GSI(V_b J_c) = \frac{26.5 + 8.79 log J_c\ + 0.9 log V_b}{1 + 0.0151 log J_c - 0.0253 log V_b} \qquad 2.26$$

Where, s1, s2 and s3 are joint spacing, p1, p2 and p3 are joint persistence factor, Jws is large scale waviness, Js is small scale smoothness and JA is joint alteration factor.
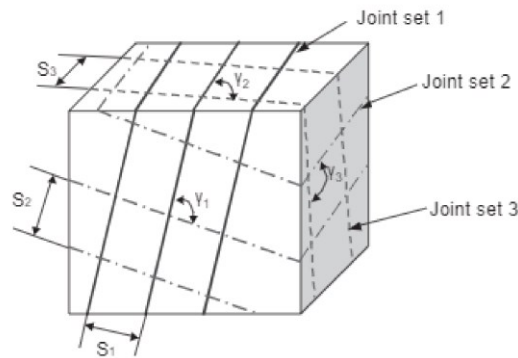
Figure 2.8: Rock Mass with Joint sets (Cai et al., 2004)

The geological character of the rock material and the rock mass it forms is used as input parameters. This approach enables the rock mass to be considered as a mechanical continuum where the influence of geology on the mechanical properties is still considered (Marinos et al., 2005).

2.4.2. Rock Mass Rating (RMR)

The RMR system was developed by (Z. Bieniawski, 1976.) and has been refined as more case records have been examined (Hoek, 2007). In this thesis, the 1989 version of the RMR system has been the basis. The following parameters are used to classify the rock mass using the RMR systems:

· Uniaxial compressive strength of rock material
· Rock Quality Designation (RQD)
· Spacing of discontinuities
· Condition of discontinuities
· Groundwater conditions
· Orientation of discontinuities

This system divides the rock mass into a number of structural regions. Each region is classified separately. The boundaries of the regions will coincide with major structural features. The RMR system with recommendation for rock support is given in appendix B. The recommendation for excavation and rock support is only given for horseshoe-shaped drill and blast tunnels with a span of 10 meters which are subjected to a vertical stress <25 MPa (Palmstrom & Stille, 2010).

The RMR value can be linked to the GSI value with the relationship given by equation 2.8. Here, the RMR value has a groundwater rating set to 15 and the adjustment for joint orientation is set to zero (Hoek & Brown, 1997).

2.4.3. Q-system

The Q system was developed by(Barton et al., 1974) of the Norwegian Geotechnical Institute.   The numerical value of index Q varies on a logarithmic scale from 0.001 to a maximum of 1000 and is defined by:

$$Q = \frac{RQD}{J_n} X \frac{J_r}{J_a} X \frac{J_w}{SRF} X \qquad 2.27$$

Where RQD – Rock Quality designation, describes the joint density of the rock mass

Jn – Describes the number of joint sets

Jr – Describes the joint roughness

Ja – Describes the joint alteration

Jw – Describes the water conditions in the rock mass

SRF – Describes the stress conditions in the rock mass

(Hoek, 2007)

These parameters are measures of:

1. Block size (RQD/Jn)

2. Inter-block shear strength (Jr/Ja)

3. Active stress (Jw/SRF)

(Palmstrom & Broch, 2006)

The block size factor represents the structure of the rock mass, differing the extreme values (100/0,5 and 10/20) by a factor of 400. The inter-block shear strength factor represents the friction characteristics of joint walls or filling materials. Clay mineral coatings and fillings significantly reduce this factor (Hoek, 2007).

The active stress factor consists of two stress parameters. The Jw parameter is a measure of water pressure, which reduces the shear strength of joints due to a reduction in effective normal stress. Water will also act destabilizing by softening clay fillings in joints. SRF is a measure of

1) Loads during excavation through weak zones,

2) squeezing loads in plastic, incompetent rock, and

3) rock stress in the competent rock, which is the most relevant for this assignment. SRF is regarded as a total stress parameter.

Combining Jw and SRF to a consistent parameter for inter-block effective stress is complex. This is because paradoxically, a high value of effective normal stress can result in less stable conditions than a low value, despite the higher shear strength (Hoek, 2007). However, by combining the estimated Q-value, the span (or wall height) of the excavation and an excavation support ratio (ESR), a recommended amount of support can be found in the Q-value chart (Appendix A.5). The Q-values can also be

obtained from RMR values by formulas published by Bieniawski (1989) equation 2.6 and (Grimstad & Barton, 1993a)equation 2.7.

Empirical methods in the form of rock mass classification systems suffer from several limitations. The classification systems are significant tools to describe the stability characteristics of the rock mass and their best applications are in jointed rock masses where instability is caused by block falls (Palmström & Stille, 2010).

Today's classification systems are simplified to cover a wide spectrum of conditions. These simplifications may result in overlooking local geometrical and structural features. Classification systems give averaged values. There might be a significant variation between the highest and the lowest values. The support charts are derived from cases where the installed support is based on varying contractual conditions. The different excavation and rock support practices in various countries will also contribute to uncertainties (Palmstrom & Stille, 2010).

2.5. Rock stresses

For stability of any underground caverns and openings, rock stress plays a vital role in obtaining the self-supporting capability for safe excavation and construction works. In any case, the distribution of the rock stress surpasses the rock mass strength, and the stability of the cavern is compromised.

2.5.1. In-Situ Stresses

According to (Nilsen & Thidemann, 1993), in-situ stresses are the result of the following components:
- Gravitational stress: Rock stress originated due to gravity alone.
- Topographic stress: Topography affects stress when the surface is not horizontal.
- Tectonic stress: Stress produced due to tectonic movement.
- Residual stress: Remnant stress has been locked into rock material during an earlier stage of geological history.

The General conventions used in rock engineering are compressive stresses are taken as positive while the tensile stresses as negative. Principal stresses are the representation of resultant stresses at any point in the rock mass. Principal stress is the stress in a principal plane, which is acted upon by only normal stresses and no shear stresses. There are 3 principal stresses namely, Major principal stress (σ_1), Intermediate principal stress

(σ_2) and Minor principal stress (σ_3) that are important for stress analysis. (Nilsen & Palmström, 2000)have given away to measure these stresses.

2.5.1.1.   **Gravitational Stresses**

Due to overburden, stress gets induced in two directions, namely vertical and horizontal directions. At a depth z below the rock surface, and with the horizontal surface assumption, the vertical gravitational stress is given as equation 2.28.

$$\sigma_v = \sigma_z = \gamma_r H \qquad\qquad \text{2.28}$$

where γ_r is the specific gravity of rock mass in MN/m3.

There have been many site measurements of vertical stresses from tunnels, caverns and minings around the world plotted against depth. As indicated by (Carranza-Torres & Fairhurst, 2000) after (Hoek & Brown, 1980) and (Panthi, 2006), Figure 2.9 shows the relationship producing a straight line with a slope of 0.027 which is fairly correct since the value is the mean specific gravity of rock. The values, however, can have significant deviations near the surface or at considerable depth because of the limits of measuring equipment at shallow depths and the presence of residual stresses at great depth (Nilsen & Palmström, 2000).

2.5.1.2.   **Tectonic Stress**

With reference to (Panthi, 2006), horizontal stress or tectonic is calculated as the sum of effect due to gravity and tectonic condition and is given as an equation 2.29.

$$\sigma_H = \sigma_{tect} + \frac{\vartheta}{1-\vartheta}\sigma_v \qquad\qquad \text{2.29}$$

where the first term is the gravitationally dependent term. The vertical gravitational stress is assumed reduced by the ratio defined by the Poisson's ratio v.

In addition, the stress factor (k) varies significantly due to topography and tectonic movements as shown in Figure 2.9 (Hook, 2007). According to (McCutchen, 1982), the ratio(k) is greater than 1 at shallow depth and less than or attains a constant value as the depth increases. (Panthi, 2006) found that plate tectonic movement affects the magnitude of the stress factor(k) to a great extent. This variation emphasizes the vitality of in-situ stress measurement for any underground excavation to start. Most often tectonic stress do not align normal and parallel to the cavern alignment,

therefore necessary resolving in equivalent in-plane and out-of-plane stress are done using equation 2.30 and 2.31.

$$\sigma_{in-plane} = \sigma_{tect}.\cos\beta + \frac{\vartheta}{1-\vartheta}\sigma_v$$ 2.30

$$\sigma_{out-plane} = \sigma_{tect}.\sin\beta + \frac{\vartheta}{1-\vartheta}\sigma_v$$ 2.31

where, β is angle made by tectonic stress with the equivalent in-plane stress.
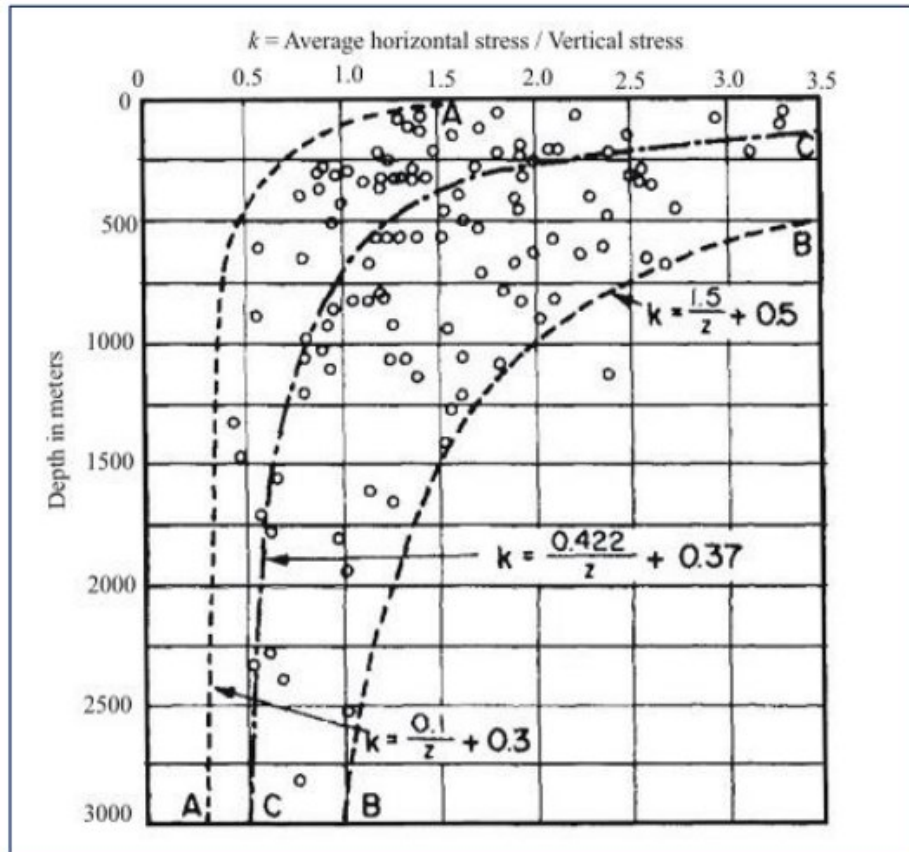
Figure 2.9: *Variation of ratio of average horizontal stress to vertical stress with depth below surface (Panthi, 2006)*

2.5.2.   Stress Distribution around the underground excavation

During and after the excavation of an underground opening, the stresses in the rock mass will be redistributed around the periphery of the excavation. The load carried by the mass removed must be transferred to the remaining mass. The stresses induced by the excavation will depend on the magnitude and direction of the principal stresses and the geometry of the opening (Nilsen & Palmström, 2000).
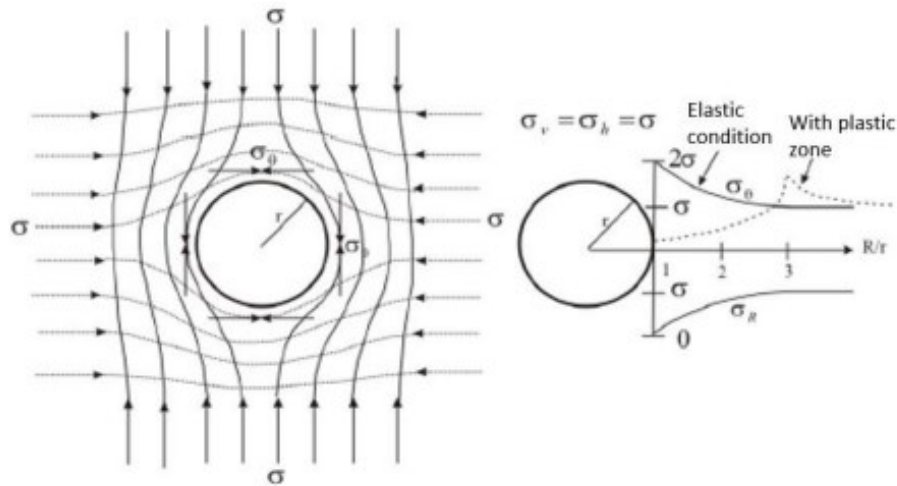
Figure 2.10: Stress trajectories around a circular opening(left); Tangential and radial stress distribution in elastic and non-elastic conditions(right) (Panthi, 2006)

Figure 2.1 illustrates how the redistribution of the stresses can be expressed around a circular opening, for an elastic material in iso-static stress conditions ($\sigma_h = \sigma_v = \sigma$). Inelastic material, the tangential stress (σ_θ) will be twice the principal stress (σ) at the wall of the opening, and the radial stress (σ_R) equal to zero. Moving away from the opening, the stresses will normalize as the ratio between radial distance (R) and opening radius (r) increases (Figure 2.10 right). Formally, this theory is known as the Kirsch solution:

$$\sigma_\theta = \sigma \left(1 + \frac{r^2}{R^2} \right)$$
2.32

$$\sigma_r = \sigma \left(1 + \frac{r^2}{R^2} \right)$$
2.33

For non-isostatic stress conditions, the Kirsch solution states that the maximum tangential stress ($\sigma_{\theta max}$) will occur in the direction where the major principal stress (σ_1) is tangent to the contour. Likewise, will the minimal tangential stress ($\sigma_{\theta min}$) occurs where the minor principal stress (σ_3) is tangent to the contour. According to the Kirsch solution, the magnitude of the tangential stresses is defined as:

$$\sigma_{\theta,max} = 3\sigma_1 - \sigma_3$$
2.34

$$\sigma_{\theta,min} = 3\sigma_3 - \sigma_1$$
2.35

The Kirsch solution is valid for a homogeneous, isotropic and elastic rock mass with widely spaced and tight joints (Panthi, 2006). For weak and anisotropic rocks, the tangential stresses will cause destruction and cracking of the material, resulting in a gradual reduction of the strength. A zone of broken rock will form around the opening, the so-called plastic zone,

where the material loses its load-carrying ability. In such rock masses, the maximum tangential stresses are moved further from the periphery of the opening, until 20 the elastic zone is reached (Panthi, 2006). This is illustrated by the dotted line to the right in Figure 2.10.

A non-circular opening will change the locational and magnitude of the tangential stresses. Sharp corners, in particular, may strongly influence the magnitude; the sharper the corner, the higher the stress concentration in that corner will be (Nilsen & Palmström, 2000). The magnitude of the maximum tangential stress depends in theory on the shape of the excavation, and not its size. However, the zone of influence increases when the size increases. Consequently, the more masses are removed, the more stress is redistributed to the remaining masses (Myrvang, 2001).

3. DESIGN AND STABILITY ASSESSMENT OF UNDERGROUND POWERHOUSE CAVERN

3.1. Design Aspects/Criteria

The planning, design, and construction of powerhouses and powerhouse complexes, particularly underground powerhouse caverns, has grown in favour as technology has advanced. However, critical considerations must be made during the planning and design stages of large-scale powerhouse caverns, since this significantly impacts powerhouse construction's cost, serviceability, and structural stability. The general characteristics of these structures are controlled by the geography and geology of the rock mass. The structure must be properly conceived, planned, and designed based on geological investigations and rock mass characteristics, taking into account the location, purpose, nature of the surrounding rock mass, and the standardized rules and practice codes. (Gattinoni et al., 2014). The compatibility of the structural design with standard codes and safety margin that covers the prevailing uncertainties should be maintained. The following design approaches: systematic and general design procedures as described by (Selmer-Olsen, 1977), are highly recommended for cost-effective and safe underground powerhouse caves.

3.1.1. Location

The most important aspects of engineering geological investigation are to find the best location for the underground structure of a hydroelectric power plant, as an investigation defines the quality of the rock mass that prevails in the environment in question. This step is one of the most important decisions to be made during the preliminary design and planning phases of the project. The site selection can be risky with the presence of young or friable sedimentary rocks that form a very complex geology that can present very unfavorable structural stability problems and should be avoided if possible (KC & Panthi, 2011). Mountainous regions with weak, porous, and highly jointed rock masses are prone to subsidence due to seismic activity and inherent stresses that threaten the stability of caves at shallow depths. To ensure cave stability, the site must be investigated for topographic and inherent stresses due to deposition (Hoek & Moy, 1993). In addition to seismic stresses at specific locations, weathering can also be a problem. This means that the cave opening must be deep enough to independently support the roof under normal loading and must be at an appropriate depth of weathering-resistant strata in caverns with shallow and deep underground openings (Edvardsson & Broch, n.d., 2002).

According to (N. W. Hudson, 1993), there are mainly two types of failure that can occur in an underground excavation. It is block failure, when pre-existing blocks in the ceiling and side walls of an underground opening move freely after excavation. The second form is stress failure, when the induced stresses around the excavation exceed the strength of the rock. Thus, most instabilities in the subsurface excavation are depth-dependent. Near the surface, in-place stresses are generally anisotropic, and stability is determined mainly by discontinuities. In contrast, deeper in the rock, in situ stresses are greater and the frequency of occurrence of discontinuities is lower due to increased confinement, so in situ stability is controlled by induced stresses. This means that the challenges to stability vary greatly depending on how a hydropower plant is designed with respect to the location of the various underground structures such as headrace and tailrace tunnels, shafts, underground caverns, and access tunnels.

3.1.2. Orientation
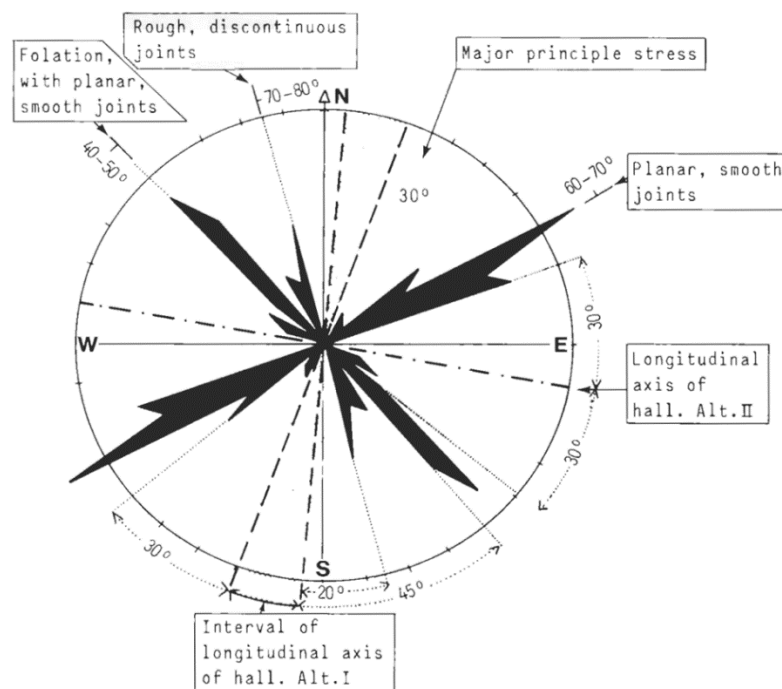
Figure 3.1: Orientation (Nilsen and Palstrom, 2000).

The orientation of the cavern opening is decided by the joint patterns predominant at the location selected for the cavern. These joint patterns and foliations are quite common within the rock mass and infrequently create weak planes that threaten stability if not tackled effectively (Hoek & Moy, 1993). The orientation of the cavern must be designed and optimized to possess low minimum support requirements, stability issues, and low overbreak (Edvardsson & Broch, 2002). For shallow or intermediate-depth caverns, it's best to orient the length axis of the cavern along the bisection

27

line of the most intersection angle between two major dominating joint sets, foliation, or bedding directions as shown in Figure 3.1.

To reduce distortion and low friction shear, avoid aligning the cavern in a parallel position with the third and fourth joint sets (Edvardsson & Broch, 2002). It is recommended to align the cavern at a 25-30 degree angle with the discontinuous joint sets beneath strong anisotropic stress to obtain stability in the cavern. Between the cavern's long, high walls and steep dipping planes, and joints filled with clays, a minimum angle of 25º should be maintained (Nilsen & Palmström, 2000). Nonetheless, in the case of deep-seated caves, the direction of major primary stress is critical, and the entrance should be aligned to avoid tangent stress plane collision. With an angle of 15-30º between the cavern length and the horizontal projection of the primary principal stress, reliable alignment has been attained based on previous experiences (Edvardsson & Broch, 2003).

3.1.3. Shape of Cavern

The rock mass's behaviour and the entrance's stability are influenced by the shape, geometry, and size of the cavern's excavation. According to the rock masses, the powerhouse cavern might take several different forms (Palmstrom & Stille, 2010). In a strong rock mass, a traditional underground powerhouse cavern configuration with a somewhat flat top and vertical sidewalls can be designed, whereas tall straight sidewalls can be bent inwards and tensile failure can occurs when used in weak rock masses, especially with significant horizontal in-situ stresses.
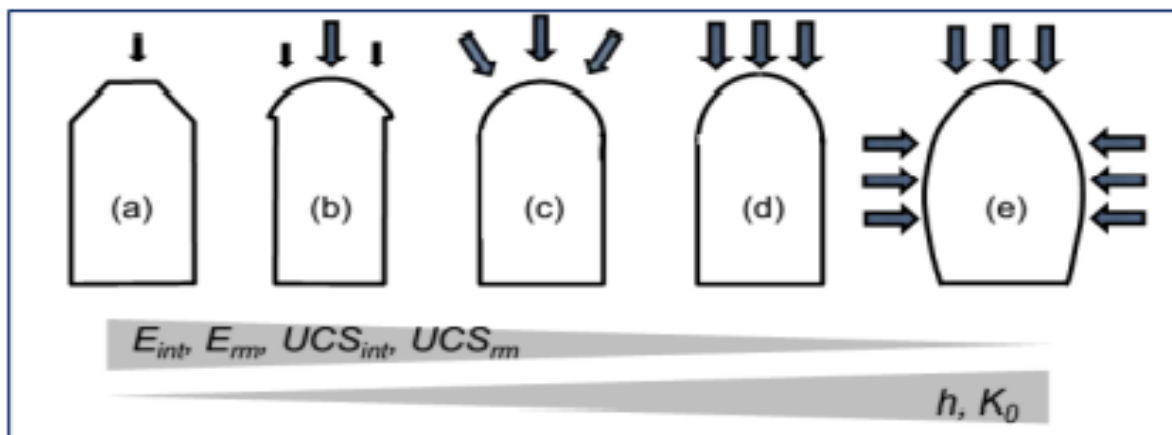
Figure 3.2: Common shapes of caverns; (a) trapezoidal; (b) mushroom; (c) circular shape; (d)bullet shape; (e) horseshoe

To support the rock mass surrounding the cavity in such caverns, significant reinforcing in the form of grouted cables or rock bolts will be necessary. The formation of a horseshoe cavern, as shown in Figure 3.2 (e) can be used to

prevent this. The disadvantage of such a design is that it requires more profile-conscious construction than a cavern with straight walls.

For the design of an underground cavern, the general principle is a shape so that the compressive stresses are evenly distributed along the periphery of the opening. The underlying goal is to make sure there is enough confinement for the roof to be self-bearing and at the same time not to cause high-stress concentrations along with points in the periphery which cause failure. Arched roof openings without intruding corners and edges distribute rock stress and give headspace for overhead cranes in the rock above the cavern, providing a greater stability margin. Although having slightly curved machine cavern sidewalls helps to eliminate high tensile failure zones and reduce support demands, the most common combination is a straight-cut wall since it is the easiest to dig and gives the greatest stability (Saurer et al., 2011). A simply shaped cavern may be developed in a short period with little effort, saving both time and money (Panthi 2015). At shallow and intermediate depths, the number of joints and their features influence the shape of the cavern's roof, but at deep depths, stress or anisotropy affects the shape of the cavern's roof (Edvardsson & Broch, 2003)

The ideal cavern shape should be closely linked to rock mechanical qualities and stress conditions from a geo-mechanical perspective; yet, neither geo-mechanical situations nor rock parameters are reliant on cavern shape. In the diagram in Figure 3.2, several cavern formations are presented, along with their applicability dependent on rock mass properties and stress conditions (Saurer et al., 2013). These shapes of the caverns are the most commonly used for the design of the underground caverns.

3.1.4.   Dimension of Cavern

The stability of the large caverns is not only dependent on the location, orientation, and shape of the cavern but also its dimension. Underground power stations require large openings, often with a span order of 25 m. Both the geometry and the size of the excavation will highly influence its stability. In general, the deformations of an opening will increase with increasing width or radius of the opening (Palmstrom & Stille, 2010). Larger excavations will decrease the in-situ strength of the rock mass since larger tunnels offer less confinement to the surrounding material (Goel et al., 1995; Palmstrom & Stille, 2010). This is why special considerations have to be made for the planning and design of large-scale caverns. Based on the layout requirements, the orientation, size, and especially the shape, of the

excavation have to be adjusted to fit the actual stability issues (Palmstrom & Stille, 2010)

3.1.5. Pillar width between caverns

For underground hydropower stations, an additional challenge will be adjacent openings mutually influencing each other. For larger projects the transformers are typically placed in a smaller cavern parallel to the powerhouse, to reduce the size of the main cavern. The engineers have to weigh the cost of having a long distance between the two caverns for better stability, versus a shorter distance to reduce the length and cost of the busbars (Hoek & Moy, 1993). In general, there should be enough rock mass between the openings for the stresses to normalize. For squeezing ground, it will be especially important that the plastic zones do not overlap, which in the worst case may cause complete failure of the pillar.

According to (Hoek, 2007), a study was carried out to find the optimum pillar width between the transformer gallery and the machine hall. The results showed that the optimum pillar width is obtained when the distance between the two openings is approximately equal to the height of the larger of the two caverns. In very poor-quality rock with larger overstressed zones, it may be advisable to increase the pillar width to 1.5 times the height of the larger cavern (Hoek, 2000). According to (Hoek & Marinos, 2007b), this rule of thumb is generally applicable for all cavern designs in weak rock masses.

3.2. Stability Assessment Methods

Unground caverns and openings are prone to failure mostly due to the in-situ stress magnitude and characteristics of rock mass as shown in Figure 3.3 (Martin, 1999). Assessment of the stability can be done using different methods depending upon the types of failure. According to (Hoek & Moy, 1993), influences of surface topography on the in-situ stress field have to be considered for the selection of the location of the underground powerhouse and assessment of the stability condition.

This thesis will focus on the assessment of the cavern location, orientation and the stability of the powerhouse.
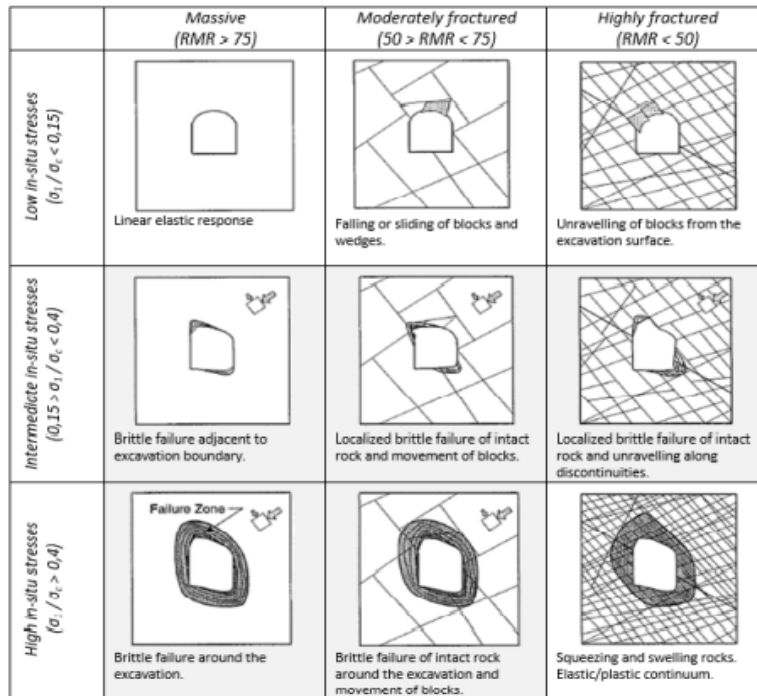
Figure 3.3: Instabilities and brittle failures (grey squares) as a function of Rock Mass Rating(RMR) and the ratio of the major principal stress and UCS. Modified after Martin et al. (1999)

3.2.1. Structurally Controlled Failure or Block Failure

The ceiling and walls of the Power House cavern fail in two ways. In weak or highly jointed rock or huge hard rock subjected to very high loads, failure of the rock mass around the excavation is the most common failure mode. The most prevalent kind of failure in hard rock excavation in shallow depths is wedge failure, which is characterized by crossing structural discontinuities (three structural planes intersecting to form a block with the excavation boundary as the fourth plane) (Hammett & Hoek, 1981). If the loose wedges are allowed to fall, the cavern's stability will quickly decrease, generating further issues such as reduced constraint and interlocking of the rock mass. The other wedges will be destabilized as a result of this impact, and the failure process will continue until the natural arching stage is achieved. The structurally controlled instability is influenced by the orientation of discontinuities, the geometry of the cavern, and the state of the structural feature, such as friction and weathering. The influence of in-situ stresses is ignored throughout the study since it is deemed sensible, i.e. to guarantee conservative support design in Figure 3.4 depicts possibly unstable rock blocks in the vicinity of the subsurface cavern, with failure mechanisms varying based on the wedge's placement.
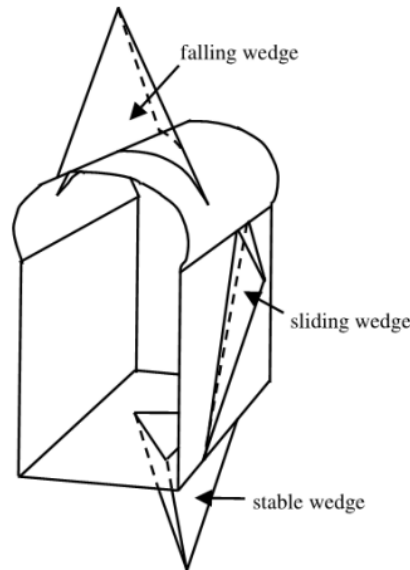
Figure 3.4: Sketch of potentially unstable rock blocks around the underground chamber of the Rio Grande hydroelectric power plant (Cordoba district – Argentina) (Oreste and Cravero, 2008)

3.2.1.1.   **UnWedge Analysis**

UnWedge is a three-dimensional numerical tool for analyzing the geometry and stability of underground openings in a rock mass with structural discontinuities. Goodman and Shi's block theory are the foundation to wedge stability analysis in UnWedge. Potentially unstable wedges are modelled and support system requirements are checked around tunnel opening to calculate the factor of safety.

Deterministic Analysis in UnWedge

The principle of deterministic analysis involves the determination of the factor of safety with the fixed values of effective parameters. UnWedge software has a built-in option to calculate the safety factor of falling wedge under excavation and supporting the cavern in a rock mass. The following steps are used to deal with wedge/block failure in the software.

• Determination of average dip and dip direction of discontinuity sets.

• Identification of potential wedges.

• Factor of safety calculation.

 • Reinforcement calculation.

Probabilistic Analysis in UnWedge

There are various uncertainties related to input parameters such as rock mass strength, the inclination and orientation of discontinuities in the rock mass, and the internal friction of rock joints to be used in the program. Figure 3.4 can best address the real site problem. So, probabilistic analysis deals with calculating safety factor distribution for each potential wedge

from which probabilities of failures are calculated. The interface allows the user for pseudo-random number or random number generation. The input parameters are distributed about their mean, described by one of the distribution functions such as normal distribution and distribution of safety factor and probability of failure are calculated.

The Monte Carlo method or *Latin Hypercube* sampling is a standard sampling method. Monte Carlo simulation uses random or pseudo-random numbers for sampling probability density functions specified in input parameters. The method is applicable for both deterministic and stochastic analysis. The statistical attributes of model results are based on the performance function in a sample of input variables. As a result, it is easier to solve complex engineering problems involving various distribution and highly non-linear engineering models.

Latin Hypercube simulation is a recent development that gives comparable results to the Monte Carlo simulation. Every input parameter range is divided into a space of equivalent probability, and a value is selected randomly from every space in the *Latin Hypercube* simulation. As a result, the simulation is much faster and more efficient than the *Monte Carlo* simulation. The computation uses a specified number of iterations to determine wedge results, such as maximum wedge depth, weight, and safety factor.

3.2.2. Tensile failure

Rock can withstand subtle tensile loads due to its discontinuous aspect and brittle nature. Due to cavern geometry, tensile strains might build on the powerhouse cavern wall around the crown and invert of the cavern. When the cavern orientation is aligned with the primary principal horizontal load, tensional jointing may occur.

3.2.3. Compressive failure

Compressive failure of the rock mass will occur if the compressive tangential stress Figure 3.3 exceeds the compressive strength of the rock. Depending on the character of the rock, the failure usually takes the form of either: i) rock/burst spalling, or ii) squeezing or plastic deformation.

3.2.3.1. Rock burst/Rock spalling

Rock spalling is fracturing parallel to the cavern contour induced by high compressive stresses and typically occurs for strong and brittle rocks. The fracturing process is often accompanied by loud noises and vibrations and

is then referred to as heavy spalling or rockburst. Rock burst or heavy spalling typically only occur for very high rock stresses and are therefore most relevant for deep excavations. For moderate stress levels, the fracturing will result in the loosening of thin rock slabs, referred to as rock slabbing or spalling (Nilsen & Palmström, 2000). Rock bursting may at times be quite violent and dramatic. In extreme cases, the process can have the character of popping large rock slabs with considerable force and speed. The activity is often most intensive in the vicinity of the face (10-20m behind the face) and may therefore be a significant threat to the safety of the workers if the appropriate support is not installed (Nilsen & Thidemann, 1993). Risk assessment for rockburst or spalling is generally based on the ratio between the maximum tangential stress given by equation and the rock mass strength (Section 2.2.1).

3.2.3.2.   **Squeezing or Plastic deformation**

Weak and soft rocks will due to their plastic nature behave very differently when subjected to tangential stress. In such rocks, the potential problem will be plastic deformation. In extreme cases reduction of the original cavern width/diameter by several tens of centimetre due to squeezing may occur (Nilsen & Palmström, 2000). The major cause of stability problems at the caverns with weak rock mass is plastic deformation. Hence, analysis and risk assessment of the squeezing phenomena for Tamakoshi V HEP will be discussed in detail.

3.2.4.   **Plastic Deformation**

An important underground opening instability in the weak and deformable rock mass is plastic deformation or squeezing. Plastic deformation was first described by Heim in 1878 during tunnelling in the Alps (Shrestha, 2006). As per (Shrestha & Panthi, 2014), there are two types of plastic deformation, namely instantaneous deformation and long-term deformation. Instantaneous deformation is the instantaneous response of rock mass under excavation of opening due to advancement of the face (Panet, 1996). International Society for Rock Mechanics (ISRM) Commission in 1995 has defined squeezing as time-dependent large deformation which occurs around tunnels or caverns and is associated with creep caused by exceeding limiting shear stress. Simplified, squeezing can be described as the time-dependent inward movement of the rock material towards the tunnel when subjected to tangential stress (Panthi, 2013). Thus, plastic deformation can occur instantaneously or by creeping effect.

3.2.4.1.   **Instantaneous deformation**

As explained in section 2.5.2, when an underground opening is excavated there is a redistribution of stresses around the opening. Weak rocks such as shale, slate, and phyllite behave differently when subjected to high tangential stress (Panthi, 2006). When the rock mass strength is lesser than induced tangential stress along tunnel contour, gradual formation of micro-cracks along the foliation or schistosity occurs. So, a viscous-plastic zone of micro fractured rock mass is formed deeply into walls. This causes induced tangential stress to move beyond the plastic zone as illustrated in Figure 3.5. This causes a time-dependent inward displacement of rock mass causing support to experience a gradual increase in pressure. This is illustrated with a dotted line in Figure 3.5, where P_i is the support pressure. This type of failure due to overstressing of the rock mass is usually referred to as instantaneous squeezing or deformation. The inward movement, squeezing of the rock mass, is usually highest in the areas of maximum tangential stress. However, if the minimal tangential stress is very low, it may also cause stability problems (Shrestha, 2006).
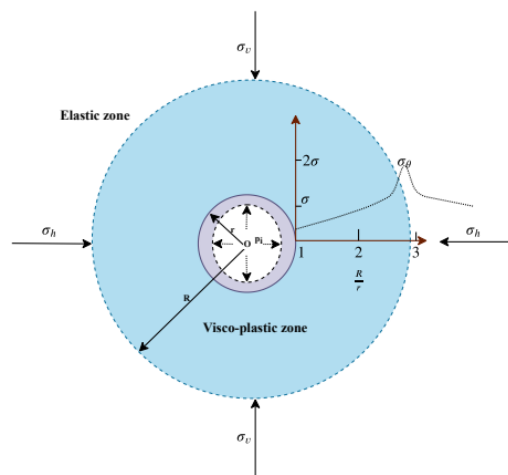
Figure 3.5: Illustration of the visco-plastic zone of micro fractured cracks (blue section) around the squeezed tunnel. Based on Panthi (2006)

3.2.4.2.   **Time-dependent deformation (Creep)**

According to (Shrestha & Panthi, 2014), long-term deformation or creep in rock mass occurs due to long exposure of rock mass to constant loading. The deformation is dependent on time. Creep is categorized into three distinct stages. They are Primary creep, Secondary creep, and Tertiary creep in Figure 3.6 (Goodman, 1989). Primary creep involves the rapid increase in a strain which lowers with time. In the case of secondary creep, the deformation occurs at high deviatoric stresses and involves a constant increase in strain. Tertiary creep involves deformation when loading is nearer the rock mass peak strength. In this stage, strain rate accelerates,

and uncontrolled propagation of crack causes failure of the rock mass. An idealized creep curve is illustrated in Figure 3.6.
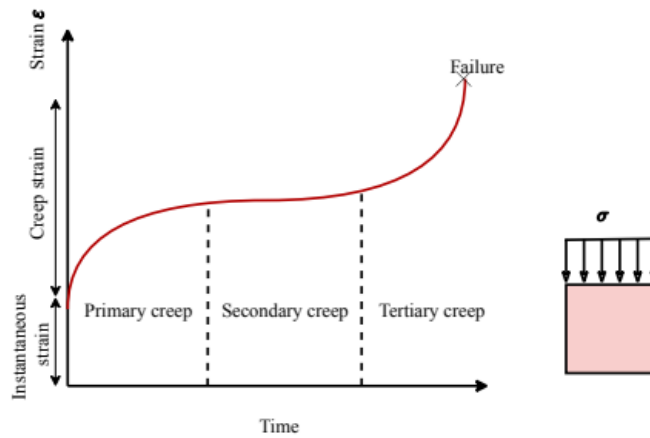
Figure 3.6: Illustration of strain-time (creep) curve indicating three major stages. Redrawn based on Shrestha (2014)

The G-U line marks the critical stress level. Above point G, crack propagation will accelerate into the tertiary stage and terminate in rupture. This means that creep initiated at point A in Figure 3.7 will terminate in failure at point B after a relatively short time. Creep starting in point C (initial stress further from peak load), will terminate in D after a much longer time than for A-B. Creep initiated at point E below the critical stress level will approach point F and stop at a finite strain level without rupture after a long time (Goodman, 1989). Point T marks the "creep threshold", below which no creep will occur. The line T-U is the terminal locus for long-term creep tests. This illustrates how materials may creep to failure, even if it has not failed immediately after excavation.
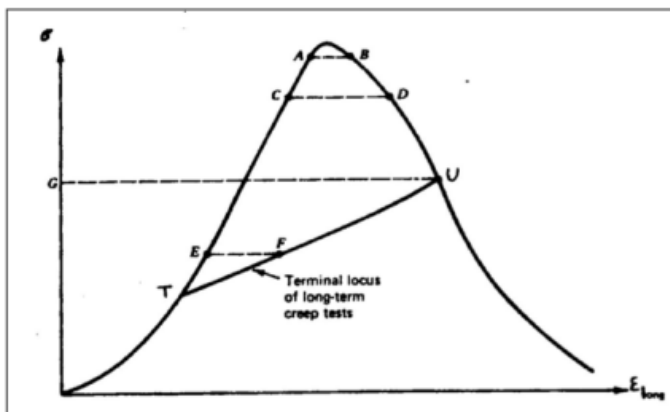
Figure 3.7: Creep in relation to the complete stress-strain curve (Goodman, 1989)

3.2.5.   Evaluation Methodologies Of Plastic Deformation

Common methods which are useful for evaluating tunnel plastic deformation include empirical methods such as (Singh et al., 1992), Q-system (Grimstad & Barton, 1993a), and (Goel et al., 1996) methods. Semi-empirical methods include (Hoek & Marinos, 2000) & (Panthi & Shrestha, 2018) methods. Similarly, the analytical method of Convergence Confinement Method (CCM) (Carranza-Torres & Fairhurst, 2000) and numerical method with finite element software like Rocscience are very useful to quantify squeezing around tunnel contour.

3.2.5.1.   Empirical methods

Empirical methods are solely based on experience and case histories. (G. L. Shrestha, 2006) has categorized empirical methods into three categories based on indicators used, namely Strength stress ratio, strain estimation & rock mass classification methods. In the strength stress ratio method, the ratio of rock mass strength and in-situ stress is calculated and if the ratio is less than 2, the ground is considered over-stressed (Wood, 1972). In strain estimation, tangential strain in the tunnel is used as a parameter to investigate squeezing (Aydan et al., 1993). This thesis uses the third type of empirical method which shall be discussed below.

Singh et al. (1992) method

This method is based on the rock mass classification system. (Singh et al., 1992) have suggested an empirical relation between tunnel depth (overburden) and rock mass quality (Q-value), both in the logarithmic system in ₛₘₐₗₗFigure 3.8 (a). 41 sections of the tunnel including 24 sections from Himalaya were used to plot the relation. A demarcating line was suggested which separates the squeezing rock mass from non-squeezing. This equation is given as equation 3.1. The approach is relatively simpler but the estimation of the Q-value is difficult since the estimation of correct SRF is challenging.

$$H = 350Q^{0.33} \hspace{4cm} 3.1$$

Goel et al. (1995) method

In order to overcome the problem of defining SRF, Goel has developed an empirical approach for predicting squeezing based on rock mass number (N) which is defined as the Q-value with SRF value of 1 Figure 3.8 (b)). 99 different tunnel sections have been studied to find the relation between tunnel depth (H), tunnel diameter (B), and rock mass number (N). (Goel et al., 1995) suggested a relation between HN0.1 and N in log-log form, as

shown in Figure 3.8. The demarcating line AB separates squeezing conditions from non-squeezing. Line AB is represented by equation 3.2.

$$H = 275N^{0.33}B^{-0.1} \qquad\qquad 3.2$$

Goel has suggested the classification scheme for squeezing as shown in Appendix B2.
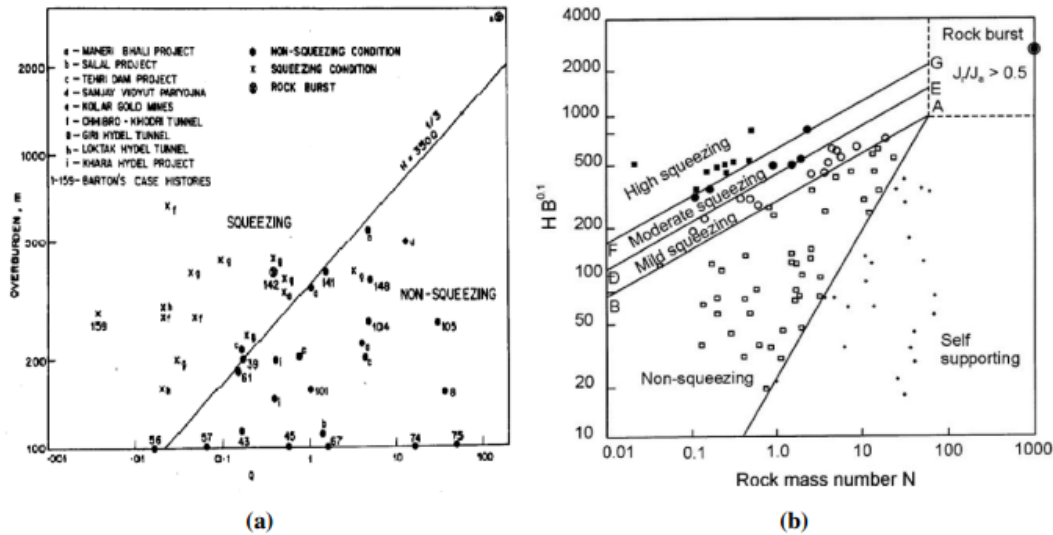
Figure 3.8: (a) Singh's method to predict squeezing by Q-value (Singh et al., 1992). (b) Goel's method to predict squeezing by rock mass number (N) (Goel et al., 1995)

Q-system

Q-system for rock classification was suggested at Norwegian Geotechnical Institute (NGI) by (Barton et al., 1974). It was updated later by Grimstad and Barton (1993). Q-system is useful for estimating required tunnel support and calculated with equation 2.27. These three parameter sets are the measures of: Block size. inter-block shear strength and active stress (Barton et al., 1974). Appendix A.5 shows details of Q-value determination. Squeezing conditions are determined based on active stress which evaluates the effect of water and the ratio of maximum tangential stress and rock mass compression strength (Barton, 2002). Table 3.1 suggests the squeezing condition according to Q-system (Barton, 2002).

Table 3.1 :Squeezing conditon according to Q-System as suggested by Barton (2002)

Squeezing rock: plastic flow of incompetent rock under the influence of high rock pressure	$\sigma_{\theta max}/\sigma_{cm}$	SRF
Mild squeezing rock pressure	1 - 5	5 - 10
Heavy squeezing rock pressure	> 5	10 - 20

According to Q-system, the plastic deformation is either Mild or Heavy based on $\sigma_{\theta max}/\sigma_{cm}$. $\sigma_{\theta max}$ can be calculated using the Kirsch equation described by

equation 2.32. For the normal stress condition, the value of $\sigma_{\theta max}$ is equal to σ_1 which is gravity stress. With reference to (Shrestha, 2006), as per (NGI, 2013) "Squeezing rock cases may occur for depth greater than 350 $Q^{1/3}$. Also, rock mass strength can be estimated using $\sigma_{cm} = 0.7 \gamma Q^{1/3}$ where γ is the density of rock mass in kN/m3. But (Shrestha, 2006) , claims this method of squeezing estimation leads to a loop of dependency. Using the equation defined above to calculate rock mass strength, σcm is dependent on the Q value. For estimating Q-value, SRF has to be estimated first. And to estimate the SRF value, it should be known whether or not there is squeezing. Thus, to eliminate this loop of dependency, different empirical methods suggested in Table 2.2 can be used.

3.2.5.2. **Semi-empirical methods**
Semi-empirical methods give an idea about extent of plastic deformation around tunnel opening and support system required to counter them. Most often semi-empirical methods use the term Competency factor which is the ratio of rock mass strength to in-situ stress to quantify squeezing phenomena. This term has been used by different researchers like (Barla et al., 1995) and Hoek (1999) .

Hoek and Marinos (2000) method
(Hoek & Marinos, 2000) method is the most common semi-empirical method used for quantifying plastic deformation. The competency factor (ratio of rock mass strength & in-situ stress) is used to show the potentiality of plastic deformation in the circular tunnel. (Hoek & Marinos, 2000)have used the approach suggested by (Sakurai & Takeuchi, 1983) to find the relation between competency factor and strain percentage (ε%) in the tunnel which is the ratio of tunnel closure to original tunnel diameter expressed in percentage. The results from a closed-form analytical solution in the circular tunnel with a hydrostatic stress field as suggested by (Duncan Fama, 1993) and (Carranza-Torres & Fairhurst, 1999) have been used in this analysis. Monte Carlo simulation has been performed for the determination of tunnel strain under conditions with in-situ stress varying between 2 to 20 MPa, tunnel diameter of 4 to 16 m, uniaxial compressive strength of 1 to 30 MPa, GSI of 10 to 35, dilation angle of 0° to 10° and Hoek & Brown constant (mi) of 5 to 12. The result of the simulation suggested that tunnel opening follows a specific pattern with the equation as illustrated in Figure 3.9 (a).
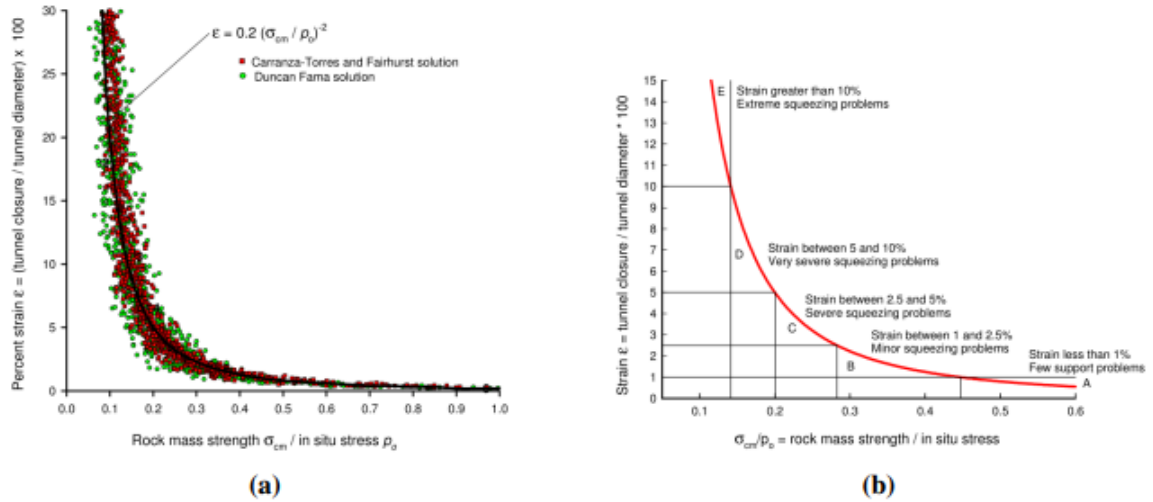
Figure 3.9: (a) Result of Monte Carlo simulation by Hoek and Marinos (2000) showing tunnel strain against competency factor. (b)Classification of degree of squeezing in an unsupported tunnel as suggested by Hoek and Marinos (2000).

(Hoek & Marinos, 2000) have suggested a classification system to quantify the degree of squeezing as illustrated in Figure 3.9. There are five different classes with different squeezing problems ranging from few support problems to extreme squeezing. Rock mass strength is estimated using (Hoek, 2007) and generalized Hoek and Brown failure criteria as described in section 2.3.2 are used. (Hoek, 2007) have considered plastic zone and the effect of internal pressure due to the use of a support system with equations 3.3 and 3.4.

$$\frac{d_p}{d_0} = \left(1.25 - 0.625 * \frac{P_i}{P_0}\right) * \left(\sigma_{cm}/P_0\right)^{\left(\frac{P_i}{P_0} - 0.57\right)} \qquad 3.3$$

$$\frac{d_s}{d_0} = \left(0.002 - 0.0025 * \frac{P_i}{P_0}\right) * \left(\sigma_{cm}/P_0\right)^{\left(\frac{2.4 * P_i}{P_0} - 2\right)} \qquad 3.4$$

where, d_p is tunnel plastic diameter (m), d_o is original tunnel diameter (m), d_p is sidewall deformation of tunnel (m), p_i is internal support pressure (MPa), p_o is in-situ stress in (MPa), σ_{cm} is rock mass strength (MPa) and ε_t is tunnel strain as the ratio of tunnel closure to tunnel diameter.

Panthi and Shrestha (2018) method
As indicated in section 3.2.4, the total deformation consists of both time independent and time dependent deformations. The extent of total deformation in such tunnels is much influenced by in-situ stress and rock

mass deformability properties of the surrounding area. Moreover, due to the anisotropic in-situ stress, the magnitude of deformation differs along the longitudinal alignment as well as the contour of the tunnel (Panthi and Shrestha, 2018).

$$\varepsilon_{inst} = 3065 * [(\frac{\sigma_v * (1+k)/2}{2G(1+P_i)})^{2.13}] \qquad 3.5$$

$$\varepsilon_{final} = 4509 * [(\frac{\sigma_v * (1+k)/2}{2G(1+P_i)})^{2.09}] \qquad 3.6$$

For the long-term stability of the tunnel, support design should be made by considering both time-independent and time-dependent deformation. Time-independent deformation occurs during and immediately after the tunnel excavation whereas time-dependent deformation is related to creep. (Panthi & Shrestha, 2018) studied the long-term squeezing phenomenon of three different hydropower tunnels in the Himalayas of Nepal and found a relationship between time-independent and time-dependent strain using a convergence equation as proposed by (Sulem et al., 1987).

An attempt was made to establish a link between tunnel strain (for both instantaneous and total tunnel strain), vertical gravitational stress (σ_v), horizontal to vertical stress ratio (k), support pressure (p_i) and shear modulus of rock mass (G). A power function was established between tunnel strain (ε) and the ratio of shear modulus (G) and in-situ vertical stress (σ_v) in which the constants of the function could be estimated for any value of support pressure (p_i) which is illustrated in Figure 3.10. The instantaneous closure (ε_{inst}) and final closure (ε_{final}) values are indirectly proportional to the rock mass shear modulus and support pressure values and directly proportional to the in-situ stress conditions which are expressed as equation 3.5 and equation 3.6 respectively.
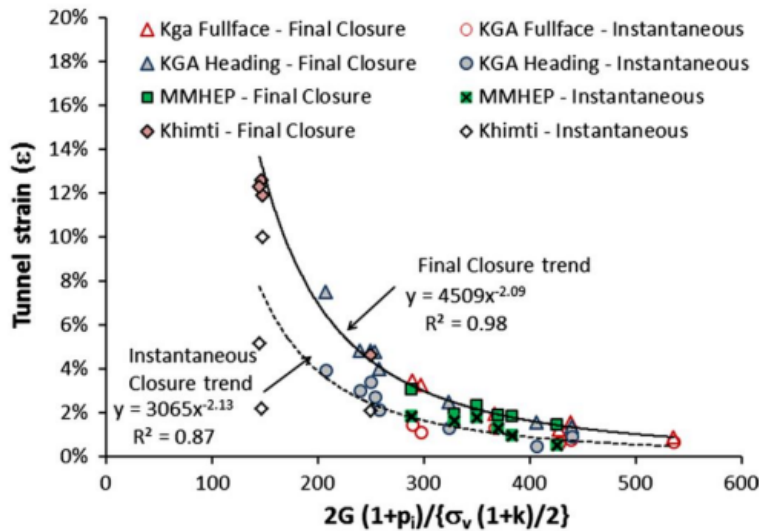
Figure 3.10 : Tunnel strain (ε) against the ratio of shear modulus (G) and in-situ vertical stress (σv)(Panthi and Shrestha, 2018)

where, G = Rock shear modulus, p_i = Tunnel support pressure and k = Stress ratio. Tunnel strain is thus, a function of a rock mass, applied support and in-situ stress. Weaker the rock mass, higher is the deformation extent. Stiffer the supports, lesser is the deformation in the tunnel, and higher the in-situ stress, higher is the tunnel deformation.

3.2.5.3.   **Analytical method**

Tunneling in a rock mass is a four-dimensional problem. Stress distribution around the tunnel occurs in three dimensions and each of them is influenced by time-dependent straining and the type of rock mass unless it gets exposed in the face. Referring (Carranza-Torres & Fairhurst, 2000), Labasse (1949) explained the procedure how standardization of support to minimize disturbance in underground constriction works. He described how need of immediate support behind the face does not require detail accurate calculations. Each cross section in tunnel would have to be studied separately for determining accurate solution in each faces which requires more time and by that time tunnel would have already been collapsed. With reference to these constraints, analytical methods can be considered as a very useful way to simplify the interplay between rock mass and installed support. This method refers variation to assumed rock properties and supports load system.

Convergent-Confinement Method

To understand the issues involved in the process of designing support in case of the tunnel in weak rock mass, it is necessary to examine some very

basic concepts of how a rock mass surrounding a tunnel deforms and how the support systems acts to control this deformation. The Convergent-Confinement method is a procedure that allows the estimation of load imposed on the support installed on the face of a tunnel. This method provides an interaction between the installed support and ground-based on stresses and strains around a circular tunnel. This approach is mainly based on three different curves; Longitudinal Displacement Profile (LDP), the Ground Reaction Curve (GRC) and the Support Confining Curve (SCC) which are combined in order to calculate the equilibrium state between the support and the ground. The schematic representation of GRC, SCC and LDP is shown in Figure 3.11.
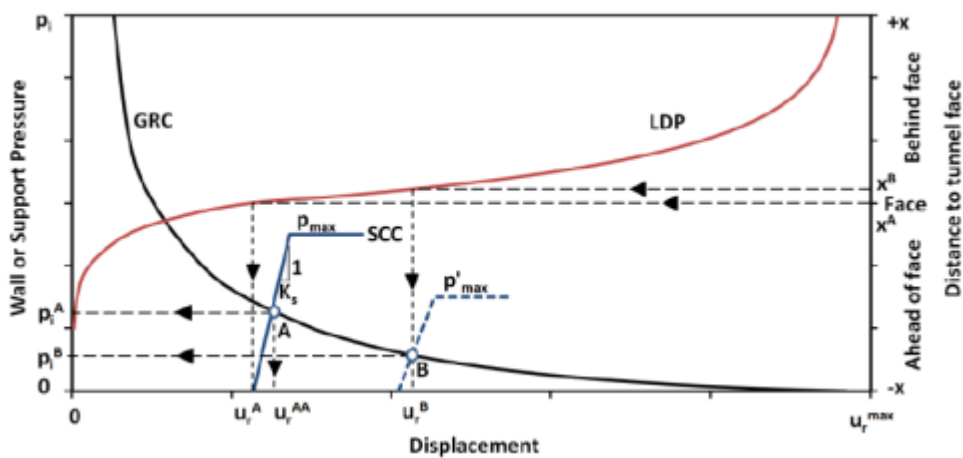
Figure 3.11: Schematic Representation of GRC, SCC and LDP of a circular tunnel (Shrestha, 2014)

CCM allows for estimation of the load imposed on the support installed immediately behind the face. Support installed immediately behind the face of a tunnel will not carry the full load for which it is designed; a part of the load will be carried by the face itself. As the tunnel advances, this 'face-effect' will decrease, and the support progressively carries more load. When the face has moved sufficiently far from the installed support, the full design load of the support is reached.

The Ground Reaction Curve (GRC)
GRC describes the relationship between the decreasing internal pressure (pi) and the increasing radial displacement of the wall. The internal pressure is not a true representation of reality, but rather a surrogate for the effect of the gradual reduction of the radial resistance provided by the initially present tunnel core (Vlachopoulos & Diederichs, 2009).

The Longitudinal Deformation Profile (LDP)

It is a graphical representation of radial displacement occurring along the axis of an unsupported cylindrical excavation, for sections behind and ahead of the face (Carranza-Torres & Fairhurst, 2000)).

Support Characteristic Curve (SCC)

SCC is the relationship between the increasing internal pressure on the support, and the increasing radial displacement of the support. As shown in the schematic representation as per Figure 3.10, K corresponds to support pressure at time of installation. Point R corresponds to the maximum pressure the support can accept before collapsing, p_{max} .

CONCLUDING REMARKS ON PLASTIC DEFORMATION

• Empirical and semi-analytical methods can primarily be used to find the extent of squeezing. Empirical methods are based on experiences from numerous underground projects. The geometrical features of discontinuities and other parameters of the rock mass cannot be represented in the support charts (Shrestha, 2006) A good understanding of the geological conditions of the rock mass is a prerequisite of using the empirical methods.

• The method by (Hoek & Marinos, 2000) includes support pressure, but as emphasized out by the authors themselves; their methodology does not provide a final design for the tunnel excavation sequence and support system. The CCM is the only method, besides numerical modelling, that consider the interaction between rock mass deformation and installed support. However, the methods is constraint by many non-realistic assumptions, making the method limited for design purposes.

• The empirical and analytical methods are developed for circular tunnels. The Q-method does not directly depend upon the dimension of the opening, and makes it applicable to all underground structures. However, the degree of squeezing depends upon the size and shape of the excavation. This non-dependency is therefore an advantage as well as a limitation of the Q-system. In this regard, numerical modelling show as the the most applicable option for analysis of large scale caverns, as few limitations are set for the geometry of the excavation.

3.2.6. Estimation of rock support

The diameter and spacing of the rock bolt are estimated for the rock pressures in the crown and the side walls as per Barton's Q values.

Table 5-1. Empirical formulas to calculate the design pressure

Description	Formula Used	
Design pressure on the roof	$$P_{roof} = \frac{2}{J_r} Q^{-\frac{1}{3}}$$	3.7
Design pressure on the walls	$$P_{roof} = \frac{2}{J_r} Q'^{-\frac{1}{3}}$$	3.8

Where,

$$Q' = n \times Q \qquad\qquad 3.9$$

n = factor depending on rock mass quality

The support pressure for the rock bolt is computed by the relationship:

$$P = \frac{T}{S} \qquad\qquad 3.10$$

Where P is the rock pressure in the crown/wall, T is the working load of the rock bolt, S is the area supported by each rock bolt (Rathore, 2016).

Theres are several empirical rules of thumb to determine the anchor length of rock bolts together with support spacing. Empirical relations found in the literature are presented in Table 3.2 and Table 3.3. Rules of thumb for support design have been developed for blocky and fractured ground. These are based on data from tunnels, caverns, and mine openings and they summarize support practice. It should be noted that such guidelines should be used in conjunction with other design tools (Hutchinson & Diederichs, 1996).

Table 3.2: Empirical formulas, estimating the necessary length of rock bolts as a function of cavern span/height. S = span, H = height, Sp = Spacing of primary bolting.

Bolt length	Reference	Comment
$L = 0.67 \times S^{0,67}$	Lang & Bischoff, 1984	
$L = 0.3 \times S$	Farmer & Shelton, 1980	Span > 15m, alternate with secondary bolting
$L = 0.3 \times Sp$	Farmer & Shelton, 1980	Secondary bolting
$L = 2 + 0.15 \times S$	Hoek, 2000	Suited for weak rock masses (roof)
$L = 2 + 0.15 \times H$	Hoek, 2000	Suited for weak rock masses (walls)
$L = 1.40 + 0.184 \times S$	Myrvang, 2001	Norwegian approach
$L = 2 + \dfrac{0.15B}{ESR}$	Barton et al. (1980), Hoek (2007)	ESR = 1 for powerhouse
$L = \dfrac{S}{4}$	U.S.C.E.	Roof

$L = \dfrac{H}{4}$	U.S.C.E.	Wall

Table 3.3: Empirical formulas for determining spacing between rock bolts.

Spacing	Reference	Comment
$Spacing = \sqrt{T/P}$	Hoek, 2000	T=working load of bolt or cable P=support pressure
$Spacing = 0.5 \times L$	Farmer & Shelton, 1980; U.S.C.E., 1980	Primary bolting
$Spacing = 0.5 \times L$ (secondary)	Farmer & Shelton, 1980	Secondary bolting
$Spacing = 0.5 \times L$	Myrvang, 2001	Applicable to jointed rock mass

3.2.7. Numerical Methods

Analytical methods are best suited for simple geometries in a homogeneous medium. Most underground excavations have a complex shape and are located in an inhomogeneous rock mass. In addition, openings are frequently grouped close to other excavations. The equations for such cases will be too complex to be solved analytically. Over the past few decades, several computer-based numerical methods have been developed to provide means for obtaining approximate solutions to these problems. These methods for analyzing stress-driven problems in rock mechanics can be divided into two classes:

· *Boundary discretization methods*, where only the excavation boundary is divided into elements. The interior of the rock mass is represented as an infinite continuum. This division will normally restrict the methods to cover elastic analysis.

· *Domain discretization methods*, in which the interior of the rock mass is divided into elements with assumed properties. The collective behaviors and interaction of these simplified elements yield a model for the complex and inhomogeneous rock mass. This means that the domain methods allow an analysis of more complex material models than boundary methods. Within the domain of discretization methods, finite element and finite difference methods techniques treat the rock mass as a continuum. The distinct element method models each block of rock as a unique element.

The two classes can be combined in the form of hybrid models to maximize the advantages of each method (Hoek, 2007)

Finite Element Methods

The finite element divides the domain into finite elements. Each element contains material with certain properties. The method is connecting many simple elements to approximate a more complex state over a larger domain. The problem contains differential equations, which can be solved numerically by minimizing an associated error function. The finite element method is suited for solving problems involving heterogeneous or non-linear material properties since each element explicitly models the response of its contained material (Hoek, 2007)

UnWedge

Unwedge is a 3D stability analysis and visualization program for underground excavation in rock mass containing structural discontinuities, i.e., to analyse structurally controlled instability, provided by Rocscience Inc. (Rocscience, 2022a)

RS2

RS2 is a versatile two-dimensional finite element program for designing underground or surface excavations and their support systems, provided by Rocscience Inc. (Rocscience, 2022a). The program consists of three modules: modelling, computing and interpreting. RS2 offers a wide variety of options when it comes to modelling, meshing, material properties and behaviour, support, far-field stress, loads, joints, and data interpretation.

RS3

RS3 is a 3D finite element program used for rock applications i.e., underground excavation, tunnels, and support design, provided by Rocscience Inc. (Rocscience, 2022c)

RocData

RocData is a software program for determining rock mass strength parameters, based on the generalized Hoek-Brown failure criterion (Rocscience, 2022b). From the input parameters: UCS, GSI, intact rock property mi and disturbance factor (D), RocData calculates the HoekBrown parameters Mb, s and a (these parameters are described in section 2.3.2)

4. TAMAKOSHI V HYDROELECTRIC PROJECT

4.1.   Project Description

The 99.8 MW Tamakoshi V Hydroelectric Project is a cascade development of the 456 MW Upper Tamakoshi Hydroelectric Project (UTHP). It is planned to operate through the discharge from the UTHP tailrace. This project is a tandem operation under UTHP by NEA (Nepal Electricity Authority). The project will be constructed on the right bank of the Tamakoshi River in Nepal's Bigu Village council of Gaurishankar Gaupalika, Dolakha district, Bagmati province. Tamakoshi V, with a gross head of 174 meters and a rated discharge of 66 m3/s, is planned and projected to create 507 GWh of annual energy with Four Francis Turbines. The underground interconnection system for the cascade scheme with Upper Tamakoshi HEP is located in Mathillo Jagat, while the underground powerhouse site is proposed at Suri Dovan.
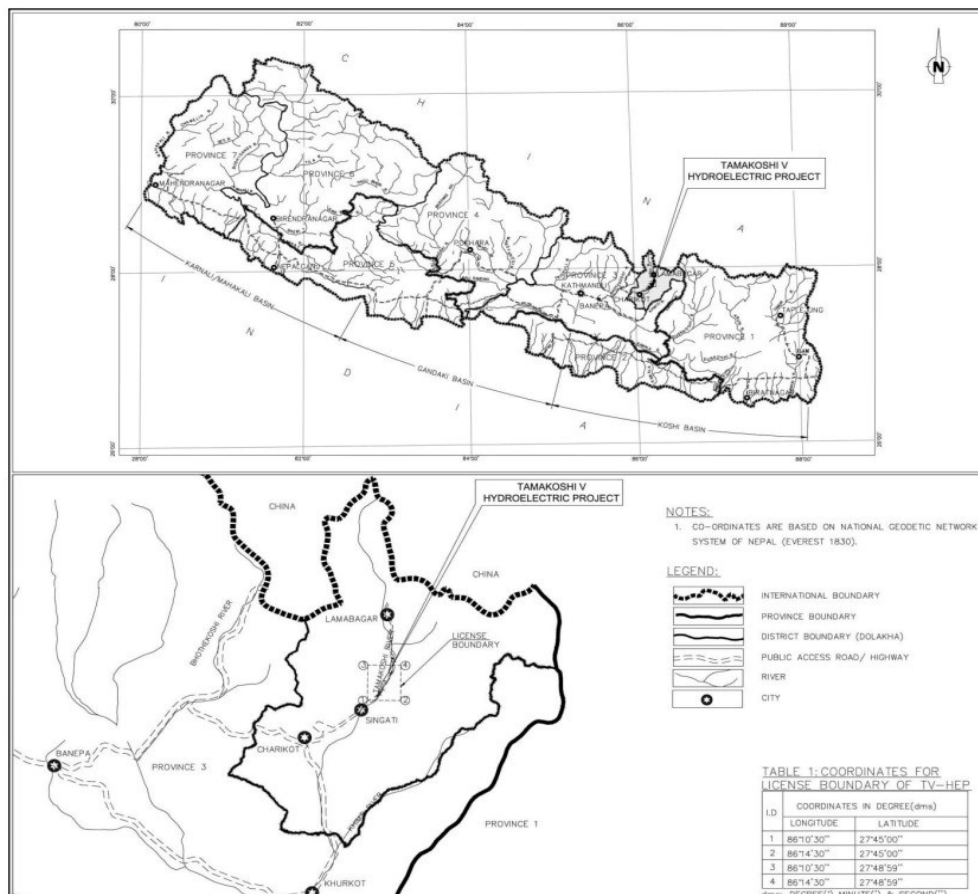
Figure 4.1: Location of the Tamakoshi V Hydroelectric Project

4.1.1.   Project Location

The project area is around 170 km north of Kathmandu, Nepal's capital, and roughly 40 km from the district headquarters of Dolakha District-Charikot Bazaar. The project area is defined by latitude 27º49'50" to 27º45'00" North and longitude 86º10'30" to 86º14'30" East. There is no need to build a

separate access road because the UTHP-built road linking Singate Bazaar and Lamabagur goes right through the project's powerhouse and headwork site. However, just a few km of project road must be built. Tamakoshi Jal Vidhyut Company has begun work on the Tamakoshi V Hydroelectric Project's Permanent Camp Facility, which is anticipated to be finished in May 2022. The project's location map is shown in Figure 4-1. Proposed Tamkoshi V HEP parameters are given in the table, and project layout features are mentioned in Appendix C.

4.1.2. Project Geology

Tamakoshi V HEP is located in both the Higher Himalayan Tectonic Zone and the Lesser Himalayan Tectonic Zone of the Himalayas of eastern Nepal; however, most of the project areas lie in the lesser Himalayan zone. Rock mass of the project can be divided into two categories, i.e., medium to high-grade Higher Himalayan Crystalline sequence and low-grade metamorphic rocks of the Lesser Himalayan rock sequence, separated by Main Central Thrust (MCT). The majority of rock masses in the project area are Augen gneiss, chlorite schist, graphite schist, garnet schist, meta-carbonate, and phyllite of the Lesser Himalaya and banded gneiss of the Higher Himalaya.
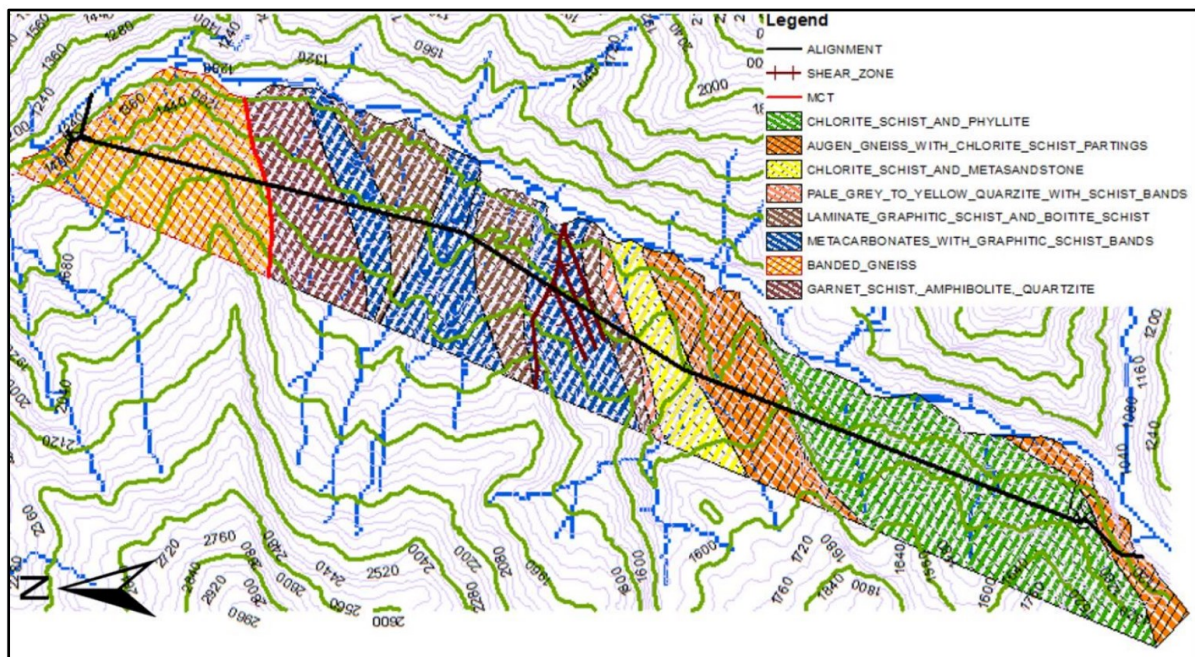
Figure 4.2: Project layout of Tamakoshi V Hydroelectric Project along with the geology, (Chauhan, 2020)

As per (Basnet & Panthi, 2017; Schelling, 1992), rock mass downstream of MCT is a tectonically disturbed, sheared, and mainly distressed zone. Along the alignment of the project, rock mass has been evaluated as fair to extremely poor rock mass. Around 65 % of the rock mass in the project area is of fair to poor rock mass quality (NEA 2019). From the results of

surface mapping, rock masses of fine to coarse-grained, fresh to moderately weathered, having three major joint sets which are close to widely spaced with tight to relatively open joints filled with silts, sand and clay have been expected around the alignment as shown in Figure 4.2.

The rock mass is gently dipping (5-15°) towards North-West or the hillside along the foliation joints at the Powerhouse and Outlet. The dipping angle pattern increases gradually towards the north and reaches an angle of 65° to 70° at the head pond area. The regional strike of the foliation joints of rock mass trend WNW to ESE with a gradual change in anti-clock direction with a strike of WSW to ENE from the head pond towards the tailrace tunnel.

4.1.3.   Assessment of Earthquake History at Project Location

As discussed in 2.5.1.2, the project site is vulnerable to earthquakes due to the continuous movement of the Indian plate toward the Eurasian plate. According to the Indian Standard (IS) for Earthquake Resistant Design of Structures (IS 1893 (2002)), Nepal is classified as zones IV and V, which are high-risk zones (Nobuo et al., 2015). Some major earthquakes in the past in the region were the Nepal-Bihar earthquake in 1934 with a magnitude of 8.1 and the Gorkha earthquake in 2015 with a magnitude of 7.86. The magnitude of these earthquakes is given on the Richter scale. One of the strongest aftershocks had an epi-centre near (about 14 Km) the project area and had a magnitude of 7.3 Richter scale. This highlights the need for an assessment of seismic impacts on underground structures excavated in this region. According to Panthi and Basnet (2019a), the peak ground acceleration (PGA) at the surface of the power plant area is about 0.5 g to 0.6 g or 6m/s2. The average value of PGA is considered for the study, which is 0.55 g or 5.5 m/s2. However, the effect of the earthquake on the rock mass below the surface is relatively small. For the study, a PGA value of 0.55 g is assumed based on (Panthi and Shrestha, 2017; 2018a, 2019a).

Actual data from the 2015 Gorkha earthquake are used for modelling. Strong ground motion data of the main event and aftershock recorded at Kanti Path station and obtained from USGS[1] are considered for the analysis. The time series of acceleration and velocity in the eastward direction and along the height is in Figure 4.3. A PGA of 0.16 g in the east direction and 0.17 g in the Z direction is observed with ground velocities of 107.32 cm/s and 57.98 cm/s, respectively.

---

[1]https://www.strongmotioncenter.org/
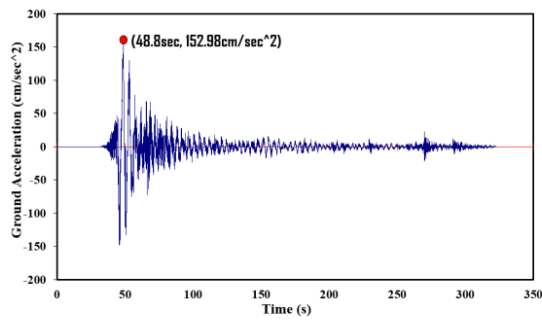
(a) Ground acceleration along east direction recorded at Kanti Path Station, Kathmandu, Nepal (**USGS Database**)
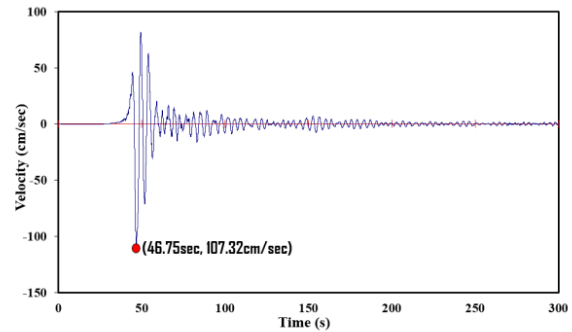
(b) Ground velocity along east direction recorded at Kanti Path Station, Kathmandu, Nepal (**USGS Database**)
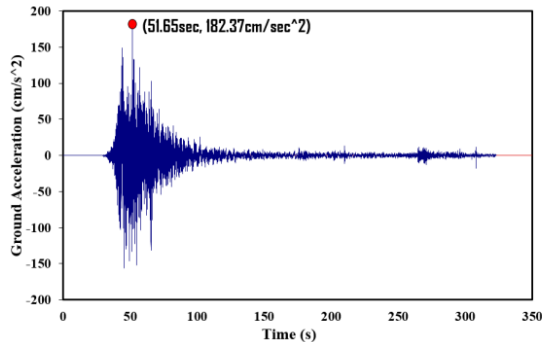
(c) Ground acceleration along elevation (Z) recorded at Kanti Path Station, Kathmandu, Nepal (**USGS Database**)
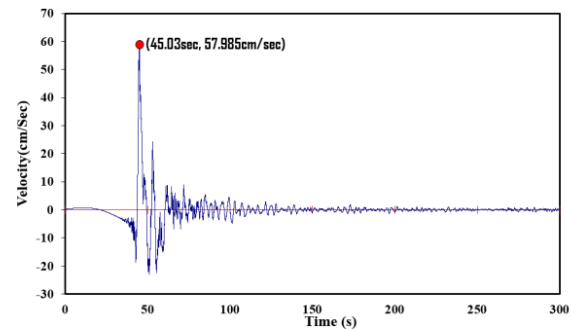
(d) Ground velocity elevation (Z) recorded at Kanti Path Station, Kathmandu, Nepal (**USGS Database**)

Figure 4.3: Strong Ground acceleration and velocity of Gorkha Earthquake 2015

4.1.4.   Ground-Structure Response

Understanding the soil-structure response of subsurface openings during a seismic event is an important task. The complexity of an approach increases when moving from the simple application of reduced PGA in-depth to dynamic analysis using the finite element or finite difference method. Bilotta et al. (2007) presented three methods for analyzing load increases due to an earthquake in a tunnel lining which will be implemented in our case of underground caverns. These methods are briefly discussed below:

4.1.4.1.   Pseudo-Static Analysis

Seismic input is measured as peak amplitude and/or inertial force at the ground surface. These data are recorded at the ground surface and should therefore be reduced with increasing depth. Power et al. (1998) established a relationship between the reduction ratio and depth, as shown in Table 4.1. Using this ratio, the PGA in the horizontal direction for our case is 0.385 g and the PGA in the z-direction is 0.128 g (1/3 of the horizontal coefficient as discussed with the supervisor (04/05/2022), as the underground caverns are at a depth of more than 30 m.

51

When a seismic load is implemented as a PGA, the force is calculated as the inertial force, which is the product of the mass element and the acceleration acting on the mass element. This seismic load is then implemented as a seismic coefficient that simulates only the peak value and does not consider the time series of the seismic motion. The variational independence of this method is a limitation and leads to an exaggeration of the risk of damage in earthquakes.

Table 4.1: Reduction ratio of ground motion Vs depth Power et al. (1998)

Depth(m)	Ratio of ground motion at depth/ground motion at depth at surface
≤6	1
30	0.9
15-30	0.8
>30	0.7

4.1.4.2.   **Simplified Dynamic Analysis**

In this type of analysis, the kinematic soil-structure interaction is ignored. But ground response parameters such as acceleration time series, shear stresses, and strain time series are determined. These values are then applied to the pseudo-statistical analysis.

First, dynamic data analysis is performed to obtain time series of ground velocity, acceleration, and displacement under seismic loading at the cavern site. Then, in the second phase, the peak ground motion value resulting from the dynamic analysis in the first phase is obtained at the cavern location of interest and implemented into the model domain as a seismic load coefficient, similar to the pseudo-statistical method.

4.1.4.3.   **Full Dynamic Analysis**

Full dynamic analysis is a complex model solved using numerical models that take into account the interaction between the soil and the cavern. Finite element or finite difference methods are used in this method.

In contrast to pseudo-static analysis and simplified dynamic analysis, the fully dynamic analysis uses a time series of ground motions at the cavern site as input parameters. In this case, the dynamic data analysis in the first phase is performed similarly to the simplified dynamic analysis. The result of the first dynamic analysis is a time series of ground motions at the cavern site during a seismic event. These results are used as input for the second stage of analysis. This analysis method provides results that take into account the vibrations of the ground in time. The computation time increases significantly because the analysis must be performed for a large

amount of data. The results obtained are more meaningful than the other two approaches already presented.

4.2. Geology of Powerhouse and transformer cavern
4.2.1. Rock masss

The rock mass of the powerhouse and transformer cavern is composed of Augen gneiss with the parting of chlorite schist, which exhibits a gneissic texture. The rock mass also contains quartz, feldspar, muscovite & biotite, and phenocrysts of quartz and feldspar. The borehole logs for 'SW-1' (NEA, 2019) and the rock mass assessment done at the test adit near the public road near the powerhouse show that rock mass underlying is Augen gneiss which is coarse-grained, having close to moderately spaced foliation joints (spacing >6cm to 60cm), slightly to rather weathered and moderate strong to strong. Foliation joint (JS0) & other joints are filled with sandy, silty, and at places with clayey material up to 5 mm in thickness. Four well-developed joint sets, including foliation joint (JS0, JS1, JS2 & JS3), are observed nearby the powerhouse area. The dip angle & dip direction of the said joints are as follows:

JS0 (Foliation joints): 050 -15° /330° - 000°,

JS1: 75° -85° / 010° -030°,

JS2: 65° -75° /065° -085°&

JS3: 70° -85° / 170° -210°.

The rock mass quality assessment of the test adit has been used for our rock mass quality in powerhouse and transformer cavern areas as they lie nearby, and the rock mass is assumed to be similar. The rock mass assessment as per the DPR of the Tamakoshi V HEP is presented in Table 4.2.

Table 4.2: Rock mass assessment (Tractebel,2019)

S.N.	Parameter	Ranges of values	Remarks
1	Uniaxial Compressive Strength (UCS)	6	Strong to medium-strong (25-100 MPa)
2	RQD	3	< 25%, Very poor quality
3	Spacing of discontinuities	7	>6cm to 60 cm
4	Condition of discontinuities	20	Rough surfaces, separation <5mm, Fresh to slightly
5	Ground water condition (dry)	15	Dry
6	Orientation of discontinuities	-5	Fair
RMR = 46			

The Assessment of the Q value for the powerhouse area is given in Table 4.3

Table 4.3: Q Assessment of the Powerhouse Area (Tractebel, 2019)

53

S.N.	Parameter	Ranges of values	Remarks
1	RQD	20	>27 joints per m3, very poor
2	Joint set number (Jn)	12	Three joint sets plus random
3	Joint roughness number (Jr)	15	Rough irregular, planer
4	Joint alteration number (Ja)	3	Silty or Sandy clay coatings, small clay fraction (non-softening)
5	Joint water reduction (Jw)	1	Dry excavation or minor inflow, i.e., 5 lt/min locally.
6	Stress reduction factor (SRF)d	1	Medium stress, favorable stress condition
	Q=0.833		

4.2.2. Engineering Geological Investigations around Powerhouse

The study of the geological condition is significant for constructing the hydroelectric structures, especially when most of the structures of the Tamakoshi V HEP are all underground. As a part of the geological engineering investigation, the desk study, reconnaissance survey, preliminary geological investigation of engineering geology, geological mapping, and geological structures were done by Nepal Electricity Authority (NEA) in 2011. The detailed geographical mapping of the project area and the complex engineering geological study has been carried out by TRACTEBEL ENGINEERING GmbH several times, taking traverses through different locations, and the final detailed design report was submitted in July 2019.

During its planning stages, various detailed investigations applied for the underground excavations have been done for different surfaces and sub-surfaces. Clear and precise geographical mapping was carried out to study the nature and behaviors of structural features of the rock mass, which provides us with information on the possible challenges during the construction phase and proper arrangement of the civil components, design, location for open and underground structures, tunnel alignment and the appropriate construction methodology. Challenges most faced during underground excavation are the overbreak and water ingress, which is very closely associated with geological structures; hence a detailed study about the fold, fault, shear zone, and fracture has been done. Figure 4.4 shows the flow chart of the investigation cycle in the preconstruction phase in the Himalayas (Panthi & Nilsen, 2007).
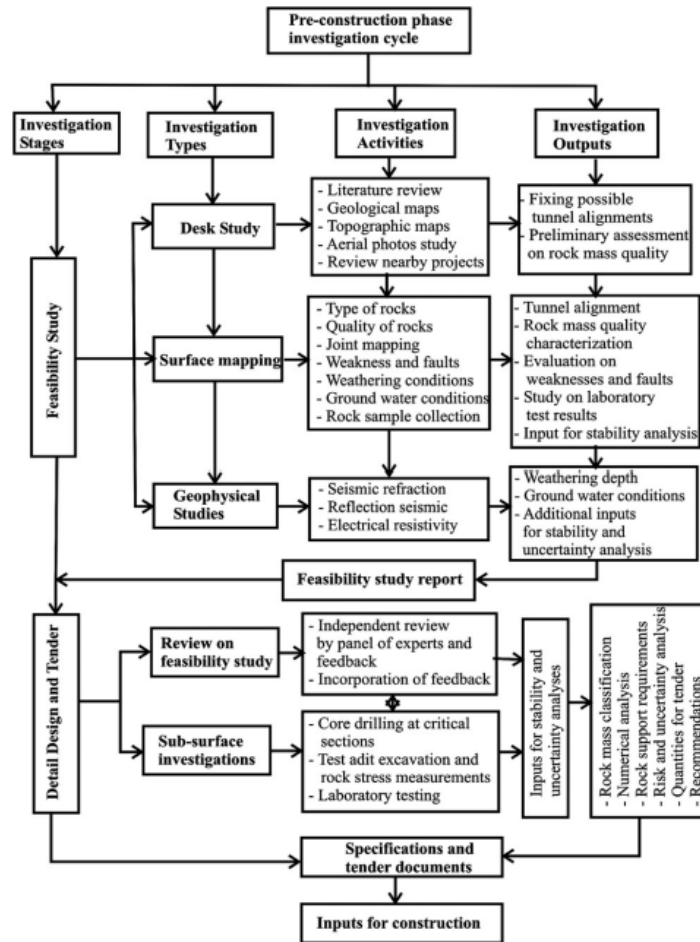
Figure 4.4: Recommended pre-construction phase engineering geological investigation for underground projects in the Himalayas (Panthi and Nilsen, 2006)

The following investigation has been done presently for engineering geological investigations during the Feasibility stage and Detail design stage;

4.2.2.1.   Topography and Geomorphic Features (Desk Study)

The project's initial study was conceptualized from the reports provided by NEA, which gave insights into the project, engineering geology, geological mapping, and geological structures.   During the feasibility study, Core drilling of approx. 100m was done along with the point load and uniaxial compression tests. To verify the results of the core logs, drill core samplers and lab tests were sent for petrographic analysis outsourcing.

A seismic Refraction Survey of length 1875m has been done at the powerhouse area and along the expected MCT zone and Electrical Resistivity Tomography (ERT).

4.2.2.2.   **Reconnaissance Survey:**

A reconnaissance survey along the project areas has been conducted to verify and update the geological/engineering geological map with sufficient field records. Geological reports and the geological map has been updated based on the geological field observations done with geological data (Dip and strike of foliation surfaces & joints) at several rock outcrops and field visits. Geological maps and geological reports determined all civil components, and the appropriate location of adits, underground powerhouse cavern, surge tank, headrace tunnel alignment, spillway, and tailrace tunnel alignment were determined.

4.2.2.3.   **Exploratory Boreholes**

Five exploratory boreholes have been carried out during the Feasibility Stage (FS) at different locations of structures. A total core drill depth of 277m had been done at the TRT outlet structure (TT-1), Tailrace tunnel alignment (SW-1), HRT/Shear zone intersection/Tatopani (HB-1'), Orang Khola intersection (HB-2') and at spillway portal (SP-1) which provided with the information to assess the characteristics of the sub-surface material, establishment of bedrock to find out groundwater level. At present, 487.6m of drilling has been done

Additionally, in-situ tests have been done in boreholes, as mentioned below.
i.   Standard Penetration Test (SPT)
ii.   Dynamic Cone Penetration (DCPT)
iii.   Permeability Test and
iv.   Water Pressure (Lugeon) Test

1. Laboratory Testing of rock samples and construction materials

The rock core sample from the core drilling was selected for laboratory test to undergo the following tests;
i.   Elastic Parameter- modulus of elasticity and Poisson's ratio
ii.   Indirect Tensile Strength (Brazilian Test)
iii.   Triaxial Compression Test
iv.   Point Load Test (PLT)
v.   Uniaxial compressive Test (UCS)

Laboratory testing was also done for the availability, sufficiency, and suitability of the construction material.

4.2.2.4.   **Electrical Resistivity Tomography (ERT)**

2D ERT surveys have been conducted at four project locations- HRT / MCT intersection, HRT / shear zone area intersection, tailrace tunnel alignment,

proposed powerhouse location, and terminal & ventilation building take-off yard post-FS and during FS. The completed linear length of the ERT test was 1000 and 1788m at post-FS and during FS, with a total of 2788m. At present, the total length of ERT done is 3973m.

4.2.2.5.   **Sub-Surface Study**

Test adit portal is located at Suri Dobhan on the right side of the Tamakoshi River, having an inverted 'D' shape and 2.5m x 2.5m size with the gradient of 0-10% at the length of 175.7m. It has been constructed within Powerhouse hill at the level of the Ventilation tunnel; however, a test adit at the powerhouse cavern top elevation is proposed to conduct a few in-situ tests to confirm sub-surface geological conditions for the design of the powerhouse cavern. Hydrofracture, Block Shear, and Plate Load tests were performed for In-situ testing.

4.2.2.6.   **Evaluation of rock mass or surface mapping**

To determine the rock mass characteristics of the underground excavations, two well-established evaluation methods were used:
  i.   Geomechanics Classification/ Rock Mass Rating(RMR)
  ii.   Rock tunnelling Quality Index (Q-system)

4.2.2.7.   **Rock mass classification Criteria**

The rock mass class in the tunnel alignment in Tamakoshi 'V' HEP is determined in a combined way with the criteria based on the Rock Mass Rating (RMR) classification system by Bieniawski (1989) and the Tunnelling Quality Index (Q) by Barton (1974). The rock mass classes are then categorized more or less as per ranges of RMR and Q, as shown in Table 4.4.

Table 4.4: Rock mass classification Criteria for Tamakoshi V HEP

S.N.	Rock Classes	RMR Value	Q-Value
1	I	81-100	>10.0
2	II	61-80	4.0-10.0
3	III	41-60	1.0-4.0
4	IV	21-40	0.5-1.0
5	V	0-20	<0.5

The summary of the geological engineering investigation is given in Table 4.5**.**

Table 4.5: Summary of the Engineering Geological Investigation

Investigation Type	Description	Location
Core drilling and in-situ test	Five exploratory boreholes with 487.6 m in length. SPT, DCPT, and Lugeon Test	Spillway portal area, HRT/Tatopani Shear zone interaction (HB1'), HRT/Orang Khola intersection (HB2'), Powerhouse area, TRT, and Tailrace structure.
Seismic Refraction Tomography	Total length -1875 m	Along the Tamakoshi river at Jamune, Suritar and Tatopani shear zone.
Electrical Resistivity Tomography	Total length- 2788 m	Along with the HRT and TRT alignment, outlet area, and Test Tunnel portal area.
Test Adit and In-situ Test	Length- 175.7 m, size - 2.5 mX2.5 m, gradient 0-10%, Shear test, plate load test, and hydrofracture test	Along the Powerhouse area. Incomplete hydrofracture test due to poor rock mass condition
Surface mapping	Q and RMR	Exposed rock mass along Tamakoshi River.

4.3. Evaluation of Design Aspects

4.3.1. Location

The Powerhouse cavern proposed for Tamakoshi V HEP is 69 m (L) x 18 m (W) x 33.14 m (H) and has a conventional straight wall. It is almost perpendicular to the direction of the river valley and is a large cavern by design. The overburden varies in length from 150 to 194 meters along its orientation. The ceiling of the cavern is almost at the same level as the floor of the river valley, indicating that the tectonic stresses may be greater than those of the Tamakoshi V hydropower project along the headrace tunnel. The location of the powerhouse with respect to depth will not be changed because it may affect the net head of the project, which is not the actual objective here (discussed with supervisor 04/03/2022). However, the powerhouse cavern alignment will be evaluated in detail in the next section.

4.3.2. Orientation

The powerhouse cavern is aligned at N135°E. As shown in Figure 4.5, the cavern is advantageously oriented with respect to the foliation joint (Jf) and joint set 1 (J1). However, another dominant set of joints 2 runs almost parallel to the cavern axis, which is undesirable for large openings. Moreover, it slopes steeply and forms an angle of 15° to 25° with the high wall. Similarly, the redistribution of stresses after excavation leads to a reduction in confining stress in the walls, mainly due to the horizontal tectonic stress (Figure 4.5), which is almost perpendicular to the longitudinal axis. This ultimately leads to a reduction in wall stability. On the other hand, the redistribution of tectonic stresses during the use of the roof leads to a better limitation of the stability of the roof. Therefore, considering the tectonic stress direction and J2, an alternative alignment Alt. 1, at N15°E was proposed, aligned along the bisector of the maximum intersection angle between Jf and J2, forming an angle of 20° with the tectonic stress, as shown in Figure 4.5. This adjustment provides better confinement in both the high walls and the ceiling, limits stress-related problems to a small cavern area, and is more favourable for avoiding structurally induced instabilities.
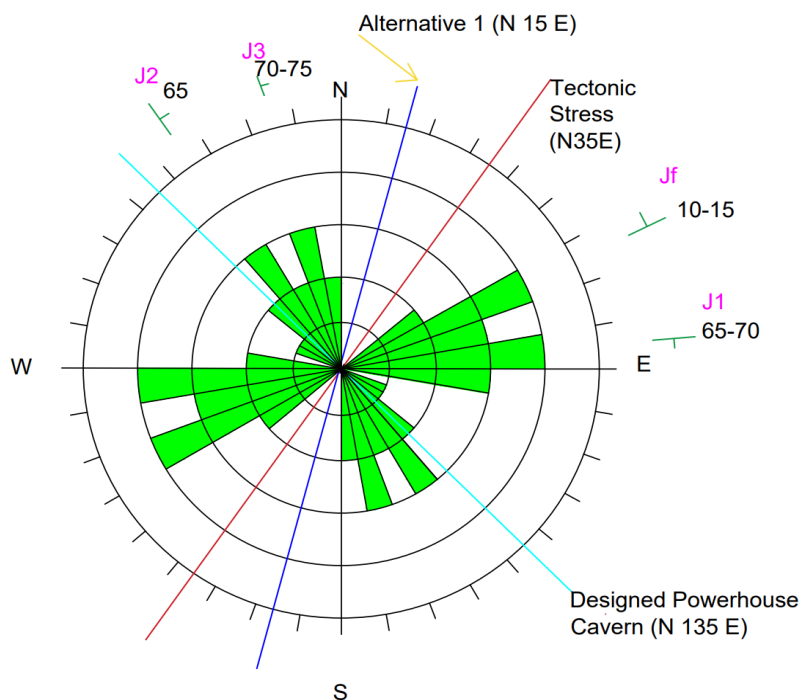
Figure 4.5: Rosette Diagram for the Original Orientation of the powerhouse and the alternative orientation with the tectonic direction.

4.3.3.   Shape of Cavern

For an underground opening of a hydropower project, inverted D or circular shaped caverns with deep wall excavated with drill and blast method is commonly used. The powerhouse and the transformer cavern of Tamakoshi V HEP are arched roofs with a smooth transition so as to reduce the development cracks on the corners which may appear between the transitional wall and arched roof if a protruding corner is made whichcontributes to the stability of the openings. The figure 4.5 show the shape of the caverns.
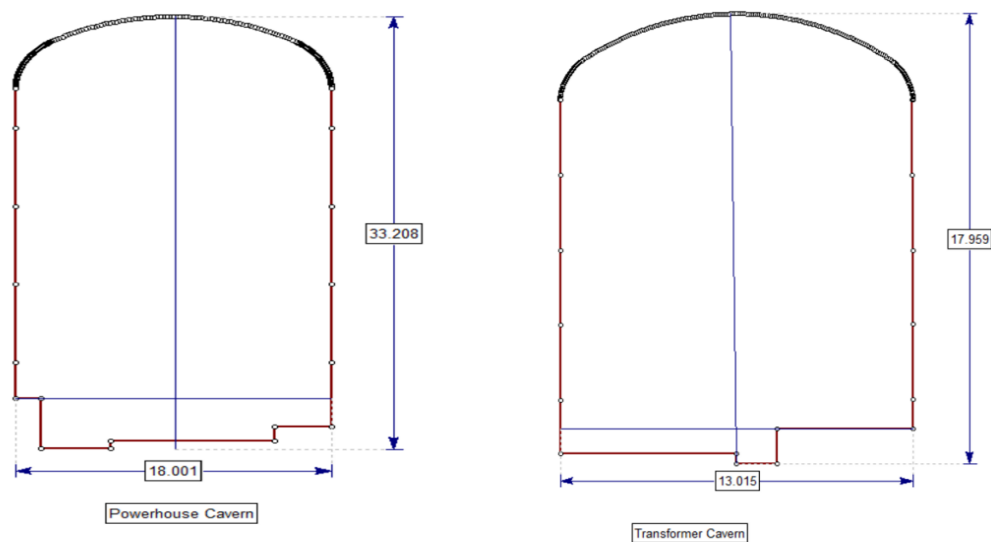
Figure 4.6: Shape of powerhouse and transformer cavern

4.3.4.   Pillar Width between Caverns

Based on the design criteria in Pillar width between caverns3.1.5, the pillar width between the powerhouse cavern and the transformer cavern is taken as 30 m (as per the drawing), almost equal to the height of the powerhouse cavern. However, for this thesis, the drawing has been modified and studied according to the dimension in the detailed project report with a height of 33.14m. According to (Hoek & Moy, 1993), it meets the minimum criteria for weak rock mass and is generally acceptable in terms of busbar length.. However, it is always preferable to perform numerical modelling to study the interaction between the stresses in the vicinity of the two caverns and to analyze the overstressed zone, especially the potential tensile failure zone, in the column, which may lead to excessive strain of the rock and consequent instability.

5. ESTIMATION OF INPUT PARAMETERS

To study the stability of the underground powerhouse caverns and openings, we must first have a thorough knowledge and in-depth insight into the rock, rock mass properties and conditions, degree of weathering, the cause and effect of the rock stresses, and the response of the rock mass strength. These parameters have an interdependence on the stability of the underground openings (Hoek, 2007). This Chapter will focus on the rock mass quality and geological strength index, in-situ rock test, and estimation of input parameters such as rock mechanical properties and in-situ stresses that are crucial for the stability analysis through empirical, analytical, and numerical modelling methods.

5.1. Rock mass quality and GSI

According to the geological mapping report by Tractebel (2019), the rock mass quality assessment has been done using RMR and Q-system. Table 4.2 and Table 4.3 show the field observation's RMR and Q value estimate, respectively. General rock mass properties around the powerhouse area are given in Section 4.2.1. From the estimated RMR and Q values from face mapping, the Geological strength index (GSI) was estimated. GSI can be calculated using an empirical approach by (Z. T. Bieniawski, 1989) and (Barton, 2002) using the equations 2.6, 2.7 and 2.8.

Table 5.1: RMR and Q from field observation and GSI calculated from equation 5.3 using the empirical approach by Bieniawaski (1989) and Barton (1995)

	Field observation		Bieniawaski (1989)	Barton(1995)	GSI		
Rock Type	Q value	RMR	RMR	RMR	From field obs	Bieniawaski (1989)	Barton (1995)
Augen Gneiss	0.833	46	42	49	41	37	44

Rock mass properties of Augen gneiss at Tamakoshi V HEP are compared with the data of the rock mass and the laboratory testing of UTHP to find the relativeness and estimate the parameters concerning scientific papers, doctoral thesis (Panthi, 2006; S. Shrestha, 2014), books, lecture notes, internet, and nearby projects. To analyze the stability of the powerhouse and transformer cavern, RMR and corresponding GSI from the field-based observation have been adopted as discussed with the supervisor (03/01/22).

The table of the relationship between Q-value and RMR (Panthi, 2006) is given in Appendix B.

5.2. In-situ rock test

For obtaining the data related to the rock mechanics, in-situ rock tests are carried out by NEA (2011) and Tractebel (2019) to get the moduli of deformation and the young's modulus of elasticity with a plate loading test.

The UCS test has been done on two test samples, and PLT tests have been done on four test samples around the adit 4. No actual deformation of the rock mass has been registered as the project's construction hasn't been done, and no extensometer has been set for the exploratory adits. Table 5.2 shows the mechanical properties of the intact rock samples obtained from laboratory testing.

Table 5.2: Mechanical Properties of the intact rock from the laboratory test (Tractebel, 2019)

Rock type		σ_{ci} (MPa)	$\sigma_{ci,r}$* (MPa)	E_i (GPa)	γ (kN/m3)	v	ϕ_i
Augen Gneiss	Average	43	43	34.24	2.7	0.25	43
	Range	40-47	40-47	20.06-48.42	-	-	-
	Std. deviation	4.95	4.95	20.05	-	-	-

5.3. Establishment of Input Parameters

Based on the rock mass quality (Section 5.1) and the in-situ rock test (Section 5.2), the input parameters have been established for the powerhouse and transformer cavern. Hoek and Brown constant, mi is determined as per Appendix A.1. The drill and Blast (D&B) method is most dominating in Nepal. Blasting is generally uncontrolled, which results in poor contour blasting. However, the average disturbance factor (D) of 0.5 has been selected for all the analyses carried out in this thesis. The disturbed zone of 4m is set around the powerhouse and transformer cavern for analysis. RocData has been used to calculate the Hoek and Brown Failure Criteria parameter given in Table 5.3**.**

Table 5.3: Intact rock parameters and Hoek Brown Failure Criteria parameter using RocData (Rocscience, 2022)

	Minimum	Maximum	Average
Intact Uniaxial compressive strength UCS, σ_{ci} [MPa]	39.79	46.71	43.25
GSI	41		
Poisson's Ratio	0.25		
Unit wt (t/m3)	27		
Disturbance Factor, D	0.5		
S Peak value	0.00038331		
a Peak value	0.510621603		
Mi	26		
Mb	1.535009267		
RMR	46		
Q	0.833		

5.3.1. Rock mass strength

Rock mass strength has been calculated using the empirical relationship given in Table 2.2. Material constants for the Hoek method to estimate rock mass strength have been extracted from the standard chart in Appendix A.1. Estimated rock mass strength with these methods has been presented in Table 5.4.

As seen in Table 5.4, (Barton, 2002) gives the highest value of rock mass strength while Panthi (2006) shows the minimum value of the rock mass strength. Hoek et al. (2002) and Kalamaras et al. (1995) methods have similar values for the rock mass strength. Panthi's (2006) method is much relevant to the Himalayan young geology rocks, which is valid for this case study. In addition, Panthi's (2006) method considers the intact strength of rock, eliminating the loop dependency problems that occur in Barton's (2002) approach.

Table 5.4: Rock mass strength using Empirical Relations

Rock mass strength, σ_{cm} [MPa]															
Hoek et al. (2002)			Panthi (2006)			Barton(2002)			Kalamaras et al. (1995)						
min	max	Avg	min	max	Avg	min	max	Avg	min	max	Avg	Min	Max	Avg	Std. deviation
6.38	7.49	6.94	4.18	5.32	4.74	9.69	11.38	10.53	7.26	8.52	7.89	4.18	11.38	7.52	2.40
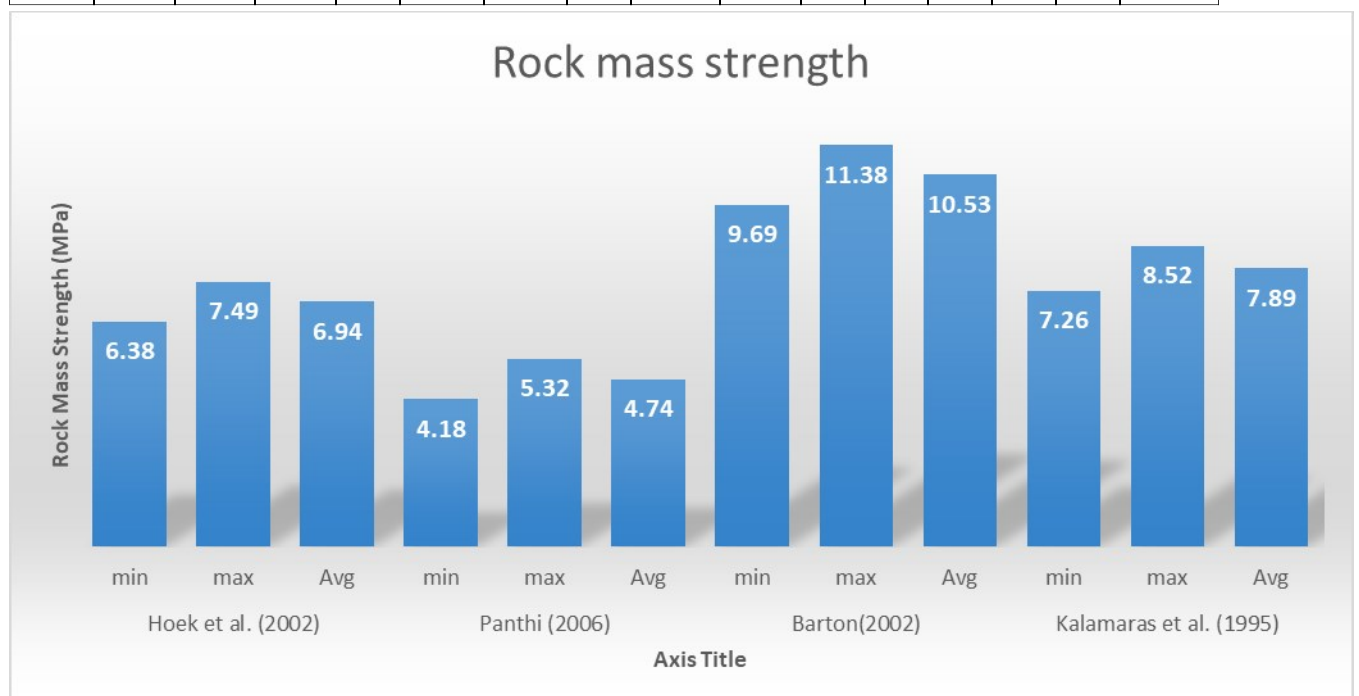
Figure 5.1: Rock mass Strength using different Empirical Relations

5.3.2. Rock mass deformability

Rock mass deformability is estimated by using the relations in Table 2.3. Table 5.5 and Figure 5.2 show that rock mass deformability by (Panthi, 2006) methods gives the average value while (Barton, 2002) method provides the

least. (Hoek et al., 2002) and (Hoek & Diederichs, 2006) method share similar values. The rock mass deformability given by (Panthi, 2006) seems to be the reasonable value of deformation modulus as the equation is based on the weak and young Himalayan rocks.

Table 5.5: Rock mass Deformability using Empirical Relations

Rock mass deformability, E_{rm} [MPa]													
Hoek and Diederichs(2006)			Panthi (2006)			Barton(2002)			Hoek et al. (2002)					
min	max	Avg	min	max	Avg	min	max	Avg	Min	Max	Avg	min	max	avg	Std. deviation
1.64	3.96	2.80	2.11	5.52	3.75	6.92	7.30	7.12	2.82	3.05	2.94	1.64	7.30	4.15	2.02
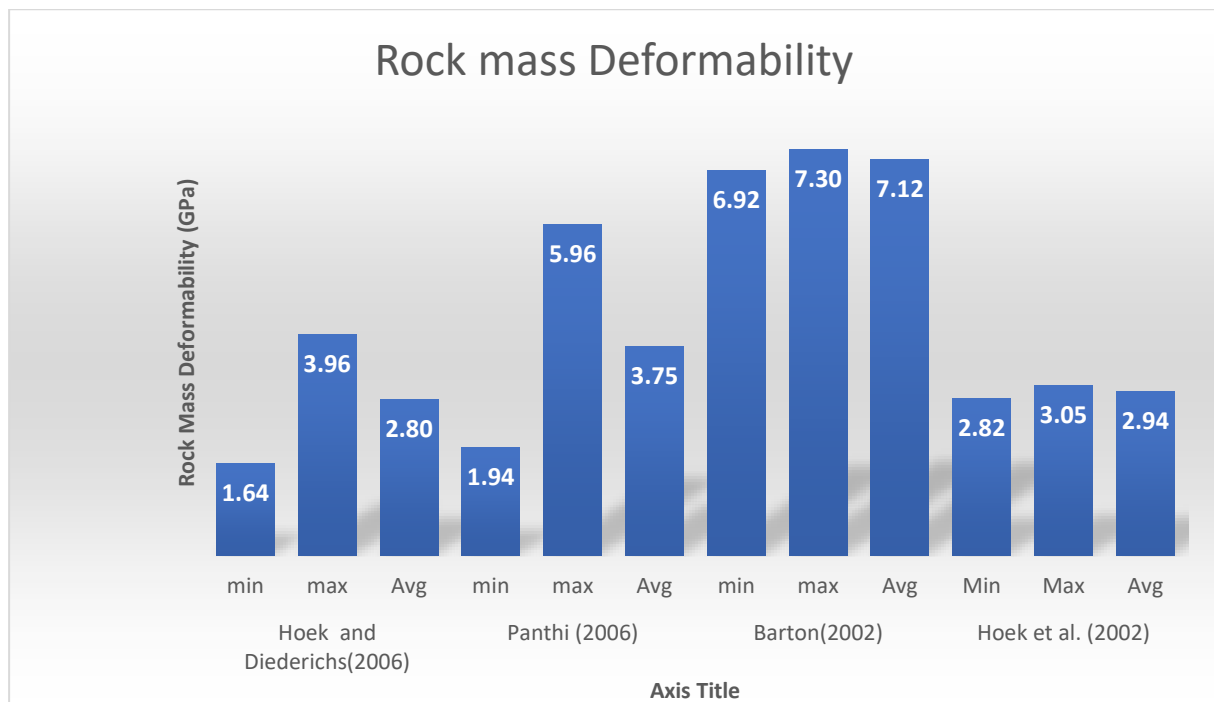
Figure 5.2: Rock mass Deformability using Empirical Relations

5.3.3.   In-situ Stress and Tectonic Stress Estimation

When the excavation is done, the virgin stress or anisotropic condition of the of the ground is disturbed. The horizontal stress acting on the underground structure is affected by two significant factors: tectonic stress and gravity with Poisson's effect on the rock mass. According to (Nilsen & Palmström, 2000), the horizontal tectonic movement of the earth's crust contributes to the total horizontal stress as given in (section 2.5.1.2).

The stability analysis of the powerhouse and transformer cavern is done in a cross-sectional profile. The tectonic stress is not aligned normally and parallels to the powerhouse alignment; therefore, necessary resolving in equivalent in-plane and out-of-plane stresses has been done. Resolved in-plane and out-plane stresses are given as equations 2.30 and 2.31 and illustrated in Table 5.6. The estimated values of in-situ stresses are tabulated in Table 5.6**.**

According to Panthi and Basnet (2019b), the stress orientation of the Himalayas is along with the NE-SW trend. The tectonic stress in the rock

64

mass for the UTPH is between 5-7 MPa according to the stress measurement done by (Basnet & Panthi, 2017, 2018, 2019) the orientations are between N30°E to N45°E from a 2D and 3D model for the TT3 of the UTHP. According to Nepal (1999), the tectonic magnitude in Nepal Himalaya lies between 3-4 MPa for schistose and sheared rock mass. The nearby project Khimti I HP lies in between MCT and MBT in Nepal as Tamakoshi V HEP which has tectonic stress of 3MP according to (S. Shrestha, 2014), so the value of 3 MPa with the orientation of N35°E is considered for the analysis (Discussed with supervisor, 03/02/2022).

In this study, the stress acting on both the powerhouse and transformer has been kept the same as the stress on the powerhouse cavern; analyzing the transformer cavern critical, which ensures the stability of the transformer cavern if the powerhouse cavern is stable.

Table 5.6: In-situ and tectonic stresses acting on the Powerhouse and Transformer cavern

	Powerhouse	Transformer Cavern
Overburden [m]	186.84	176.08
Poisson's ratio	0.25	0.25
Tectonic Stress Orientation (degree)	N35°E	N35°E
Horizontal Stress σh[MPa]	1.68	1.58
Vertical Stress [MPa]	5.0	4.8
Tectonic Out of plane [MPa]	0.52	0.52
Tectonic In-plane [MPa]	2.95	2.95
Horizontal stress (Out-of plane) [MPa]	2.20	2.11
Horizontal stress (In-plane) [MPa]	4.6	4.5
Total Stress ration (Out-of plane)	0.44	0.44
Total Stress ration (In-plane)	0.92	0.95
Locked in stress ratio(Out-of plane)	0.10	0.11
Locked in stress ratio(In plane)	0.59	0.62

6. ANALYSIS OF UNDERGROUND POWERHOUSE
6.1. Stress Distribution and rock burst analysis

To estimate the stress distribution and predict the rock burst around a cross-section of the caverns, the directions of the principal stresses must be evaluated. For the powerhouse and transformer cavern placement and orientation, the length of the axis of the caverns is oriented towards the elongation of the valley. This means that maximum tangential stress will likely appear in the part of the cavern roof facing the valley side. Figure 7-17 shows results from stress modelling; the topographical effect on the stress situation is clearly near the cavern location (Section 7.2.1.3).

Tangential stresses can be estimated from Kirsch's equation 2.34 and 2.35. Due to the cavern shape, Kirsch's equation is only applied to the arched roof. Potential tension in cavern walls is difficult to calculate analytically.

Table 6.1: Maximum tangential stress on the cavern contour based on Kirch's equations

Description	σ_1 [MPa]	σ_3[MPa]	$\sigma_{\theta max}$[MPa]
Powerhouse	5	4.64	10.50
Transformer Cavern	4.8	4.5	9.72

Table 6.1 presents the maximum values of the tangential stresses for both the powerhouse and the transformer cavern. Calculation and assessment of σ_1 and σ_3 have been documented in section 5. These tangential stress values are most applicable when the caverns are excavated to a level where the height and width are approximately the same. Especially for the powerhouse cavern, the tangential stress will increase a bit after benching down to full size.

Table 6.2: Tangential stress in roof and walls calculated from empirical method from H&B 1980

Description	A	B	k	σ_z [MPa]	$\sigma_{\theta r}$ [MPa]	$\sigma_{\theta w}$ [MPa]
Powerhouse	4	1.5	0.92	5.0	13.50	2.93
Transformer Cavern	4	1.5	0.95	4.8	13.40	2.59

Table 6.2 walls ($\sigma_{\theta w}$) of the caverns as per 2.32 and 2.33 along with Figure 5-2. Principle stresses are assumed to be oriented along the horizontal and vertical axes using an empirical method developed by Hoek and Brown (1980) and Grimstad and Barton (1993).

Table 6.3: Results of rock burst assessment using Hoek and Brown (1980)

Description	For Roof		For Wall	
	$\sigma_c/\sigma_{\Theta r}$	Prediction	$\sigma_c/\sigma_{\Theta w}$	Prediction
Powerhouse	3.19	minor sidewall spalling	14.67	stable
Transformer Cavern	3.21	minor sidewall spalling	16.59	stable

Table 6.4: Results of rock burst assessment using Grimstad and Barton (1993)

Description	For Roof		For Wall	
	$\sigma_c/\sigma_{\Theta r}$	Prediction	$\sigma_c/\sigma_{\Theta w}$	Prediction
Powerhouse	3.19	medium stress, favorable stress conditions	14.67	medium stress, favorable stress conditions
Transformer Cavern	3.21	medium stress, favorable stress conditions	16.59	medium stress, favorable stress conditions

The rock burst assessment is shown in Table 6.3 and Table 6.4There is a minor sidewall spalling condition on the roof of the powerhouse and transformer cavern while the walls are stable with medium and favourable stress conditions as per the assessment of the (Hoek & Brown, 1980)and (Grimstad & Barton, 1993b) respectively.

6.2. Analysis of Plastic Deformation
6.2.1. Stress Distribution around the cavern
The powerhouse and the transformer cavern of Tamakoshi V HEP lie at the rock mass with a Q-Value of 0.833 which is a weak rock with possible plastic deformation. The stress distribution is seen as soon as the support is installed to the opening. Table 6.5. shows the input parameters used to plot stress distribution around the cavern. The overburden stress is 5 MPa.

6.2.2. Prediction of Plastic deformation
6.2.2.1. Empirical Methods
In order to predict the plastic deformation problems at the powerhouse and transformer cavern, three empirical methods such as (Singh et al., 1992), Q-System (Grimstad, 1993) and (Goel et al., 1995)) have been used. Three approaches mentioned in section 3.2.5.1 has been used to know the

squeezing condition of the ground. As per (Wood, 1972), when Competence Factor 'Fc' is less than 2, the ground will be overstressed immediately and can result into potential squeezing problem. The Fc is ratio of unconfined compressive strength of rock mass (σ_{cm}) to overburden stress. For our case the value returned is 0.93 < 2, which means that there will be squeezing in the cavern. Table 6.5 shows the result of the analysis for the squeezing by the rock mass classification approach.

Table 6.5: Squeezing Prediction According to Singh et al. (1992), Q-system (Grimstad and Barton, 1993) and Goel et al. (1995)

Rock Type	Overburden Depth (m)	σ_1 (Mpa)	σ_3 (Mpa)	Singh et al. (1992)		Q-System (Barton and Grimstad, 1993)				Goel et al.(1995)	
				Limiting value of H(m)	Squeezing Condition	$\sigma_{\theta max}$	σ_{cm}	$\sigma_{\theta max}/\sigma_{cm}$	Squeezing Condition	Limiting value	Squeezing Condition
Augen Gneiss	186.239	5.0	4.6	329.32	NO	10.45	4.74	2.20	minor squeezing	193.92	mild squeezing
Augen Gneiss	176.345	4.8	4.5	329.32	NO	9.74	4.74	2.20	minor squeezing	193.92	mild squeezing

The results for squeezing or plastic deformation from Table 6.5 show the mixed results. (Singh et al., 1992) shows that no deformation is expected in the powerhouse and transformer cavern at depths of 186.84 m and 176.345 m, respectively. However, according to the Q system (Grimstad, 1993) and (Goel et al., 1995), minor to mild squeezing will occur in both caverns.

Since Singh's method depends entirely on the Q value of the rock, which gives a rough result, the Goel method was used for analysis, as shown in Table 6.5. The Goel method predicts that some areas may deform. Squeezing with this method results in mild plastic deformation in weak rock masses such as Augen gneiss.

Discussion of the suitability of Empirical methods

The empirical method proposed by Singh requires a Q value of the rock mass to predict squeezing. However, to determine the Q value, the estimated SRF value must first be determined. To determine the SRF value, it must be known if there is squeezing or not. Therefore, the criteria proposed by Singh lead to a dependency loop. However, there is a way to solve this problem by estimating the Q value by assigning the SRF value without considering squeezing condition. For example, in the cavern considered here, the SRF value was assumed to be 1, considering the case of a single zone of weakness or a chemically decomposed rock with a depth of > 50 m (Barton Chart). Then, the equations in section 2.4.3. was checked with the Powerhouse and Transformer caverns. No deformation problem

was found when checked with Singh's equation, and this method does not prescribe any type of support requirements, which is a drawback of the method. Goel's approach is the most conservative and predicts moderate to high deformations for the entire cavern. In reality, many unexpected problems occur during cavern construction, and the design must be revised several times. With this in mind, the prediction of (Goel et al., 1995) can be considered the most appropriate to predict the actual conditions.

Semi-Empirical Methods

The analysis of the plastic deformation was done through semi-empirical methods viz. (Hoek & Marinos, 2000) and (Panthi & Shrestha, 2018). This section of the analysis also incorporated (Hoek & Marinos, 2000)) semi-analytical technique without support pressure. Only the results utilizing (Panthi, 2006) relation to estimated rock mass strength will be addressed. This is supported by prior research using σ_{cm} calculated by (Hoek et al., 2002) which revealed that the strength of the rock mass was considerably underestimated (Vestad, 2014). Table 6.6 summarizes the squeezing predictions which shows that there is no squeezing but might have some support problems. Detailed computations are at Appendix B.1.

Table 6.6: Semi-empirical methods

Component	Rock Type	Overburden Depth (m)	σ_1 (Mpa)	Hoek and Marinos (2000)		Panthi and Shrestha (2018)					
				Strain % without support	Squeezing Condition	G	K	ε_{IC}	ε_{FC}	Strain %	Squeezing Condition
Powerhouse Cavern	Augen Gneiss	186.239	5.0	0.18	few support problem	1501.19	0.92	0.00	0.01	0.90	few support problems
Transformer cavern	Augen Gneiss	176.345	4.8	0.20	few support problem	1501.19	0.95	0.00	0.01	0.91	few support problems

Analytical Methods

The analysis of the squeezing was further perfomed with the CCM suggested by (Carranza-Torres & Fairhurst, 2000). The method has been adopted in the study to see the convergence of the support and the deformation that occurs at the cavern during the excavation.

CCM: Longitudinal displacement profiles

The Longitudinal Displacement Profile (LDP) determines the ground behavior as a function of distance to the advancing face. The LDPs were constructed using the method proposed by (Carranza-Torres & Fairhurst, 2000), and the updated version by (Vlachopoulos & Diederichs, 2009) (section 3.2.5.3). Additionally, the method was applied considering mean stress. Analysis of deformation was performed taking the equivalent radius of the cavern despite the method being derived from the circular tunnel. The assumed input parameters for the analysis are shown for the detailed

calculations in Appendix B. Figure 6.1 and Figure 6.2 gives the longitudinal displacement profile and the comprehensive plot of LDP, GRC and SCC profiles.
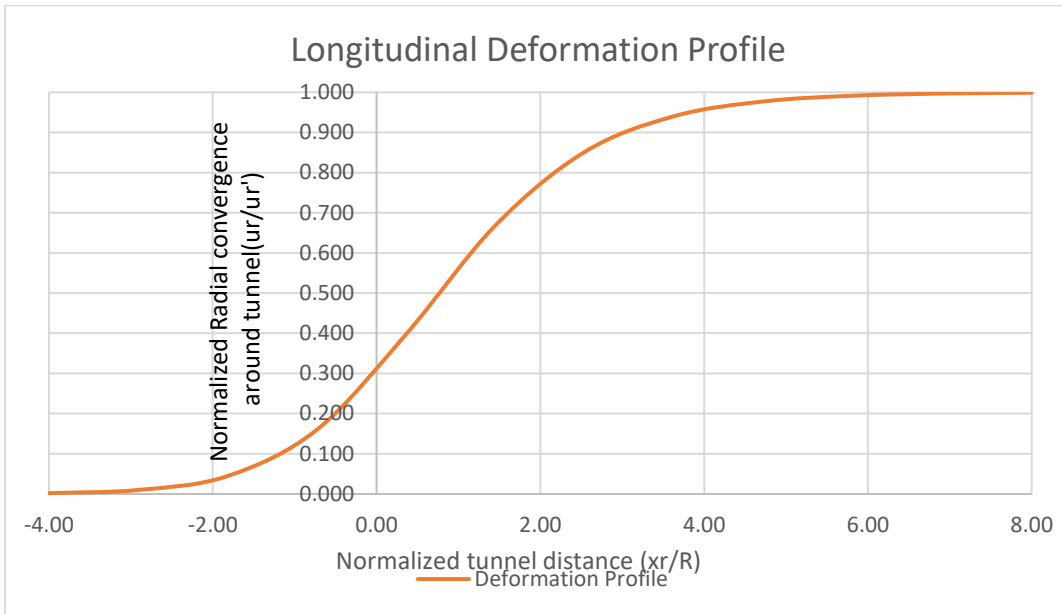
Figure 6.1: Longitudinal displacement profile
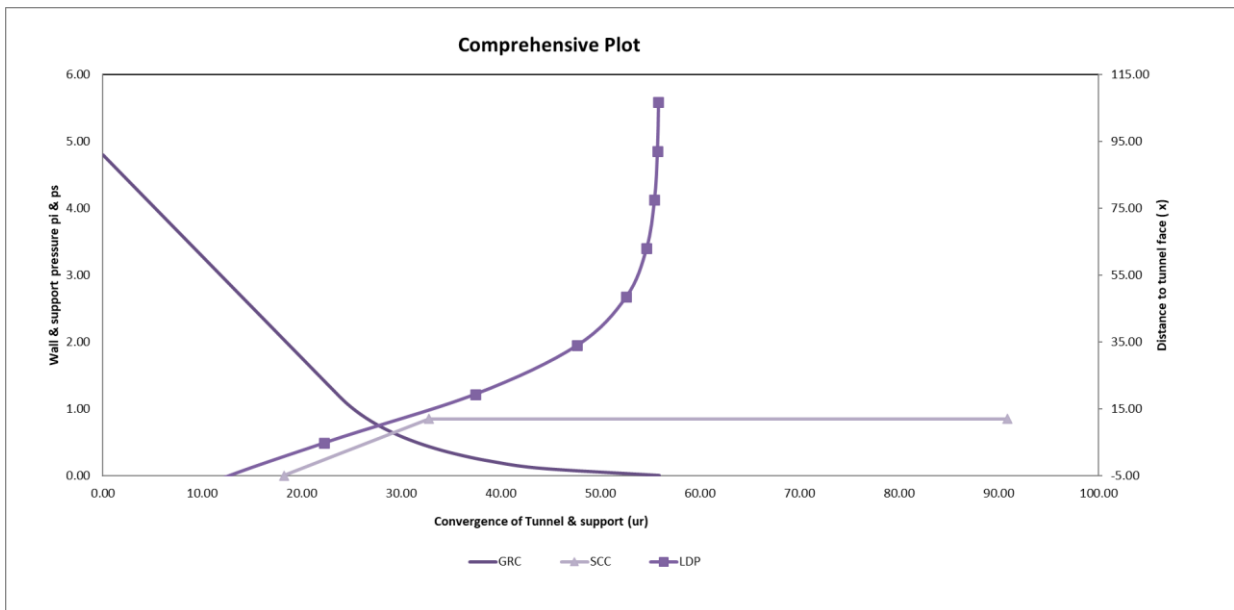
Figure 6.2: LDP, GRC and SCC profiles

7. NUMERICAL MODELLING

Throughout geological studies, various methods have been used to interpret and analyze the scenarios of subsurface structures and their interaction with the rock mass that encloses them. These problem-solving methods may be physical, analytical-mathematical, and numerical. It is not always possible to construct a physical model, which can be costly and time-consuming, limiting its use. Analytical or mathematical approaches are governed by the variability of rock parameters, which may not be sufficient to capture the actual behaviour of the subsurface excavation and the influences of such disturbance in the ground. Since physical and analytical methods are limited by their constraints in describing post-excavation soil behaviour and the effects of the various acting factors and parameters on the three-dimensional interaction of the material of interest, numerical modelling appears practical. Numerical models can perform complicated calculations through iteration and convergence criteria. Developing powerful computer hardware and software compatible with complex calculations and a wide range of applications is of great help. With this analysis method, we can input all the parameters and criteria settings suitable for excavation and check the instability and deformations that may occur. However, the actual representation and the reliable results always depend on the parameters, and the model construction follows the concept of "garbage in, garbage out" despite numerical modelling (Udpa et al., 1989). This method follows the discretization of the rock using three approaches - finite elements or differences, separated elements, or hybrid elements (Jing and Hudson 2002).

A continuum numerical modelling approach is used to develop and evaluate this study's sections. The finite element method (FEM) is used for modelling. Because of its versatility in specifying model parameters, the discipline of static modelling Rocscience packages of Rocscience engineering and science has adopted this field for continuum modelling. In engineering geology, FEM is a helpful method for dealing with the non-linearity of materials, response, and application of complex boundary conditions (Jing and Hudson 2002). In this thesis, numerical modelling of the wedge failure case study was performed using UnWedge (5.0), static and dynamic loading, and support optimization using both RS2 and RS3 as described below:

7.1. UnWedge Analysis

UnWedge is used for numerical modelling to analyze structurally controlled instability in the vicinity of subsurface excavations caused by intersecting discontinuities and excavated open areas using the stereographic diagram.

Gravity and other forces cause roof and wall wedges to fail by either falling, sliding, or twisting out of their sockets (Section 3.2.1). The analysis in unwedge can be done by either a deterministic or probabilistic analysis. The deterministic analysis assumes that all input parameters are known "exactly" (Rocscience, 2022a). The method uses constant values for each parameter, which represent specific values for safety factors (Ping, 1997). Wedge formation depends on the size and shape of the caverns and the orientation of the joints. Tractebel's (2019) geologic mapping results are used as basis for the input parameter estimation. Unwedge 5.0 was used to calculate the fixed factor of safety described below using these fixed and assumed inputs.

7.1.1.   Model setup and input data
7.1.1.1.   **Geometry**

Figure 7.1 show the cross-section of the powerhouse cavern and the transformer cavern. The bus duct tunnel and the draft tube have been excluded for easy analysis. For the unwedge research, including these features are insignificant.
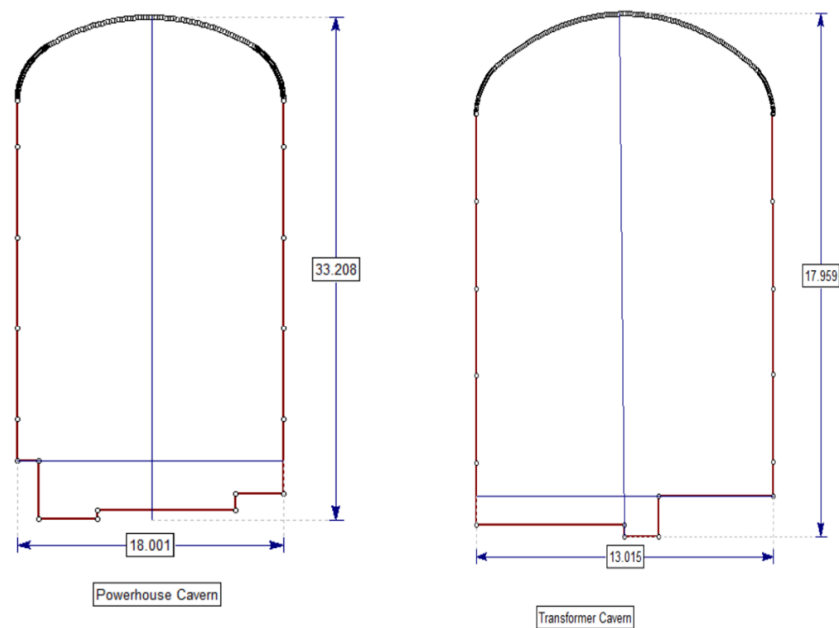
Figure 7.1 Geometry of Powerhouse cavern (left) and Transformer Cavern (right)

7.1.1.2.   **Input data**

Geometric data, rock properties, joint orientations, and joint properties were used as input data to analyze the wedge failure. Since the joint orientations and properties significantly affect the analysis outcome,

appropriate sensitivity to collective information is required. For this work, a deterministic analysis was performed.

According to Lui et al. (2004), a factor of safety greater than two is required for permanent caverns and between 1 and 2 for temporary caverns. For this analysis, a FOS of 2 is assumed. This work considered the effect of stresses (Table 5.4) to study the impact and the required support under these influences. The orientation and factor of safety for design for the powerhouse and the transformer cavern is shown in Table 7.1.

Table 7.1: Details of the orientation of Powerhouse Cavern

Description	Cavern axis orientation		Cavern length(m)	Design factor of safety	Unit weight (MN/m3)
	Trend	Plunge			
Powerhouse Cavern	N135°E	0	69	2	0.027
Transformer Cavern	N135°E	0	47.6	2	0.027

The main objective of Unwedge analysis is to assess if wedges are likely to be of concern at the construction stage. Water pressure in the joint properties is considered zero as the groundwater level in the area is not known.

7.1.1.3.   Severity of Wedges

As the severity of the hazard is dependent on the size of excavation, the size and weight of the wedge are automatically calculated by UNWEDGE and are used to quantify the severity.

7.1.2.   Deterministic and Probabilistic Analysis

7.1.2.1.   Joint Combination

The UnWedge program allows analysis without intersection when the input data contains more than three possible joint orientations. The combination analyzer automatically determines the most critical combinations of joints. The most vital wedge is generated by the joint combination of 1, 2 & 3, in deterministic analysis and probabilistic analysis for both powerhouse and transformer as shown in Figure 7.2.
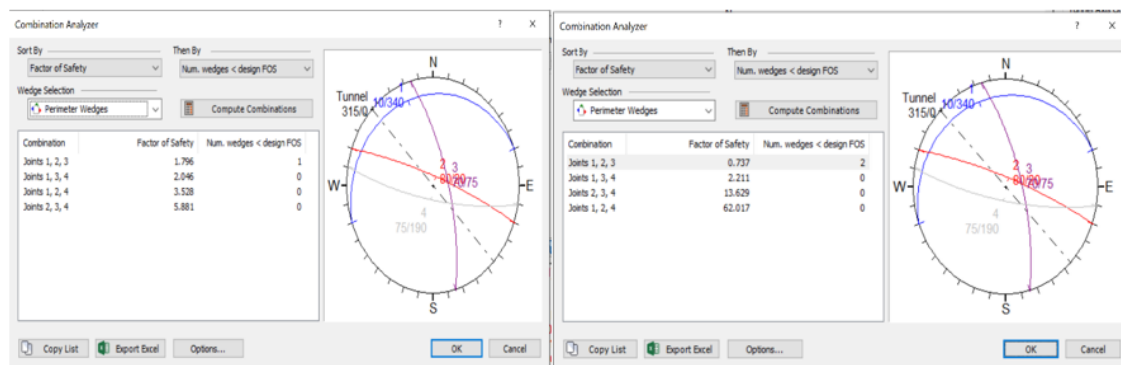
Figure 7.2: Joint Combination for Powerhouse and Transformer Caverns in Deterministic Approach

The dip/dip direction definition defines the joint alignment variability in probabilistic unwedge analysis. This method treats dip and dip direction as independent random variables.

7.1.2.2.   Deterministic Analysis Result

From the deterministic analysis, we can analyze the combination of the joints for the powerhouse cavern with an assumption that all the input parameter needed for the analysis are known. Figure 7.3 show the wedges around the caverns and the rock bolts and shotcrete support provided to ensure the factor of safety equal or greater than 2. The rock bolt and shotcrete properties are given in Table 7.2 and Table 7.3 for powerhouse and transformer caverns. The joint properties and the joint orientation are taken from Appendix C.

Table 7.2: Properties of rock bolt in Powerhouse Cavern

Perimeter Bolt Pattern for Powerhouse Cavern		Bolt Type:	Grouted Dowel
Property:	Bolt Property 1	Tensile Capacity:	0.24 MN
Strength type:	Grouted Dowel	Plate Capacity:	0.1 MN
Bolt Length:	4.00 m	Bond Strength:	0.34 MN/m
Orientation:	normal to boundary	Bond Length:	100% of Bolt Length
Pattern Spacing - In Plane:	1.60 m	Shear Strength:	0.17 MN
Pattern Spacing - Out of Plane:	1.60 m	Bolt Orientation Efficiency:	Used
Pattern Spacing - Out of Plane Offset:	0.00 m	Method:	Cosine Tension/Shear

Table 7.3: Properties of rock bolt in Transformer Cavern

Perimeter Bolt Pattern for Transformer Cavern		Bolt Type:	Grouted Dowel
Property:	Bolt Property 1	Tensile Capacity:	0.24 MN
Strength type:	Grouted Dowel	Plate Capacity:	0.1 MN
Bolt Length:	2.50 m	Bond Strength:	0.34 MN/m
Orientation:	normal to boundary	Bond Length:	100% of Bolt Length
Pattern Spacing - In Plane:	2.00 m	Shear Strength:	0.17 MN
Pattern Spacing - Out of Plane:	2.00 m	Bolt Orientation Efficiency:	Used
Pattern Spacing - Out of Plane Offset:	0.00 m	Method:	Cosine Tension/Shear
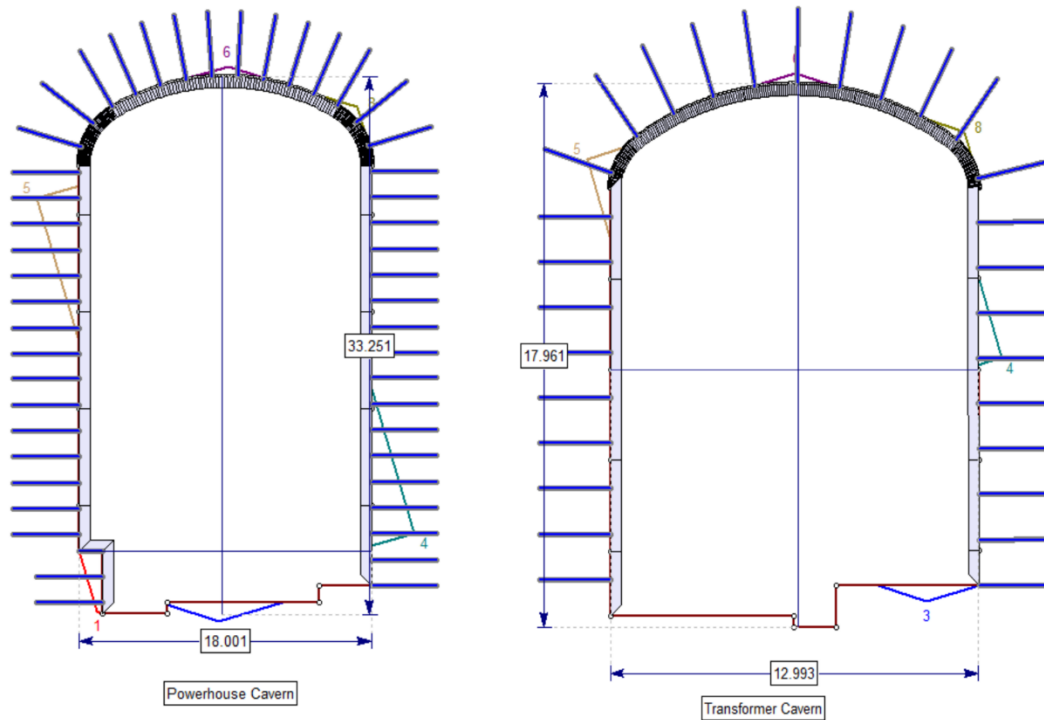
Figure 7.3: Rock Bolts and wedges in the Powerhouse and Transformer Cavern

From the deterministic analysis, the maximum wedge depth was found to be 2.67m in powerhouse and 0.97m in transformer cavern in upper left wedge 5. Therefore, bolt length of 4m for powerhouse and 2.5m for transformer cavern was installed with 4 cm thick shotcrete in powerhouse and 3cm in transformer cavern which gave the safety of factors as shown in

Figure 7.4 and Figure 7.5.
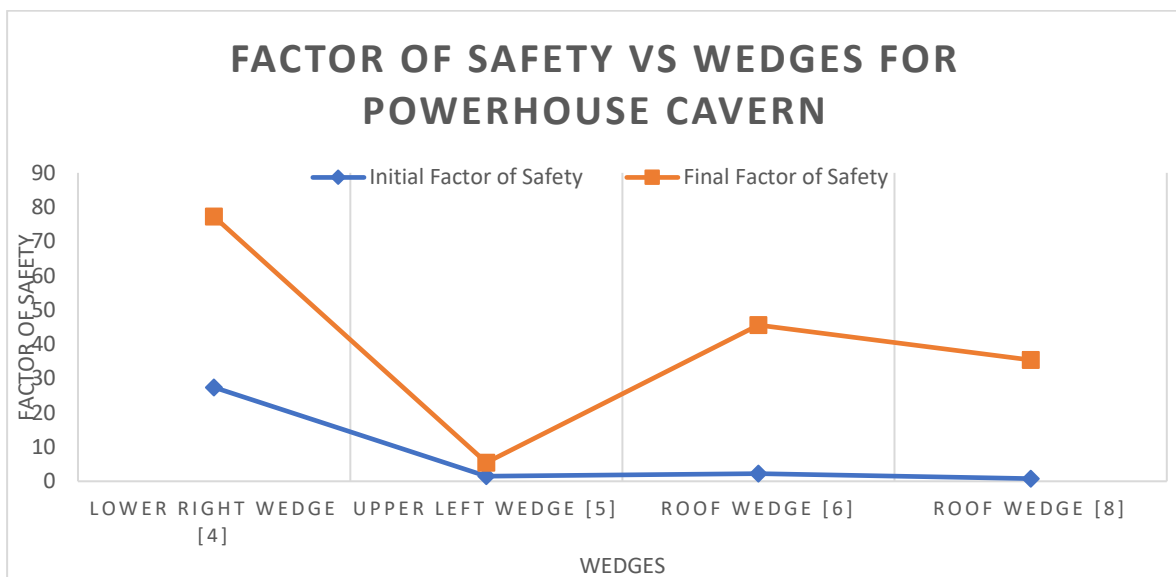
Figure 7.4: Factor of safety for Powerhouse Cavern
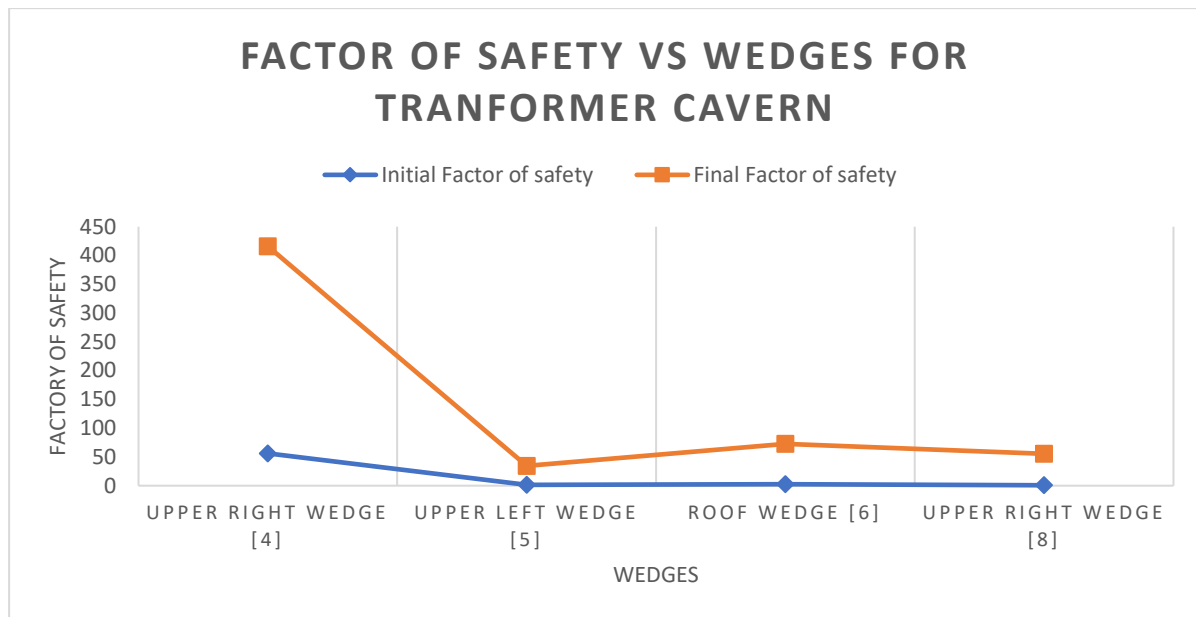
Figure 7.5: Factor of safety for Transformer Cavern

7.1.2.3.   **Probabilistic Analysis Result**

According to unwedge results based on maximum support pressure needed, maximum wedge depth, a minimal factor of safety, and chance of failure, the crown area of the cavern's perimeter and end walls is the most crucial. Certain findings show values that are highly crucial.

However, the cumulative probability of reaching critical levels is relatively small (Appendix C2). To develop the support system for this thesis, critical values with extremely low cumulative probabilities will be employed.

Maximum Support Pressure

The beginning point for designing real support systems, such as bolts and shotcrete, is the required support pressure. A safety factor larger than the design factor of safety will result from applying the necessary support pressure to the most crucial joint combination.
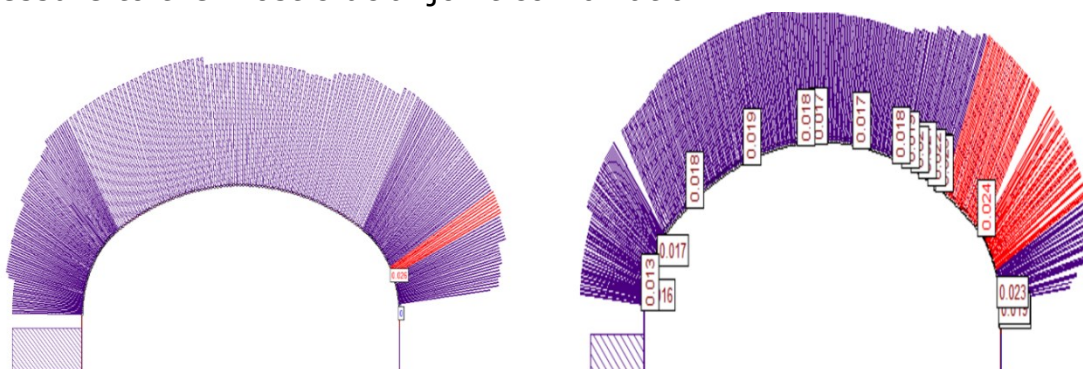
Figure 7.6: Maximum Support Pressure (MPa) probabilistic for Powerhouse (left) and Transformer Cavern (right)s

From the Figure 7.6, the maximum support pressure required for powerhouse cavern is 0.026 MPa and 0.024 MPa for transformer cavern.

Maximum Wedge Weight

From the Figure 7.7, powerhouse cavern has the maximum wedge weight ranging from 0.078 to 0.123 MN and for the transformer cavern is 0.053 to 0.096 MN. Regarding worker safety and cavern stability, the severity of the roof wedge is crucial.
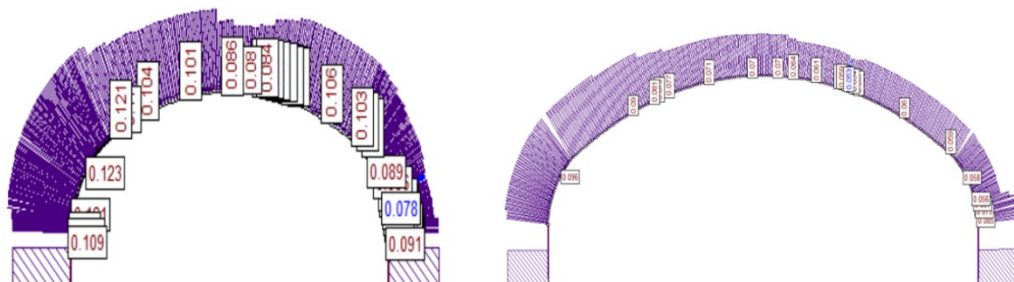
Figure 7.7: Maximum wedge weight (MN) probabilistic for Powerhouse (left) and Transformer Cavern (right)

Maximum Wedge depth

The maximum wedge depth(m) for the powerhouse cavern is 2.16 m indicated in red while 1.09 m for the transformer cavern in Figure 7.8.
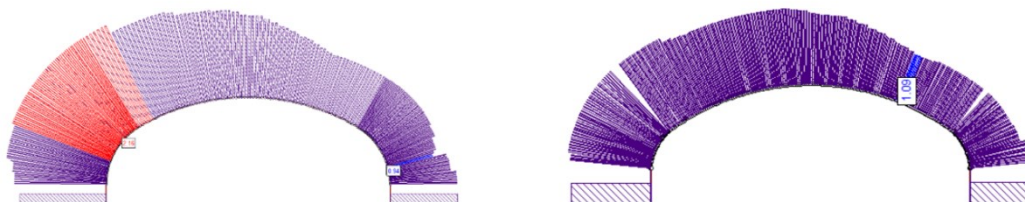
Figure 7.8: Maximum wedge depth (m) probabilistic for Powerhouse (left) and Transformer Cavern (right)

Minimum Factor of Safety

Figure 7.9 shows the minimum factor of safety for each wedge on the each segments. Both the powerhouse and the transformer cavern roof can be considered critical as the factor of safety is less than the design factor of
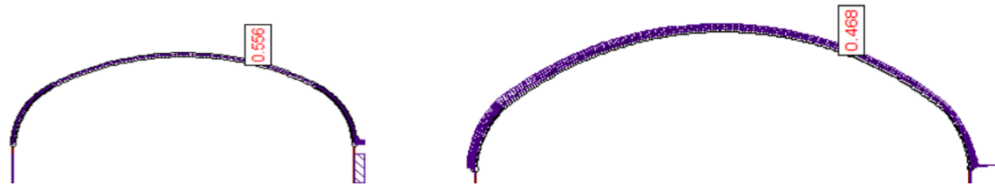
safety.

Figure 7.9: Minimum factor of safety probabilistic for Powerhouse (left) and Transformer Cavern (right)

Probability of Failure

The number of failed wedges to the total number of samples determines the chance of failure. When more valid wedges with a lower safety factor than the design factor of safety than the number of failing wedges. The application software also allows for the entry of the sample count. For the specified collection of probabilistic input data, it is the overall probability of wedge failure. Figure 7.10 show the probability of failure of the most critical segments marked in red.
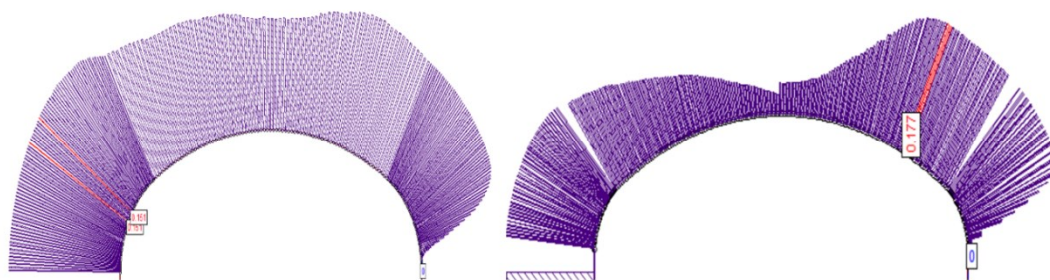
Figure 7.10: Probability of failure probabilistic for Powerhouse (left) and Transformer Cavern (right)

7.1.3.   Rock Support Design in Unwedge

A rock support system for wedges is designed to provide a stiff response to the block movement, i.e., fully tensioned mechanically anchored rock bolts or fully grouted bolts left untensioned, provided the movement of blocks hasn't taken place (Hoek, 2007). Support design in the Unwedge analysis is independent of empirical support design, Rocscience 2D & 3D support design results.

7.1.3.1.   Rock bolt length

The bolt length needed for the support can be estimated from the maximum wedge depth and minimum factory of safety given in Figure 7.4 and Figure 7.5.

7.1.3.2.   **Shotcrete support**

The failure mode of shotcrete in Unwedge is direct shear. Therefore, the shear strength of the concrete is critical to the application of shotcrete. The bearing capacity of shotcrete is a function of the extent of the exposed area, perimeter, shear strength, and thickness. Most reported values for 28-day strength are 20 to 50 N/mm2; a strength greater than 25 N/mm2 should be used only for particularly carefully constructed shotcrete work (Yun et al., 2020). In this work, a value of 35 MPa is used for the compressive strength of shotcrete (Panthi & Basnet, 2016) Table 7.4 shows the input values for shotcrete support.

Table 7.4: Shotcrete Properties

Shotcrete Property 1	Powerhouse	Transformer cavern
Compressive Strength	35 MPa	35 MPa
Shear Strength:	1.000 MPa	1.000 MPa
Unit Weight:	0.026 MN/m3	0.026 MN/m4
Thickness:	4 cm	3 cm

 7.1.4.   Discussion of the result

The model result for UnWedge are dependent on the input data. Low cumulative probability of maxium support pressure, wedge weight, wedge depth, minimum factor of safety and probability of failures has been considered for the analysis given in appendix C1. Support design has been done ensuring the design approach discussed in section 3.2.1.1.

7.2. Static Modelling in 2D

2D numerical modelling is performed in RS2 or Phase 2 (formerly), Rocscience subsurface analysis software that allows users to perform 2D modelling with finite plastic elements (Rocscience, 2022c). RS2 provides the user with a simple and friendly interactive interface to perform modelling and visualize the result explicitly with various display options. In addition to the ability to define the geometry, materials, and support types to be used, RS2 also analyzes groundwater and common rock mass conditions. The static models of the powerhouse and transformer cavern are modeled using RS2. This section explains the functions used and parameters implemented for modelling with RS2.

 7.2.1.   Project Settings

In RS2, analytical options such as the asymmetric and Plain strain models are available. Since it is a two-dimensional program, the analysis is limited to the plane of interest. This work analyzes the profiles and cross-sections of the powerhouse and transformer cavern using a plain strain model, as

shown in the figure. According to the philosophy of simple strain, the strain of material can only be observed in one plane. When modelling a subsurface excavation such as a cavern, the strain along the axis is zero. The default value in RS2 for the modelling consolidation parameter is zero, meaning that the stress under study is the total stress.

The units are used in the metric system of unity with the solver type Gaussian elimination. Stress analysis is performed with a maximum number of iterations from 1500 to 2500 with a tolerance of 0.001 and an automatic load step configuration. Convergence of a finite element solution occurs when the model reaches the acceptable energy deviation specified by the tolerance level within the set number of iterations (Rocscience, 2022a). For an accelerated initial stiffness of 0.2 to 5, the comprehensive convergence type is used, which checks the three criteria of force, energy, and displacement simultaneously and is the default in the RS2 software. The model is run in static water with a pore fluid unit weight of 9.81 kN/m3 as the pore fluid unit weight.

7.2.2. Boundary Condition

The boundary function in RS2 establishes an outer limit of the excavation boundary (cavern boundary). The design of the investigation section determines the excavation in this investigation. A box boundary model is used based on the assumption that the caverns are deep in the ground and can be represented by a box, with constraints to simulate the ground reaction near the cavern opening. In contrast, the boundary conditions for the longitudinal and cross-sections of the soil, which are essential for the stress conditions, are not defined by boxes but by actual soil surface profiles obtained using mapping and GIS tools. The expansion factor of 4 was used to analyze the extent of deformation propagation due to excavation of the model under static and dynamic loading.

7.2.3. Material Properties

The power plant cavern and the transformer cavern are used for the thesis. As indicated by the geological mapping and report on Tamakoshi V HEP, the underlying rock consists of Augen Gneiss with portions of chlorite schist containing quartz, feldspar, muscovite, and biotite, including quartz and feldspar phenocrysts. The parameters used to determine the material properties for modelling were obtained from the rock core samples collected from the exploratory adits borehole near the powerhouse. They were used to perform laboratory tests such as UCS, tensile test, PLT, etc. (see Section

5). This study introduces two material properties, one for the rock mass and one for the disturbed zone shown in Table 7.5.

Table 7.5: Material Properties of the rock mass

Material	σci [MPa]	Q-value	Erm(Hoek and Diederichs, 2006)	GSI	mi	D	v
Augen Gneiss	43	0.833	4.56	41	26	0.5	0.25

Table 7.6: Rock mass properties applied in Numerical Modelling

Parameter	Rock Mass	Disturbed zone
mb	3.16121	1.566
s	0.00038	0.00038
a	0.5106	0.5106
Dilation	0	0.05
Erm (Gpa)	5.853	2.803
Residual m_r	1.723	0.394
Residual a_r	0.5106	0.5747
Residual GSI_r	23.44	12.3
Residual S_r	0.0002151	0.00008

The numerical analysis begins with the assumption that the material is elastic. In the elastic model, the in-situ stress situation is obtained with a longitudinal and transverse profile of the ground and the strength factor from the excavation before and after.

The initial element stress conditions are the field-only stress and the body force to field stress only, according to the RS2 specification of the material. For clarification, the initial element stress refers to how the material is loaded when a force is applied. According to Rocscience (2022c), initial loading should only be used with field stress in a continuous field stress loading configuration. On the other hand, field stress and body force should be performed for gravity loading, which requires knowledge of the ground surface. Field stress and body force initial element loading are used to study the longitudinal and transverse soil sections of interest. The box model uses only field stress and field stress with body force.

A failure criterion based on Generalized Hoek and Brown is considered. As shown in Table 7.6, GSI with intact rock strength values and an empirical relationship to determine the rock mass modulus are used to define the rock material. For this study, the hydraulic properties are assumed to be drained to simplify the model without considering groundwater.

To model the post-peak behavior of the rock, the residual parameters are estimated using the equation at Section 2.4.1 and confirmed by the RocData or inbuilt calculator of GSI in RS2. The GSI value of the disturbed zone is not known, so 30% of the GSI is taken for the disturbed zone (Panthi & Basnet, 2016), and the residual parameters m_r and s_r are determined from the equations 2.16 and 2.23. The a_r parameter is independent of the disturbance factor, D so hence remains unchanged (Hoek et al., 2002)

7.2.4.   Field Stress Loading

The Rocscience in RS2 has two alternative settings for field stress: constant and gravity. Gravity loading accounts for actual ground conditions and the effective stress ratio and variable stress ratio used for the longitudinal and transverse profiles of the study section for in situ loading and for validation and calibration of the dynamic analysis of the seismic data from the corresponding source. A constant stress type was selected for the box model, used in all static and dynamic evaluations with support optimization.

Figure 7.11: Field Stress loading in RS2

7.2.5.   Mesh Setup and Restraining

A graded mesh with a 6-Noded Triangle element type is used for numerical models. As shown in Figure 7.12, a gradation factor of 0.1 is used in conjunction with the default number of nodes on the excavation. Before running the simulation, the mesh quality of each model was evaluated. IA geometry cleanup was performed if individual mesh elements were of low quality This study is free from problems such as non-convergence and erroneous simulation results. The restraint implemented in the model setup provides the displacement boundary condition for model step-up. All four sides of the box are restrained from representing the realistic situation of

underground cavern structures and interaction with the rock mass, as shown in Figure 7.12.
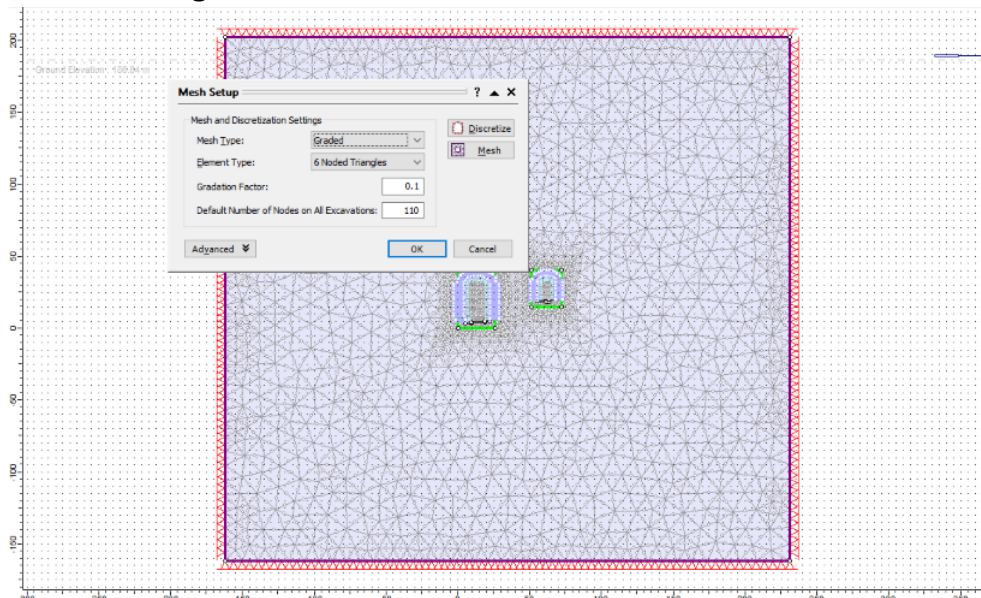
Figure 7.12:Mesh Setupd

7.2.6. Support

The life of underground openings such as tunnels and caverns depends on their stability. The rock these openings are made is fractured, and stresses build up at the edge of the outcrop. The rock mass around the cavern undergoes various reactions during this process, including decomposition, plastic deformation, spalling, and rockburst. In the worst case, complete collapse occurs if the opening is not controlled. The RS2 numerical modelling tool allows the users to apply customized supports. For this study, various support situations are explored, which will be explained later utilizing proprietary tools. Nevertheless, this section summarizes the broad support provided in this study. Liners and bolts are integrated supports offered by RS2. Support systems such as main shotcrete, RRS, lattice girders, and secondary shotcrete are used as liners. The properties of the liner and the rock bolt is given in Table 7.2. Rock bolts are also used as anchors. According to the design and Q-support diagram (Grimstad and Barton 1993) and (Hoek & Moy, 1993). Table 7.7 and Table 7.8 is obtained for the implementation in numerical modelling.

Table 7.7: Support Estimation as per Q-System, (Grimstad and Barton 1993)

	Description	Span/ESR	Support
Powerhouse	wall	33.14	Bolt length of 8m @ 1.6-2.1 c/c, fiber reinforced shotcrete of 12-15cm thickness
	Roof	18	Bolt length of 4.7m @ 1.5-1.7 c/c, fiber reinforced shotcrete of 9-12cm thickness
Transformer Cavern	wall	17.95	Bolt length of4.5m @ 1.6-1.7 c/c, fiber reinforced shotcrete of 9-12 cm thickness
	Roof	13	Bolt length of 3.9m @ 2-2.5 c/c, fiber reinforced shotcrete of 9-12cm thickness

Table 7.8: Support estimated as per (HOEK and MOY 1993)

	Description	Span/ESR	Bolt Length (m)	Bolt Spacing (m)	Cable Length
Powerhouse	wall	33.14	6.97	1.5	11.60
	Roof	18	4.7	1.5	7.20
Transformer Cavern	wall	17.95	4.69	1.5	6.28
	Roof	13	3.95	1.5	5.20

7.2.7.   Modelling of Model

In the initial phase of numerical modelling, we must first have the longitudinal and cross-sectional profile of the study subject. These two profiles are extracted from any mapping software dedicated or with additional support like Google Earth Pro, ArcGIS, QGIS, etc., from where we can get the coordinate and the point data to process in Digital Elevation Model (DEM) to have the contour and the elevation and finally get the profile from AutoCAD software. Cross-sectional and longitudinal profiles are shown in Figure 7.13 and Figure 7.14**.**
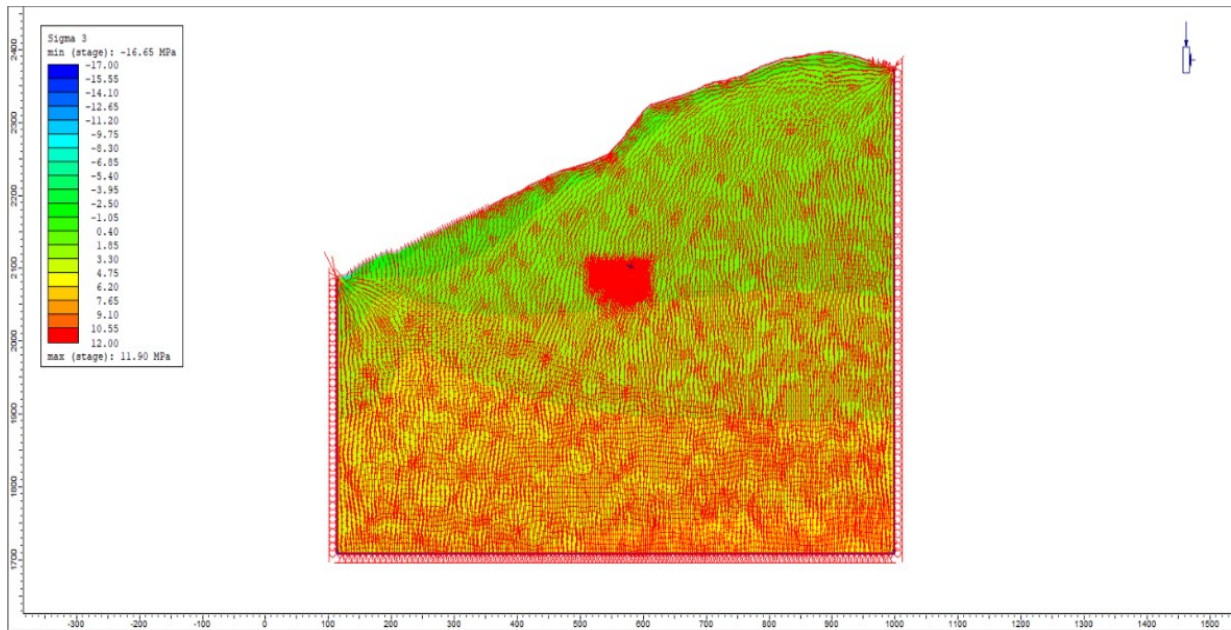
Figure 7.13: Longitudinal Profile
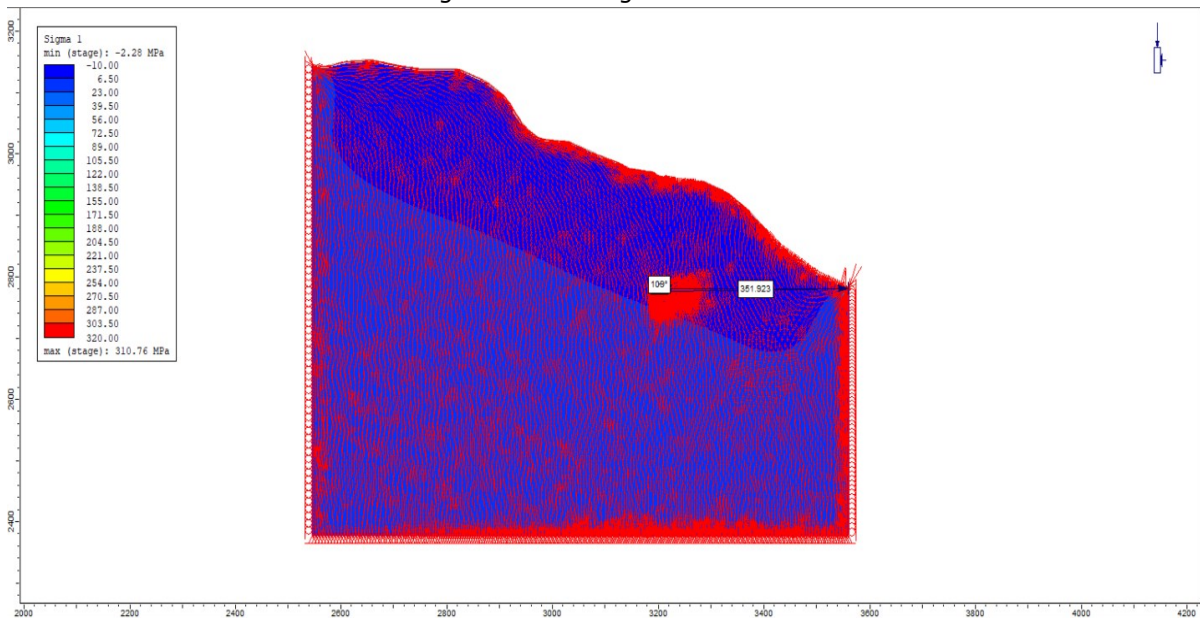
Figure 7.14: Cross-Sectional Profile

The main purpose of extracting the profiles is to study the in-situ situation and its in-plane (perpendicular to powerhouse alignment) and out-of-plane (parallel to the powerhouse alignment) orientation. The profiles also show the topographic effect, which is essential for considering stresses and the mode of failures. Assuming that the material is elastic and the rock properties, the two profiles with the data in Table 7.5 and Table 7.6 are made ready for modelling. The effective stress ratio is taken from SECTION 5.3. The transverse and longitudinal profiles are run, and the results are shown in Figure 7.13 and Figure 7.14.

7.2.8.   Excavation Sequence and Disturbed zone
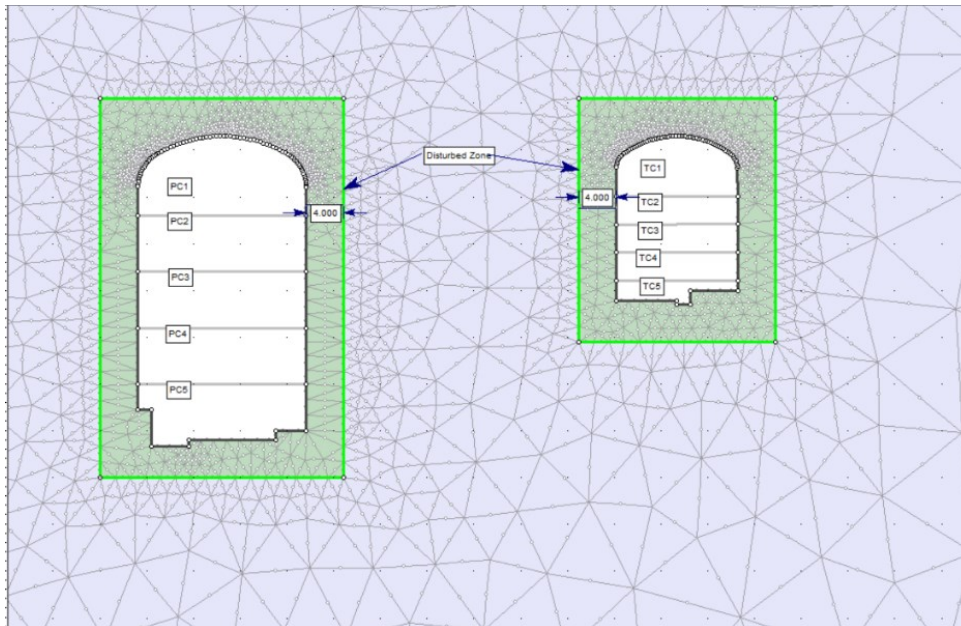
Figure 7.15: Excavation Sequence and Disturbed Zone

In reality, underground cavern excavation is performed in several phases, depending on the excavation techniques of the contractor. However, to simplify the analysis, given the complexity of the model to be run by the RS2 software and the time limitation of the work, the excavation of the powerhouse and the transformer cavern is divided into five stages to see the gradual effect of the excavation and the deformation resulting from the stress acting on the structures in the 2D plane view of the selected cross-section. The sequence is PC1 and TC1 simultaneously in the first and other stages. The disturbed zone of 4 m is set for both the powerhouse and the transformer cavern, assuming that the effects of excavation of rock mass is sensitive and will be confined within the region. In contrast, for the tunnel,the disturbed zone is set at 1-2m with a disturbance factor of D=0.5 (Hoek & Brown, 2019)

7.2.9.   Analysis Approach
7.2.9.1.   Elastic Analysis
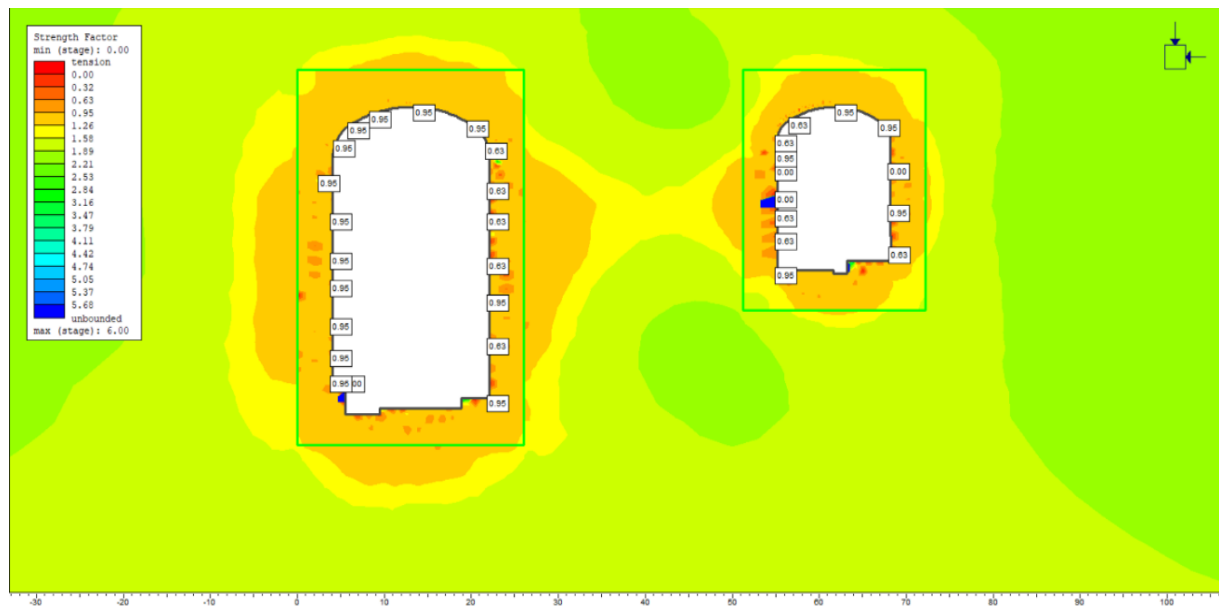
Figure 7.16: Strength factor (Elastic model)

Determining the analysis approach is as critical as the stress calculation. The analysis method determines whether the implemented model can represent the actual behaviour of the ground. The cross-sectional model of the powerhouse and transformer caverns is run through an elastic model to determine the strength factor and stress distribution around the cavern openings. A strength factor is a ratio between the strength of the rock mass based on failure criteria and the induced rock stress (Rocscience, 2022c).

If the strength factor is less than one (see Figure 7.16), the material is yielded, and this us an idea whether plastic analysis is needed or not to calculate deformation and support.

7.2.9.2.   Plastic Analysis

In this analysis, the material is set as plastic,and and the field stress values from 7.2.4. The plastic analysis focuses on the deformation when the caverns are excavated. The structure is also provided with support to check if the support is sufficient to control the deformation. The appropriate modification of the support is studied to determine the safety factor of the caverns.

7.2.10. Results of Numerical Modelling
7.2.10.1.   Spacing between caverns

Pillar width 18m   Pillar width 26m

Pillar width 30m   Pilllar width 33.14m
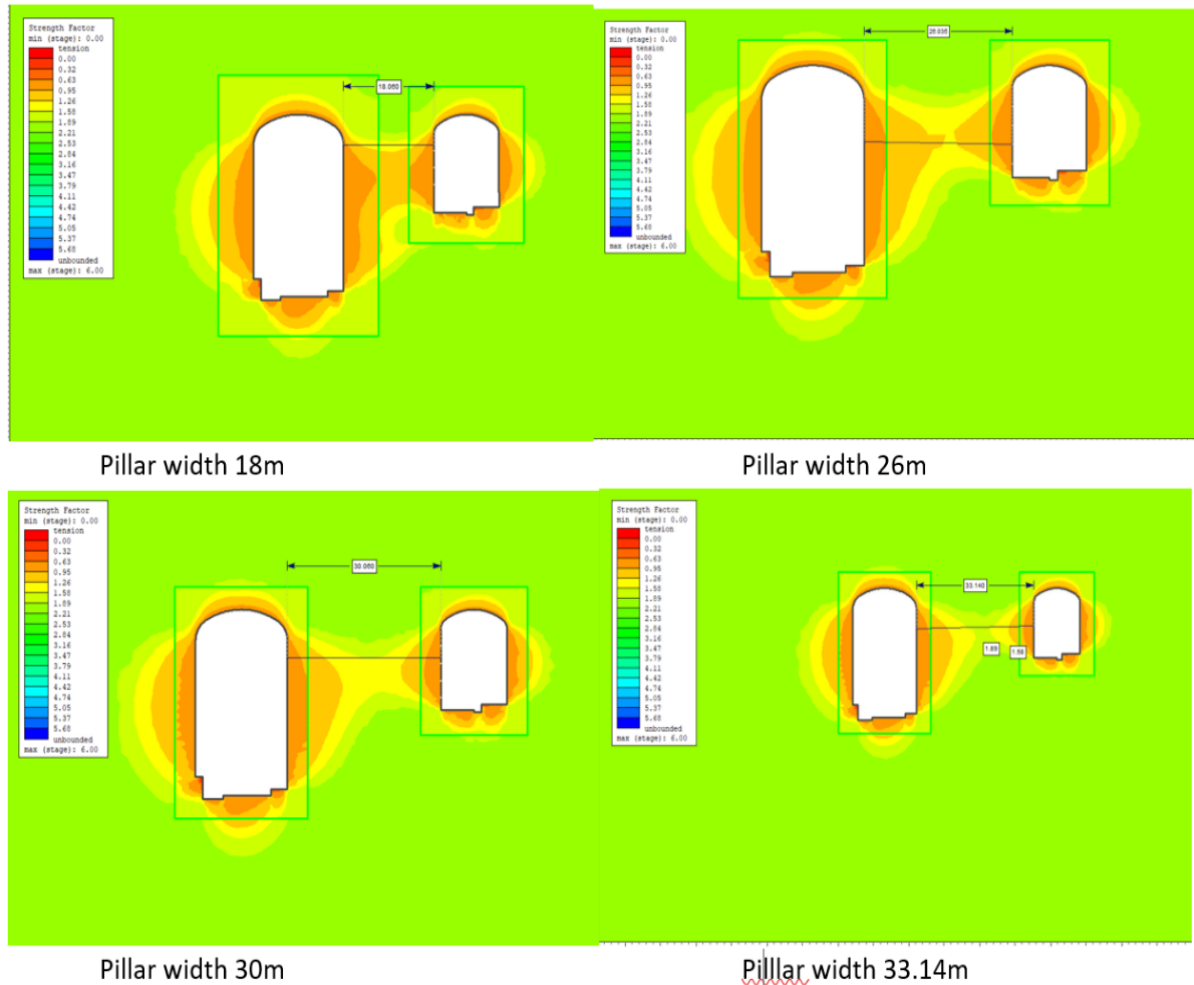
Figure 7.17: Illustration of the strength factor with pillar widths

To evaluate spacing between the caverns, different pillar widths are modelled. The strength factor is illustrated in Figure 7.17 an elastic model. According to design criteria in Section 3.1, the pillar width between the caverns should be the width or the height of the larger cavern. Models with pillar width of 18m, 26m, 30m and 33.14m has been checked to find the appropriate pillar width between the caverns which is 33.14m equal the height of the powerhouse cavern. Furthermore, plastic model is run to check for the yielded zone which aids to set the pillar width given in Figure 7.18.

The region around the disturbed zone is overstressed and likely to fail in the absence of support. The maximum elastic displacement is found to be 0.04m. for the full excavation stage of the caverns.

| 30m pillar width | 33.14m pillar width |
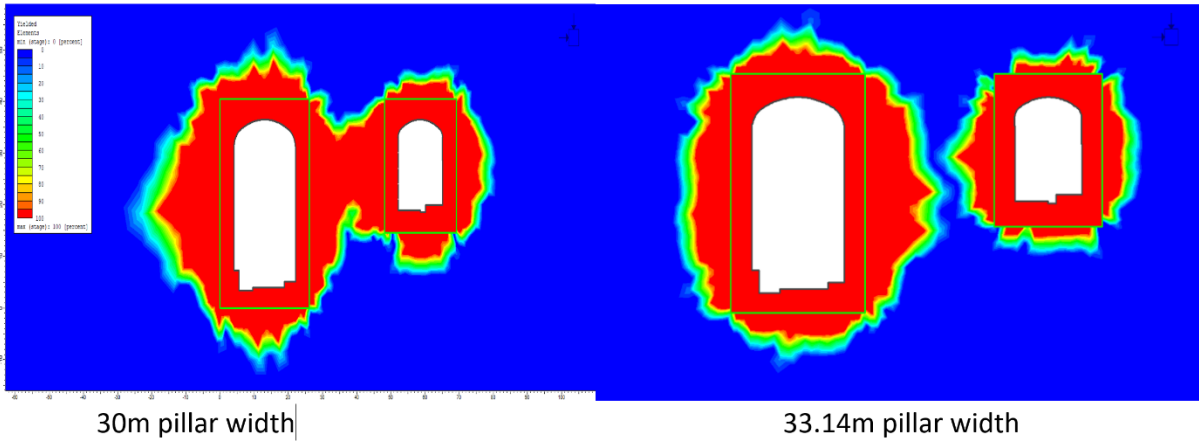
Figure 7.18: yielded elements for different pillar width between powerhouse and transformer caverns

7.2.10.2. **Stress Distribution**

The stress distribution for the opening of the caverns are modelled in elastic material properties given in Figure 7.19 and Figure 7.18. The maximum values in roof are labelled and rendered in Table 7.9. The major stress concentration is at crown and corners of invert due to overstressing. Since the disturbed zone has a lower E_{rm} than the rest of the rock mass, the stresses are distributed to the transition between the disturbed zone and the rest of the rock mass.

Table 7.9: Maximum tangential stress in the cavern roof and their ratio with UCS. Values over 0.4 indicates spalling

Description	$\sigma_{\theta max}$[MPa]	$\sigma_{\theta max}$/UCS [MPa]
Powerhouse	11.80	0.27
Transformer Cavern	11.00	0.26
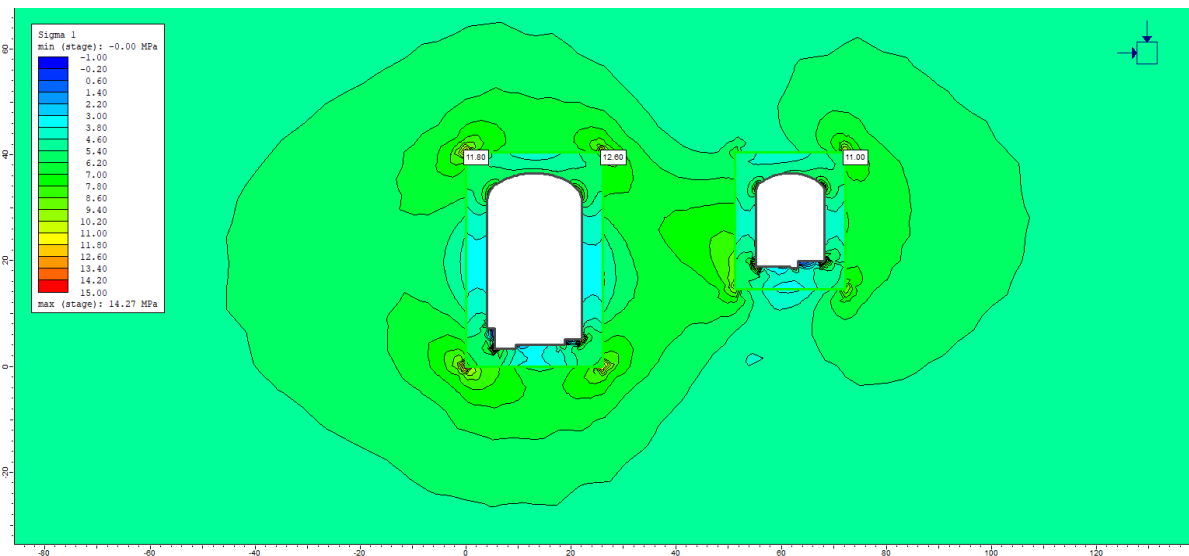
Figure 7.19: Stress distribution (Sigma 1) with maximum stress labelled from elastic model [MPa]

Negative stress might cause stability problems due to tension. The zones with negative stress are modelled in Figure 7.20Figure 7.20: Stress distribution (Sigma 3) with maximum stress labelled from elastic model [MPa]. It is primarily in the walls of the powerhouse and transformer cavern that this could be a problem. This is due to the geometry of the caverns and the direction and magnitude of the stresses.
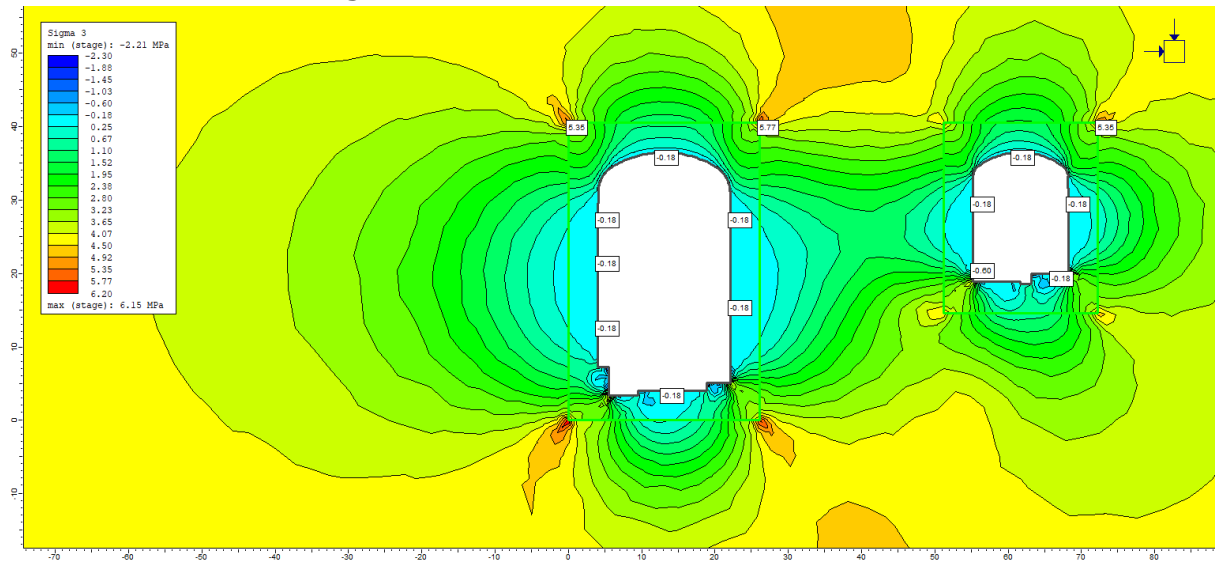
Figure 7.20: Stress distribution (Sigma 3) with maximum stress labelled from elastic model [MPa]

7.2.10.3.   **Plastic Deformation**

A plastic model is analyzed to evaluate the extent of damage when the material is allowed to yield. The numerical modeling is therefore carried out to estimate the extent of deformation at these cavern openings. Along with this, the objective of numerical modeling in RS2 is to replicate the field situation so that model represents the real ground condition.

I.   **Without Support**

The deformation around the powerhouse and the transformer cavern walls are significantly high with 0.37m for powerhouse and 0.39 for the transformer caverns. The deformation at the roof are 0.24m and 0.17m for powerhouse and the transformer cavern while 0.43m at the invert level as shown in Figure 7.21 and Figure 7.22. Likewise, rock mass has mostly failed by tension in invert, roof and wall, which might be due to the high stress anisotropy that exists because of low tectonic stress or low total in-plane horizontal stress and high vertical cover. The maximum displacement determined by numerical modelling is very high as compared to the empirical, semi empirical and Analytical methods which might be because of the 4m disturbed zone which considers the rock mass to be very weak.
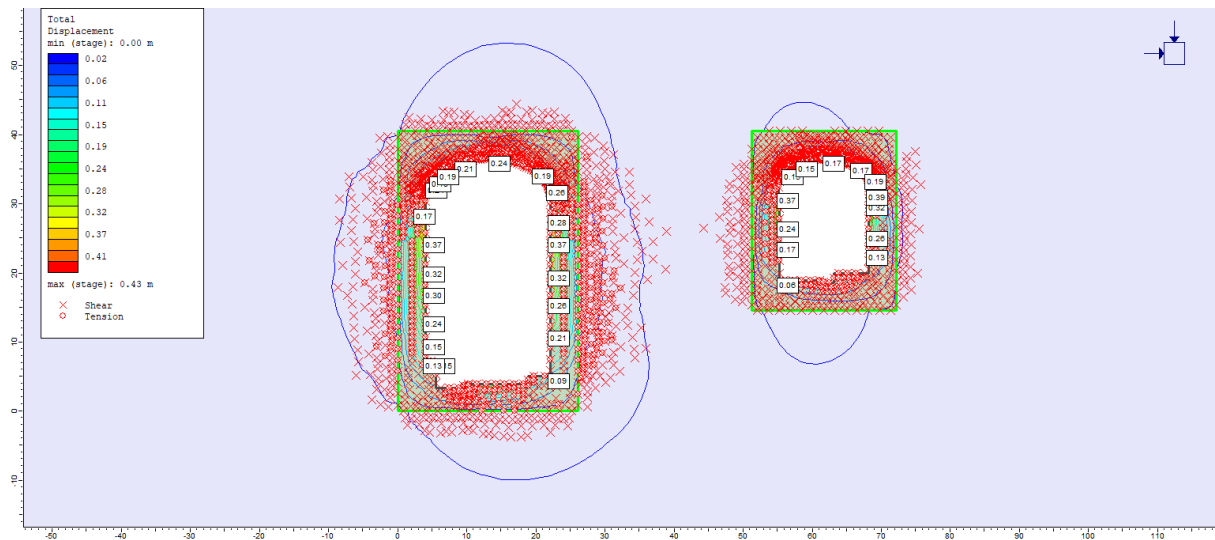
Figure 7.21: Total displacement with yielded element without support (Plastic Analysis)
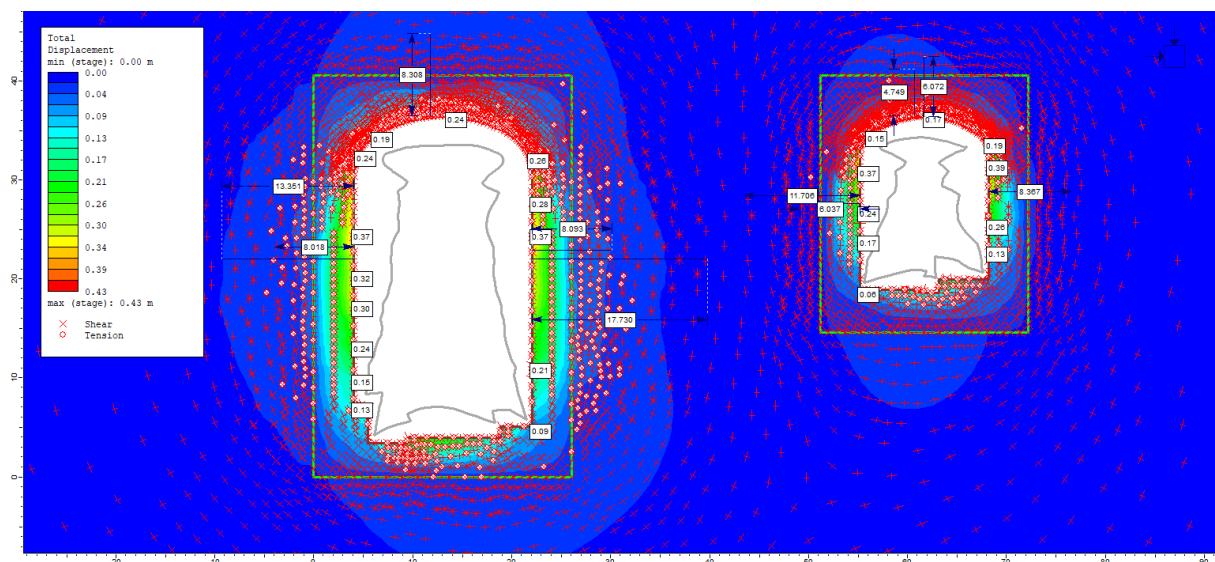
Figure 7.22: Total displacement in an unsupported state

The deformation and the yielded element are given in Table 7.10. Tension due to negative stresses can cause some problems in stability around the wall and invert, where minimum principal stresses are negative. The extension of the failure zone, which includes both tensile and shear failure, is approximately 7 meters on both sides of the powerhouse wall and within the disturbed zone of 4m for transformer cavern. Apart from this combined failure zone, future failure has been limited to shear only within 8 to 17m from the walls of caverns given in Figure 7.22: Total displacement in an unsupported state. The probable collapse zone on the roof is around 4 to 8.5m meters long. According to (HOEK and MOY 1993), if a rock mass fails gradually, continuous cracks emerge behind the walls at a particular point. A big mass of sidewall rock collapses as a result of this. Therefore, the risk of failure should be mitigated by providing extensive support.

II.   With Support

Preliminary support has been applied based on Q system-(Grimstad and Barton 1993). According to (Grimstad and Barton 1993), the recommended support system for the underground powerhouse caverns and opening with the Q value in the range of 0.1 to 4 and the excavation span ratio (ESR) equalt to 1 is presented in Table 7.7 and Table 7.8. The SFR and rock bolts were installed in total of stages to visualize the realistic pattern of support installation. Figure 7.23 shows that the deformation around the powerhouse and cavern with support installed using Q-system (Grimstad and Barton 1993).
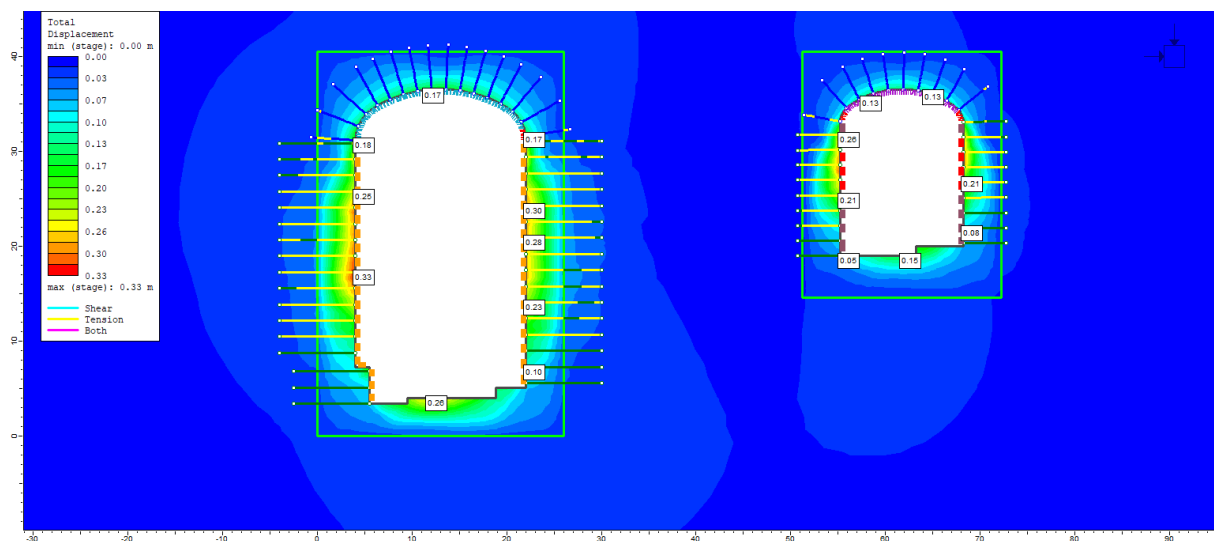
Figure 7.23: Final Stage with Support using Q-System (Grimstad and Barton, 1993)

Support estimation can also be done by the analysis of the failure zone. As the zone of failure envelops the caverns, installation of the bolt pattern is needed to reinforce the rock mass. From the Figure 7.22, Length of bolt required for the roof of the powerhouse cavern is 6m and transformer roof is 5m which enables the bolt to extend 2m beyond the disturbed zone and get anchored in undamaged rock. Length of bolt required for the walls of powerhouse is 8m and for transformer cavern wall is 6m.

Yield of the support is seen as red for the shotcrete elements, yellow for tension and light blue for shear in the bolts and cables. Bolts that are fully bonded and plain strand cables can only fail under stress. The intersection of each bolt with the solid parts of the mesh defines the failure of the bolts and cables in segments. The completely bonded bolts in the upstream wall and crown will fail under tension near to the wall, as can be observed. The support provided by the Q-system controls the total deformation with 23.25% reduction in the caverns. The deformation reduction in powerhouse is between 29.16 % to 32.43 % while for the transformer cavern is 29.72%

to 38.46%. Many bolts are yielding in the disturbed zone which is due to the applied dilation parameter within the zone. The increased deformation leads to tensile yielding in the support.

Figure 7.23, shows the yield in the shotcrete in the right side of the roof and the walls of the caverns which is due to the large span and the high horizontal stress. As most of the bolts are yielded so the support optimization has been done to reduce the deformation, contain the failure zone and the yielding of the support. Figure 7.24 shows the model with optimized support. The deformation has been contained to 0.12m from 0.24m which is 50% reduction of the initial deformation. The cable strand has been introduced in the model as per the (Hoek & Moy, 1993)) from Table 7.8. (Li, 2017)) recommends using long cable bolts in conjunction with tightly spaced rock bolts since the rock mass in the cavern is very poor to poor with a huge failure zone. Furthermore, as the height of the side walls rises, so does the length of the anchoring required.
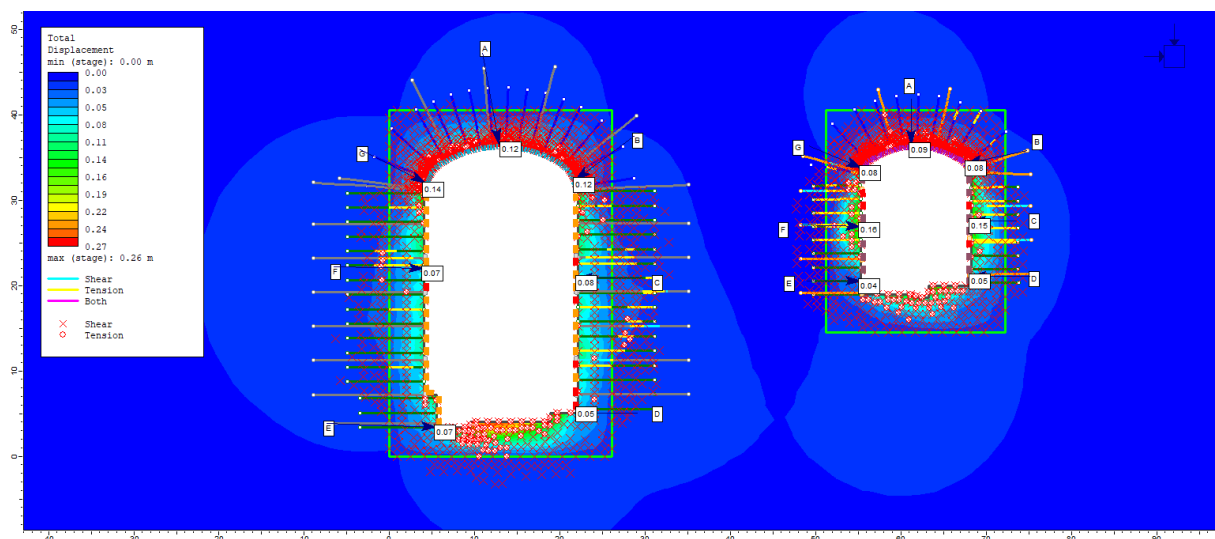
Figure 7.24: Modified support for powerhouse and transformer cavern

The support capacity curve for the shotcrete from Figure 7.25shows that, the line support is within the factor of safety of 2 in shear with some yield in the bending moment. This is because the concrete has high compressive strength and low tensile strength.
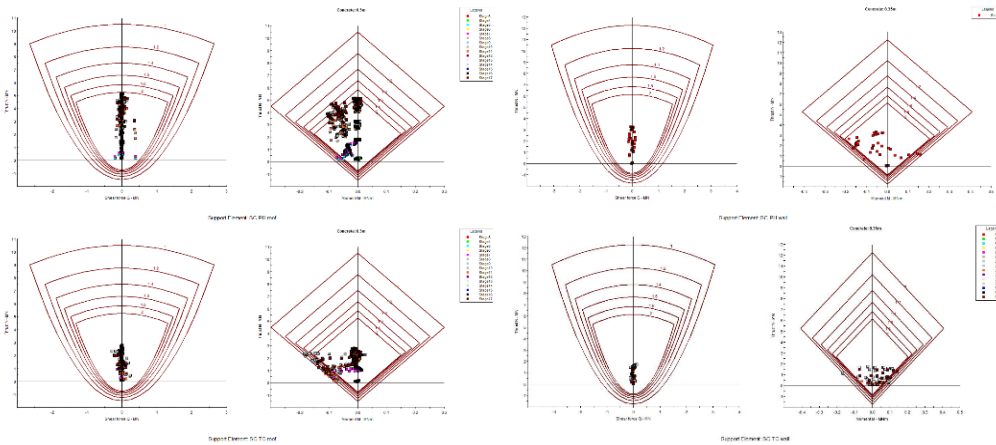
Figure 7.25: Capacity Curve for Static Analysis for the powerhouse and transformer cavern
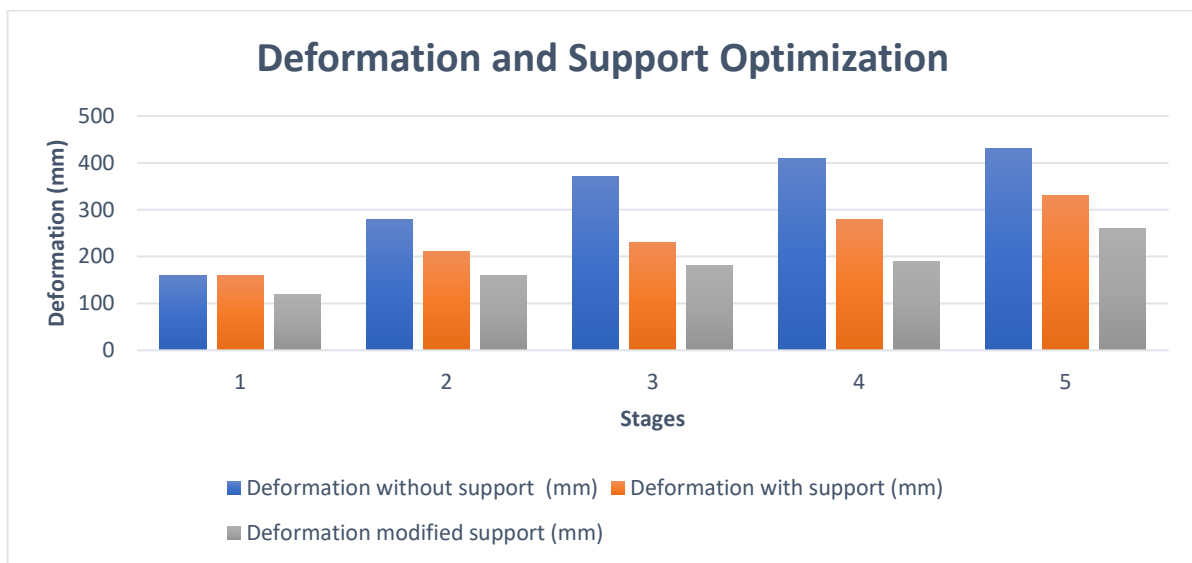
Figure 7.26: Deformation and Support optimization

Figure 7.26 and Table 7.10 show the total deformation without support, with support and optimized support. The total deformation for the powerhouse and the transformer cavern is ideally supposed to be compared or calibrated with the measured deformation given that it is provided however, for this study case no field measurement for deformation has been done.

Table 7.10: Total Deformation without support and support optimization

Stage	Without Support		With Support(Q system)				With Support(Modified)			
	Deformation (mm)	yielded finite element	Deformation (mm)	yielded finite element	yielded bolt	yielded liner	Deformation (mm)	yielded finite element	yielded bolt	yielded liner
1	160	1229	160	1229	0	0	120	1203	0	0
2	280	1425	210	1317	37	17	160	1261	37	10
3	370	1626	230	1442	87	21	180	1373	76	14
4	410	1822	280	1750	161	23	190	1665	129	19
5	430	1833	330	1764	231	26	260	1629	154	22

7.3. Static Modelling in 3D

RS3 (Rock and Soil 3) is another software package from Rocscience that allows the user to perform a three-dimensional analysis of geotechnical structures for civil and mining applications (Rocscience, 2022). The general purpose of RS3 is to perform finite element analysis for underground excavations, tunnel and lining design, surface excavations, foundation design, slopes, consolidation, ground seepage, and more. Static modelling of the dissertation study is performed in RS3 to understand the 3D effects of the powerhouse and transformer cavern excavation and the interaction between the excavation and deformation along the outer plane, which is difficult to visualize through 2D analysis in RS2.

7.3.1. Project Setting

The general project setup in RS2 and RS3 follows a similar trend except for some changes. Modelling in RS3 is performed as an uncoupled analysis using an automatic solver type. The elastic and plastic are performed for analysis with the same basis as in RS2 (see Section 7.2.1). The elastic model analyzes stress redistribution and the strength factor of the material, while displacement and deformation are examined in the plastic model. The plastic material allows the material to yield.

The analysis is carried out in two situations; one with the rock mass parameter of the powerhouse cavern (Section 5) and the other with the lowest parameter to check the worst-case scenario in terms of stability of the powerhouse and transformer cavern.

7.3.2. Model setup and input data

The cross-sectional model of the RS2 and the input data in Section 7.2 has been used for RS3 analysis with changes only at the mesh setup and displacement properties shown in Error! Reference source not found..

Table 7.11: Modal setup in RS2 and RS3

Model Setup	RS2	RS3
Analysis Type	Plain Strain	Uncoupled
Solver Type	Gaussian Elimination	Automatic
Convergence Type	Comprehensive	Absolute Force and Energy
Field Stress Type	Constant	Constant
Failure Criterion	Generalized Hoek and Brown	Generalized Hoek and Brown
Mesh Type	6 Noded Triangles Graded	4 Noded Tetrahedron

The disturbed zone of 4m just as in RS2 has been introduced in RS3 for stability assessment and support optimization. The entire length of 69m of the powerhouse and 47.6m of the transformer cavern has been introduced into the model. The external boundary has been set with expansion factor of 4 with gradation factor of 1. The restraint for the model is taken as auto restrain (underground).
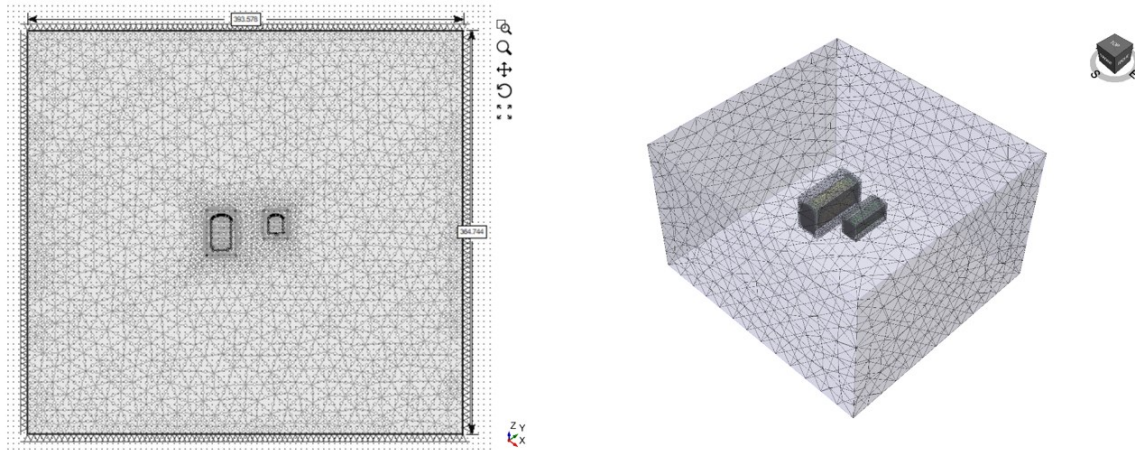
Figure 7.27: Model geometry for 3-dimensional analysis in the powerhouse and transformer cavern. Meshing in 2D model (left) and 3d model (right)

7.3.3.   Numerical Modelling Results
7.3.3.1.   Elastic Analysis
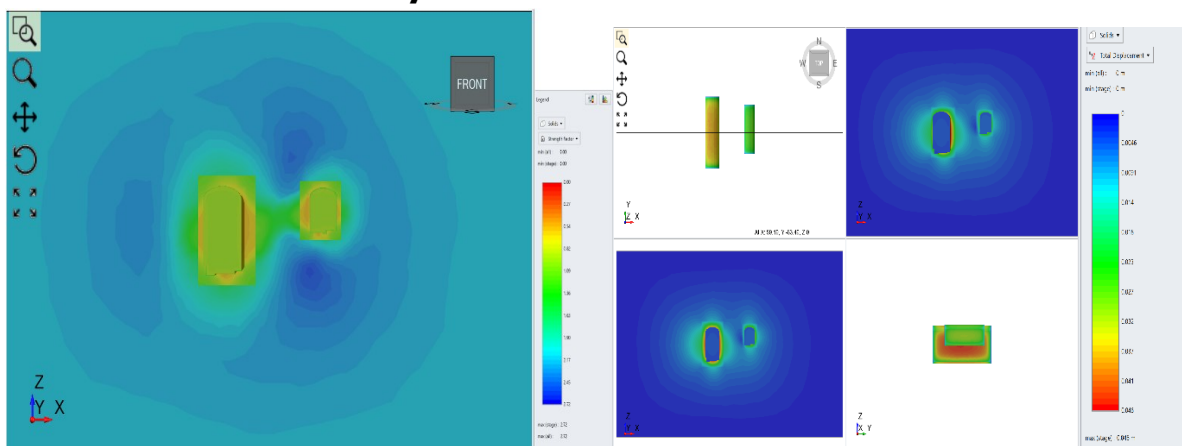
Figure 7.28: Strength Factor(left) and total displacement (right) around the powerhouse and transformer cavern

An elastic analysis using generalized Hoek and brown failure criteria shows that the total displacement is concentrated along roof of the cavern with the maximum value of 0.046m in Figure 7.28 which is slightly lower compared to 2D analysis where it showed 0.097 m (see Figure 7.16). Strength factor around the cavern is less than 1. Compared to RS2 , RS3 showed less severe rock mass state under excavation of cavern on comparing Figure 7.16 (from RS2) & Figure 7.28 (from RS3).

7.3.3.2.   **Plastic Analaysis**

Without Support

The simulation result for displacement contour is shown in Figure 7.29. It can be seen that deformation magnitude has increased significantly along sidewalls. The deformation value is as high as 0.1 m without support condition in this section. Similarly, yielding of rock mass seems to produce result 1/3 lower than that of RS2. The presence of very weak rock mass caused both shear and tensile failures around entire box model around tunnel under excavation shown in Figure 7.29.
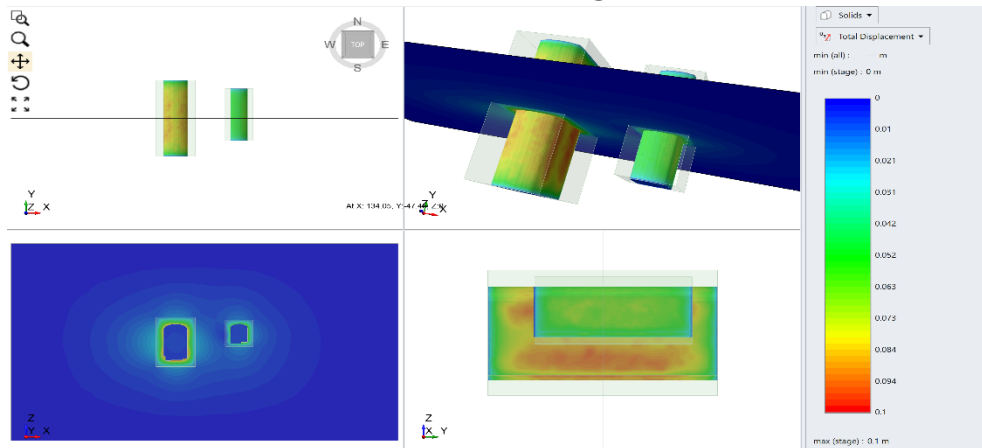
Figure 7.29: Total Displacement without support

With Support

Figure 7.30 show the support installed in the powerhouse and transformer cavern for plastic analysis. The Figure 7.31 shows the total displacement in bolt support while Figure 7.32 shows the total displacement In the liner support
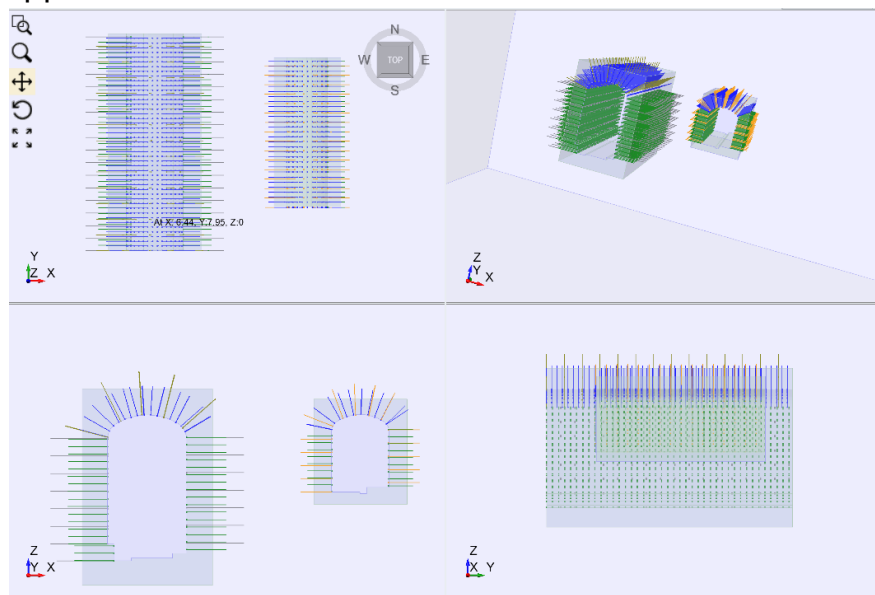
Figure 7.30: Installation of bolt in RS3
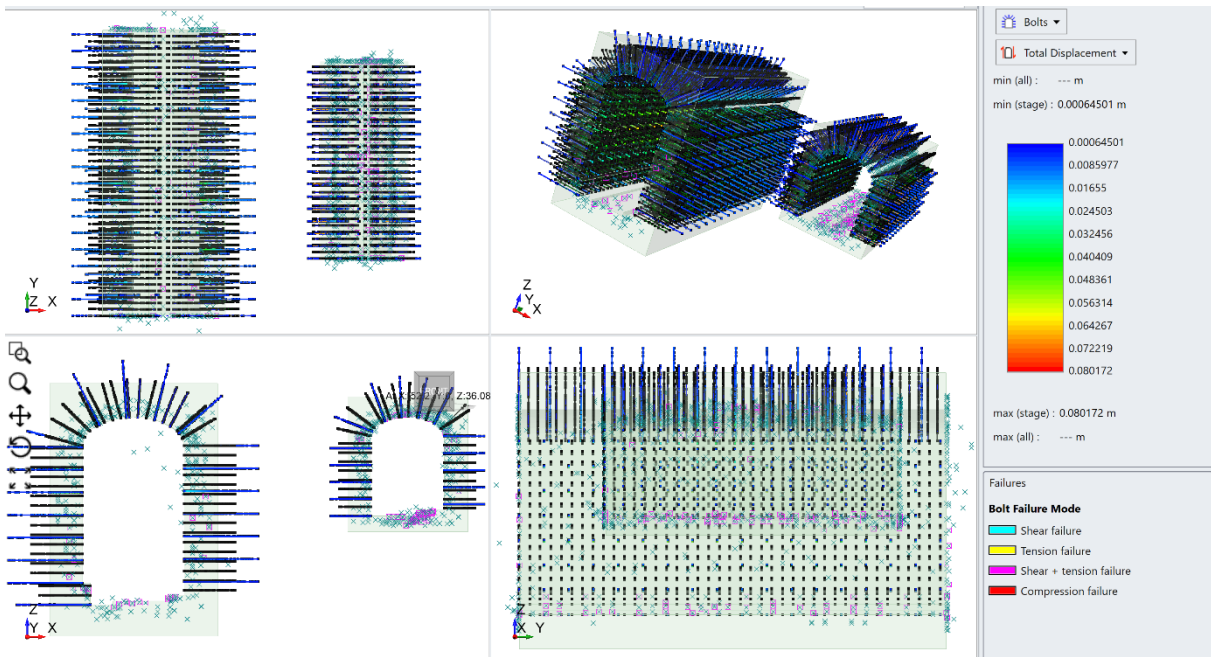
Figure 7.31: Total displacement in Bolt Support
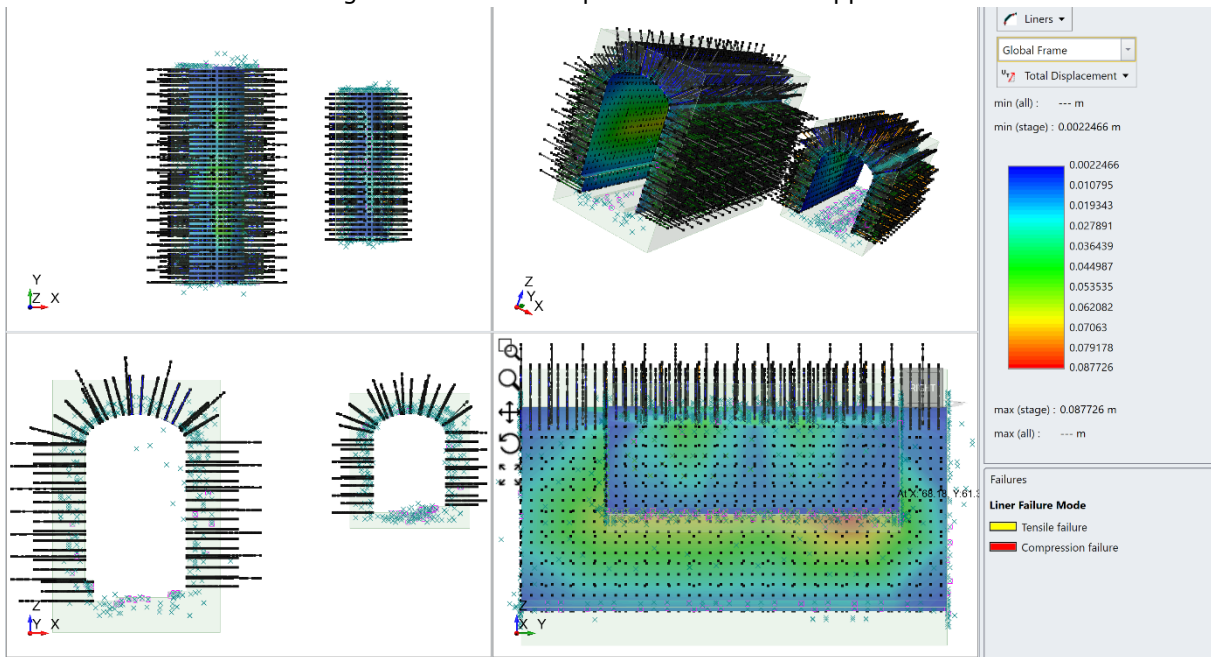
Figure 7.32: Total displacement in Liner Support

8. ASSESSMENT OF EARTHQUAKE IMPACT

As discussed in 2.5.1.2, Nepal lies in highly earthquake-prone regions, which require the underground structures to be assessed against the periodic dynamic earthquake. Permanent stress reduction occurs as a result of earthquakes, particularly in areas of weakness and shear zones (Basnet & Panthi, 2019). Since Tamakoshi V HEP is considered in an earthquake-prone zone, a dynamic analysis of the powerhouse and transformer cavern in the weak ground is carried out using the RS2 package.

The RS2 software is used to do 2D-Plain strain finite element modelling for dynamic analysis. The first stage in performing dynamic analysis is to create a static cross-sectional model of the study's relevant parts. In Chapter 7, a discussion of static modelling is done. The approach of dynamic model formation used in this work is detailed in this section. Then, pseudo-static, simplified dynamic, and full dynamic analyses are performed, as shown in Section 4.1.3.

8.1. Pseudo-static Analysis

For pseudo-static analysis, the seismic coefficient is defined in the seismic loading under the loading tab of the RS2 interface. The horizontal and vertical seismic coefficients are dimensionless factors applied to a body element (weight of each element in finite element mesh). The seismic force exerted in the model domain is calculated using Equation 8.1 and 8.2 in RS2. Furthermore, as the acceleration is recorded on the ground surface, it is crucial to obtain acceleration at a depth of interest. (Power et al., 1998) provide a factor to reduce the seismic acceleration at the depth as given in Table 3.1.

$$F_{hseismic} = \alpha_h A_{element} \gamma \qquad\qquad 8.1$$
$$F_{vseismic} = \alpha_v A_{element} \gamma \qquad\qquad 8.2$$

where,

α_h and α_v are seismic coefficients in horizontal and vertical directions in terms of acceleration due to gravity

$F_{hseismic}$ and $F_{vseismic}$ are seismic forces acting in horizontal and verticle directions

$A_{element}$ is an elemental area of mesh

γ is the unit weight of the element in the mesh

Equations 8.3 and 8.4 are used as input data for seismic coefficient, considering a factor of peak ground acceleration with gravity acceleration (Tshering, 2011). The present study incorporates the importance of PGA, as shown by the previous study (Rahman & Bai, 2018). According to (Basnet & Panthi, 2017, 2018, 2019), a PGA value in the range of 0.5 to 0.55g should be chosen for the project region. The natural damping of 5%

damping for a 2% probability of occurrence is considered for the analysis. In order to account for the depth of caverns, the amount is multiplied by 0.7 (Power et al., 1998). In the horizontal direction, the value utilized as input is 0.385g. For vertical direction, 1/3 of the horizontal seismic coefficient is implemented as the supervisor recommended (05/11/2022). Thus obtained value of vertical seismic acceleration is 0.128g.

$$\alpha_h = \frac{Acch.max}{g} \qquad \qquad 8.3$$

$$a_v = \frac{Accv.max}{g} \qquad \qquad 8.4$$

dWhere,

α_h and α_v are seismic coefficients in horizontal and vertical directions in terms of acceleration due to gravity

$Acc_{h.max}$ and $Acc_{v.max}$ are maximum acceleration in horizontal and vertical directions g is Acceleration due to gravity

Static model setups are utilized as the foundation of a dynamic model in the numerical modelling technique for Pseudo-Static Analysis. Then *seismic loading* is defined as the increased loading applied to the ground due to an earthquake.

Figure 8.1 shows the input interface and the model domain of seismic loading implementation.
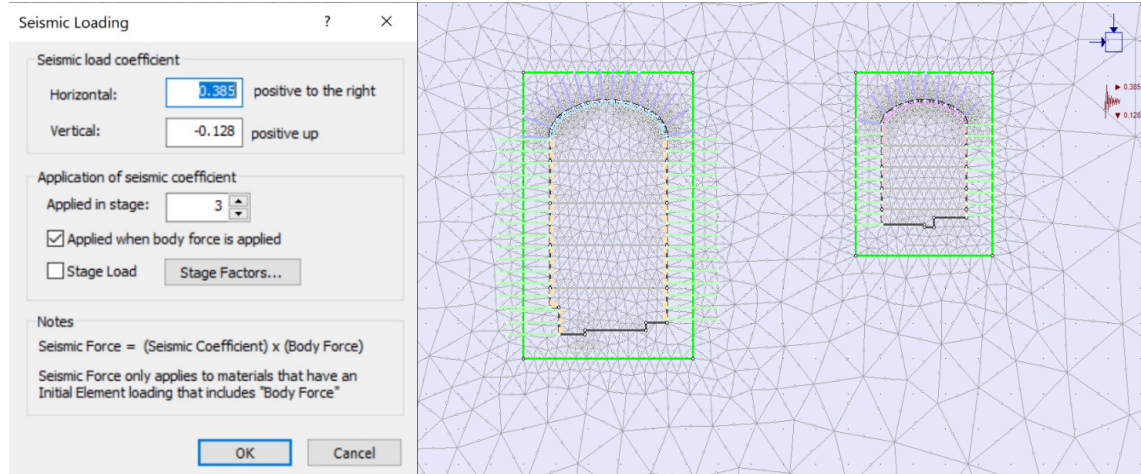
Figure 8.1: Input window for pseudostatic loading (left) and model showing the implementation of the seismic load

8.2. Simplified Dynamic Analysis

8.2.1. Dynamic Data Analysis and Nature of Damping:

For simple dynamic analysis, the 2015 Gorkha Earthquake data recorded at the Kanthi Path, Kathmandu, has been used as discussed in section 4.1.4.2. The raw data of acceleration and velocity spectrum from USGS are strong ground motions that cannot be used directly at the cavern's depth, so the data has been processed through the dynamic data analysis, a feature of

RS2 where the time series are analyzed. The amplitude spectrum, response spectrum, and arias intensity are all used in dynamic data analysis to visualize data attributes. The filter spectrum function provided in Dynamic Data analysis corrects residuals responsible for inaccuracies in data input. In addition, evaluating a local damping nature is a crucial problem for dynamic data analysis in this work. Rayleigh damping coefficients are used to compute the local damping factor.

As the distance between the source and the place of interest grows, amplitude attenuation develops. Rayleigh damping formulation is used to account for this phenomenon in numerical modelling. The damping matrix is provided by Equation 8.5 according to the Rayleigh damping formula (Rocscience, 2022b).

$$[C] = [\alpha_M][M] + [\beta_k][K] \qquad\qquad 8.5$$

Where,

α_M and β_K are mass and stiffness coefficients

[M] is the mass matrix

[K] is the Stiffness matrix

The mass coefficient (M) and stiffness coefficient (K) are estimated as the initial stage in dynamic analysis. As illustrated in Figure 8.3, cross-section profile models of the sections under examination are used to do this. Initially, a plain strain study is carried out in an elastic medium. This configuration is considered undamped, so there will be no energy dissipation. Then, under the "Define Dynamic Load" tab of RS2, the dynamic load is determined dependent on velocity. Finally, the time query function is set up at the cavern location to know the ground reaction at the place of interest. The X-velocity spectrum and Z-velocity spectrum of raw data from the Gorkha earthquake are presented in Figure 8.2.

The resulting velocity spectrum at the powerhouse and transformer caverns site is used as an input for the second undamped model after running the model and acquiring time-series data for an undamped model in the cross-sectional profile model. This velocity data is adjusted using the sinusoidal baseline correction method and filtered for a frequency range of 0 Hz to 1.9 Hz. For the Gorkha Earthquake, the frequency range is calculated from the raw data power spectrum where the most significant velocity is found, as illustrated in Figure 8.3.

Using the Natural Frequency Method, the acquired velocity is then utilized to calculate the Rayleigh damping coefficient (NFM). This approach evaluates the natural frequency of a structure to determine the resonant frequency and is recommended for usage in geological material by Rocscience (2022b). RS2 yielded values of (M) 0.2 and (K) 0.0072 for all sections. As illustrated in Figure 8.2, these values were calculated using 4.3

% damping for geological materials by Biggs and Biggs (1964). It is also worth noting that any static retraining, such as roller or fixed, is eliminated at the dynamic stage.
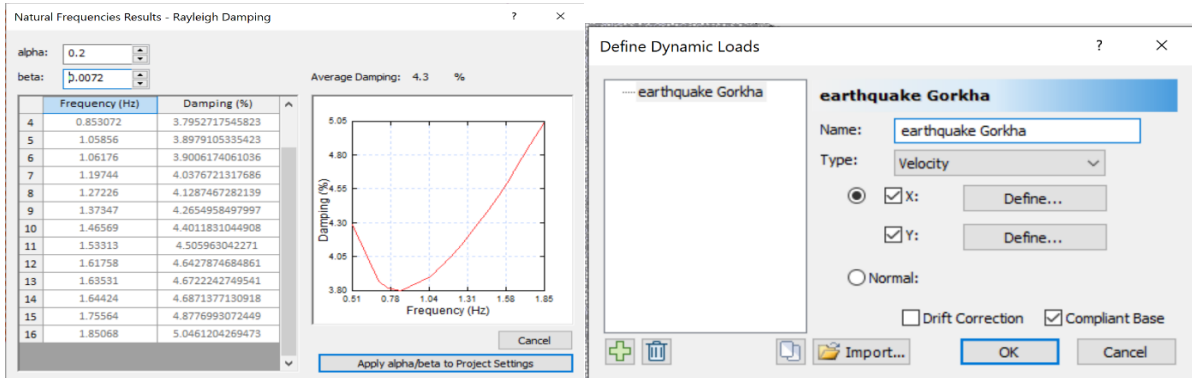
Figure 8.2: Dynamic Damping(left) and the dynamic load windows(right)
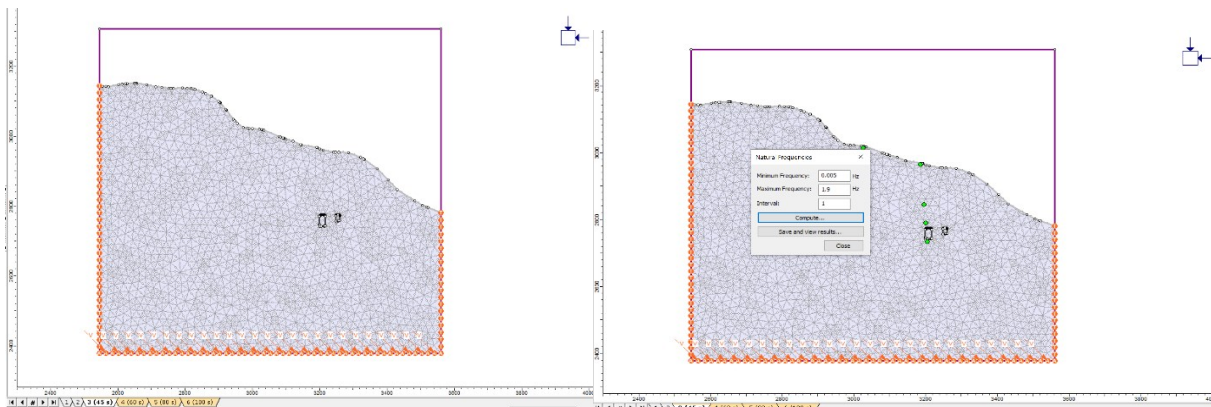
Figure 8.3: time query at the cavern depth (left) and the natural frequency modeller(right)

8.2.2.   Boundry Condition and loading

The model setup has considered dynamic boundary conditions to perform dynamic analysis of initial cross-sectional profile models. As mentioned in Section 8.1, static cavern cross-section models are taken as the base model. The dynamic stage is introduced with a 100-second time-step. The reason behind taking 100 seconds time step is the nature of the time series utilized. Figure 8.4, Figure 8.5 and Figure 8.6 shows that significant dynamic event occurrence is between time step of 0 seconds to 100 seconds for both East-West and along elevation. Two types of dynamic boundary conditions are applied for the cross-sectional profile models.

Along lateral boundaries of models, transmit boundary condition and at the base of models absorb boundary condition is implemented.

According to Rocscience (2022b), when a dynamic source is generated outside the model domain, the seismic wave in interest must transmit from the model through lateral boundaries. In the process, it should also be noted that wave reflection should be avoided. In such a case, transmit boundary condition is implemented. However, for the base, absorb boundary

condition is introduced where the base absorbs the wave and avoids transmission and reflection. Figure 8.3 show the setup used in dynamic model analysis.

8.2.3.   Deconvolution and time series of seismic data

When modelling, it's critical to understand how the input data is applied so the model may function well and create a result that accurately visualizes a real-world scenario. Deconvolution may be defined as adjusting the frequency and amplitude of seismic motion as it is implemented. The deconvolution type in RS2 can be either Rigid or Compliance Base. A compliance basis is explored in the current study, where input motion data is converted into force. The transition of ground motion into force is defined by equations 8.6 and 8.7 (Rocscience, 2022b). The usage of a compliance base is supported by the fact that downward motion should be absorbed to offer input in any outcrop motion comprising upward and downward motion in RS2 (Rocscience, 2022b)

$$F_n = (\rho V_p)v_n \qquad 8.6$$
$$F_s = (\rho V_s)v_s \qquad 8.7$$

Where,

F_n and F_s are transformed force normal and parallel force to the base
v_n and v_s are input velocity motion normal and parallel force to the base
V_n and V_s are pressure wave velocity and shear wave velocity
ρ is rock mass density

After the stepwise procedure of obtaining the raw data of strong ground motion to the deconvolution of the seismic data explained in Sections Dynamic Data Analysis and Nature of Damping: 8.2.1 to 8.2.3., the following time series is obtained for the cavern depth where the time query was setup.
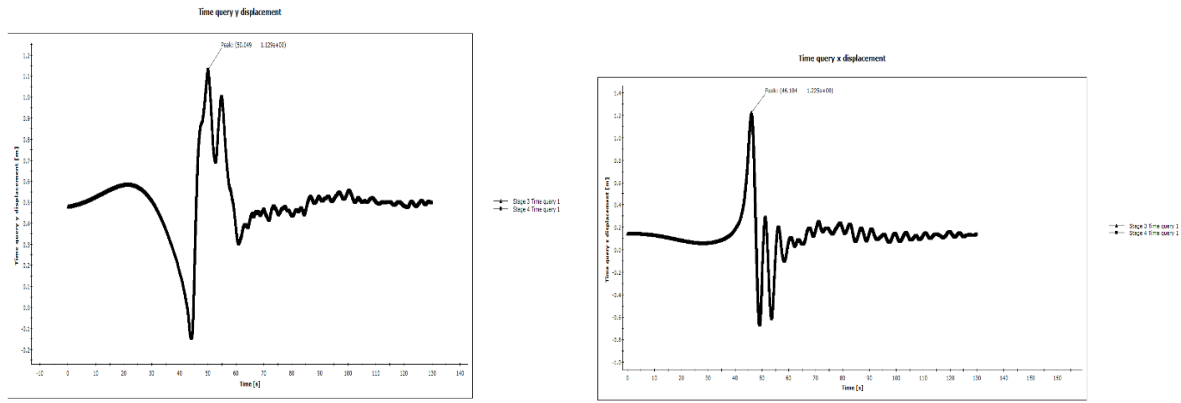
Figure 8.4: Displacement in Y-Direction (left) and Displacement in X-Direction (right)
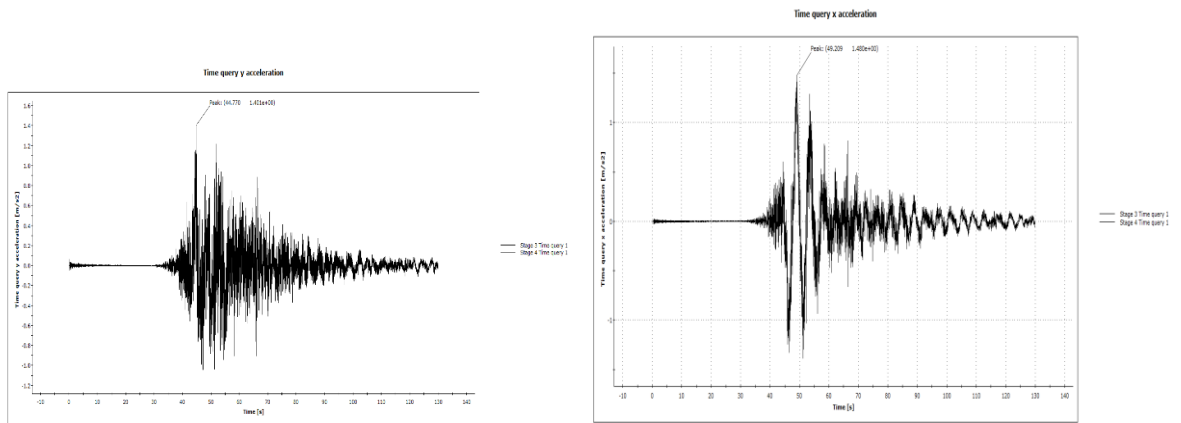
Figure 8.5: Acceleration in Y-Direction (left) and Acceleration in X-Direction (right)
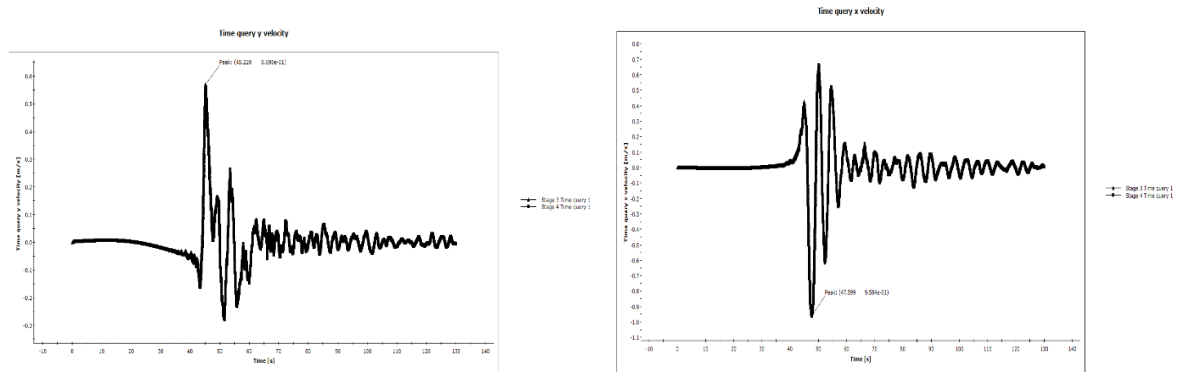
Figure 8.6:Velocity in Y-Direction (left) and velocity in X-Direction (right)

8.2.4.   Application of Simple Dynamic Load

The resulting time series of the acceleration, velocity, and displacement from Section 8.2.3 is applied to the box-boundary model using the pseudo-static method in Section 8.1. The horizontal and vertical seismic coefficient is defined in the model based on time independence philosophy. This seismic loading is an additional body force element obtained using equations 8.1 to 8.4. Figure 8.1. Shows the model setup for simplified

dynamic analysis, while Table 8.1 gives the maximum ground velocity and acceleration obtained for the cavern depth.

Table 8.1: Maximum ground velocity and acceleration

				Seismic Coefficient	
$Acc_{hmax}(m/s^2)$	$Acc_{vmax}(m/s^2)$	$Vel_{hmax}(m/s)$	$Vel_{vmax}(m/s)$	α_h	α_v
1.48	1.401	-0.958	0.569	0.151	0.143

8.3. Full Dynamic Analysis

To perform Full Dynamic Analysis, the procedure given in Section 8.2.1 to 8.2.3 are followed as simple dynamic analysis. The time series from Figures Figure 8.4 to Figure 8.6 are used at the input at the cavern location. Time series are implemented at the base with complaint base. The dynamic model is run for 100 seconds. The model setup is shown in Figure 8.7.
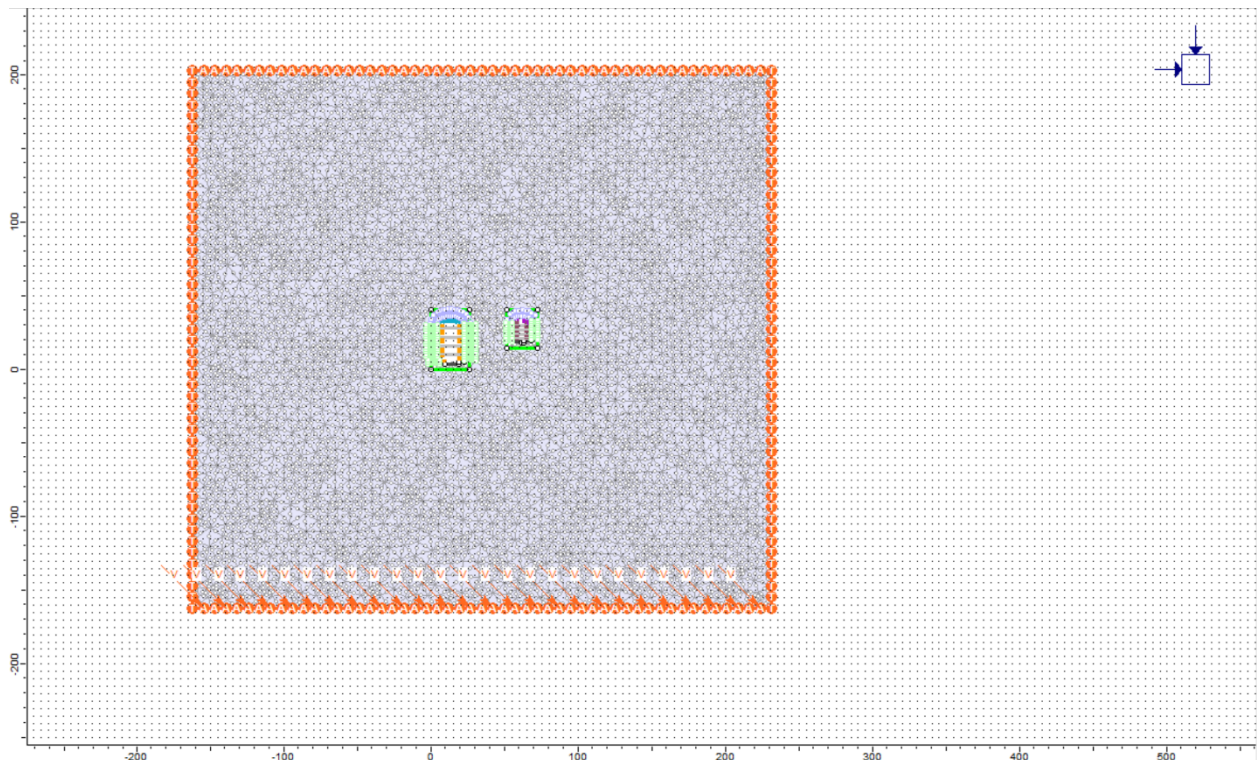
Figure 8.7: Model setup for Full dynamic Analysis

8.4. Results for Dynamic Analysis
8.4.1.   Pseudo-Static Analysis

Pseudo static analysis is carried out based on a static numerical model of sections. Here, peak ground acceleration is implemented. After the implementation of the seismic force, the number of the yield in the finite element has decreased while yield in the support bolts and liner has increased as compared to the static analysis. Figure 8.8 show the yield of the bolts and shotcrete support along the roof and walls of the caverns.

Different points of the cavern has been assigned with the letters from A to G at which the deformation is noted.
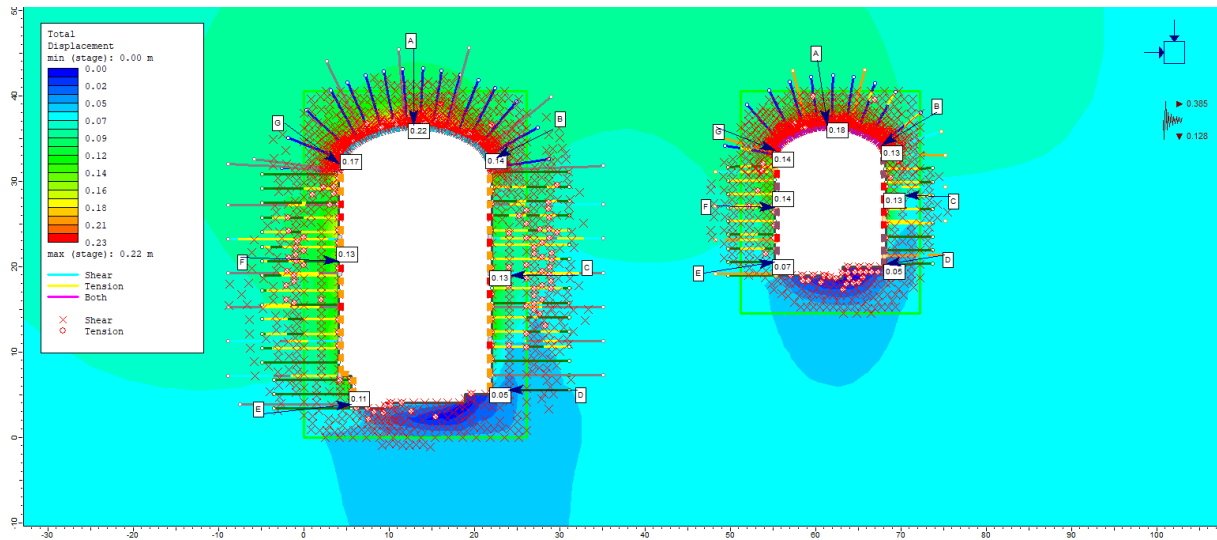
Figure 8.8: Plastic Model of Pseudo-static Analysis

The deformation in the cavern roof and walls has increased by 1.75 to 2 times with 0.07m to 0.1m in the pseudo-static analysis than in static analysis. The fully grouted and cable bolts in the walls of the cavern have mostly yielded in tension and few elements in shear. The finite element yield is increased from 1629 to 1693 which is not so much increase as compared to the bolt elements yield from 154 to 301 which is almost two times. The increment in shotcrete liner element is from 22 to 30 as indicated in red in Figure 8.8 and Table 8.2.

The capacity curve shows that the shotcrete support is taking the load and within the factor of safety of 2 with some elements yields at the edges of the roof and the walls of the powerhouse and transformer cavern as indicated in Figure 8.8 and Figure 8.10.

Figure 8.9 shows clearly that the deformation has increased with pseudo-static load applied on the static model.
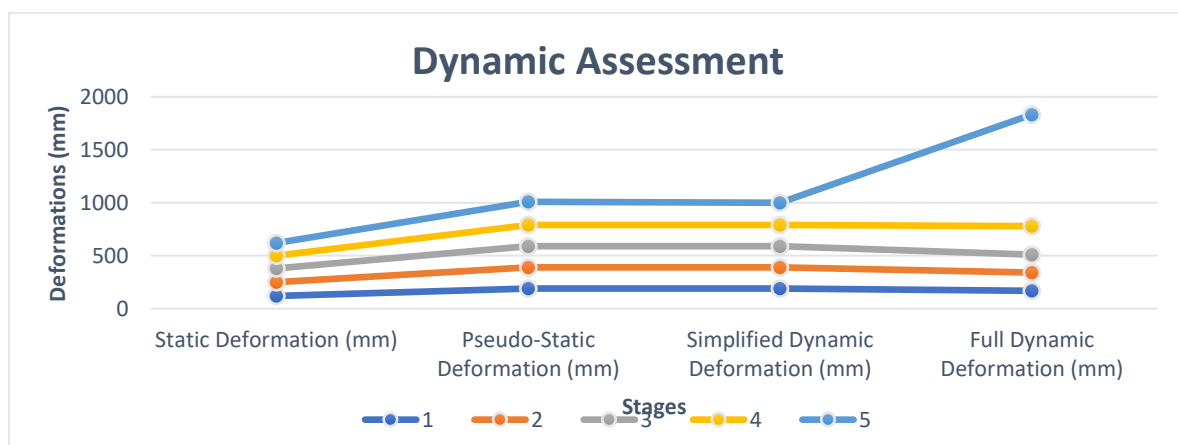
Figure 8.9: Deformation in different excavation stages after Dynamic Assessment
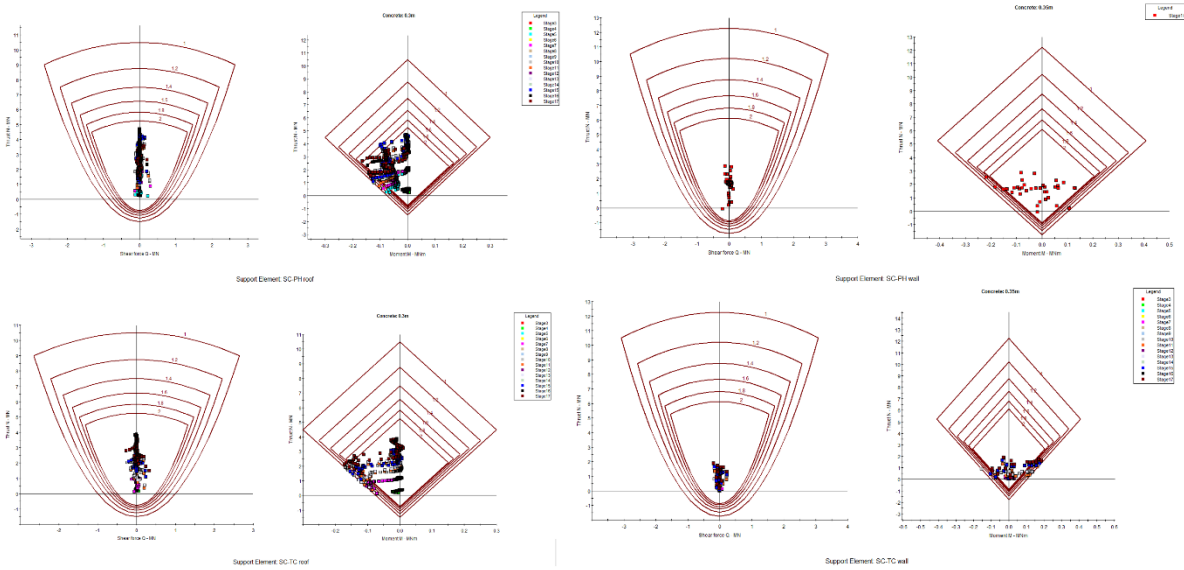
Figure 8.10: Support Capacity curve after the Pseudo-static Analysis

8.4.2. Simplified Dynamic Analysiss
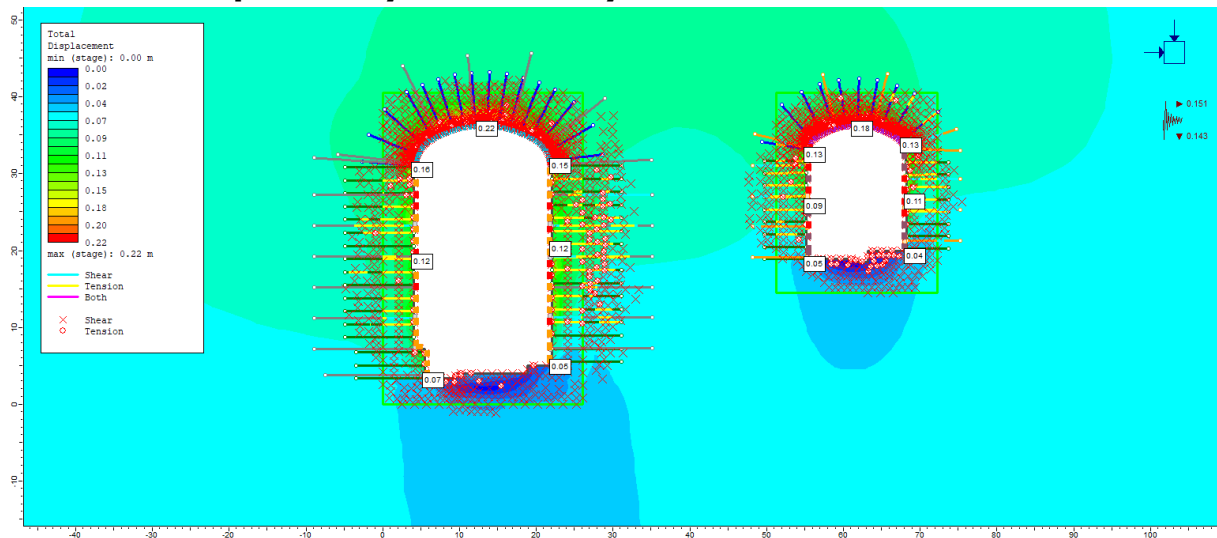
Figure 8.11: Plastic Model of the Simplified Dynamic Analaysis

A simplified dynamic analysis approach is used to calculate the dynamic load change in the caverns location. This dynamic load change is then converted to a single value representing the maximum acceleration of the ground reaction. Such dynamic analysis is performed using numerical models, shown in Figure 8.11 and as described in Section 8.2. After the value of the maximum PGA is determined, as given in Table 8.1, a seismic coefficient is defined according to Equation 8.3 and Equation 8.4 for the horizontal and vertical directions, respectively. In the simplified dynamic analysis, no reduction is made to the PGA value because the dynamic data analysis is performed directly to determine the PGA values required to estimate the seismic coefficient at the caverns location. Such an analysis is

based on finding the highest acceleration maximum at a location of interest. An approach similar to pseudostatic analysis is performed to obtain results for the analysis of the support systems of interest.
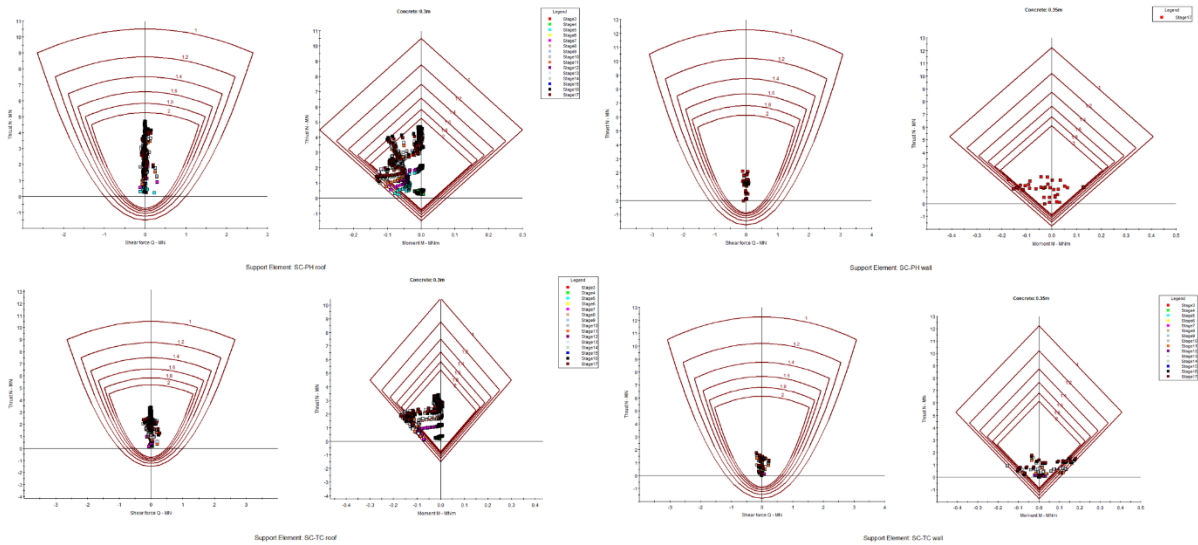
Figure 8.12: Support Capacity Curve after Simple Dynamic Analysis

The support yield in the bolt element is increased from 154 to 239, liner yield from 22 to 30 and the finite element yield from 1629 to 1651. The total deformation has increased by 0.8 times as shown in Table 8.2. figure 8.5 shows the yield in the bolts and liner while figure 8.6 shows the capacity curve where the concrete support has increased yield but still within the safety factor of 2 in Shear force and between 1 to 2 with spread of moment.

8.4.3. Full Dynamic Analysis

The full Dynamic approach considers the implementation of time series of seismic motions in the cavern depth. A dynamic model is run for up to 100 seconds to evaluate the supports over time so that high intensity seismic waves are captured (see Figure 8.6, Figure 8.7, and Figure 8.8)
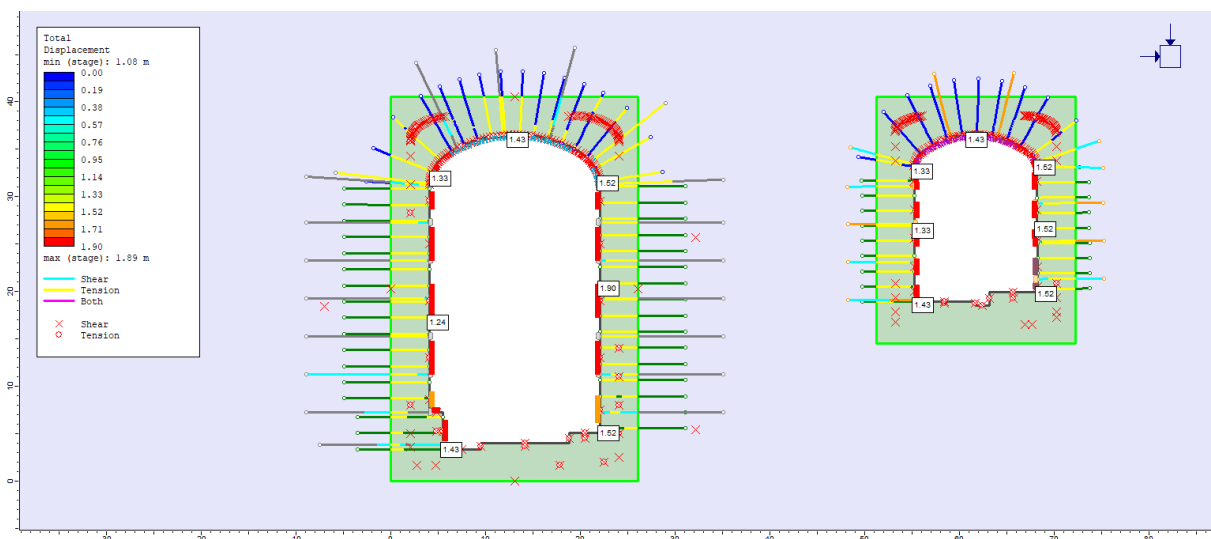
Figure 8.13: Plastic model of the Full Dynamic Analysis

Figure 8.7 shows the yield in most of the bolts and liner element in the roof and the wall of both the powerhouse and transformer cavern. The support capacity curve in Figure 8.8 shows that the concrete support has yielded with the factor of safety lying between 1.2 to 2 for powerhouse roof and between 1.6 to 2 for transformer cavern roof. Most of the liner support element has yielded with spread in moment for caverns roof while the liner support at walls are spread within safety factor of 2.
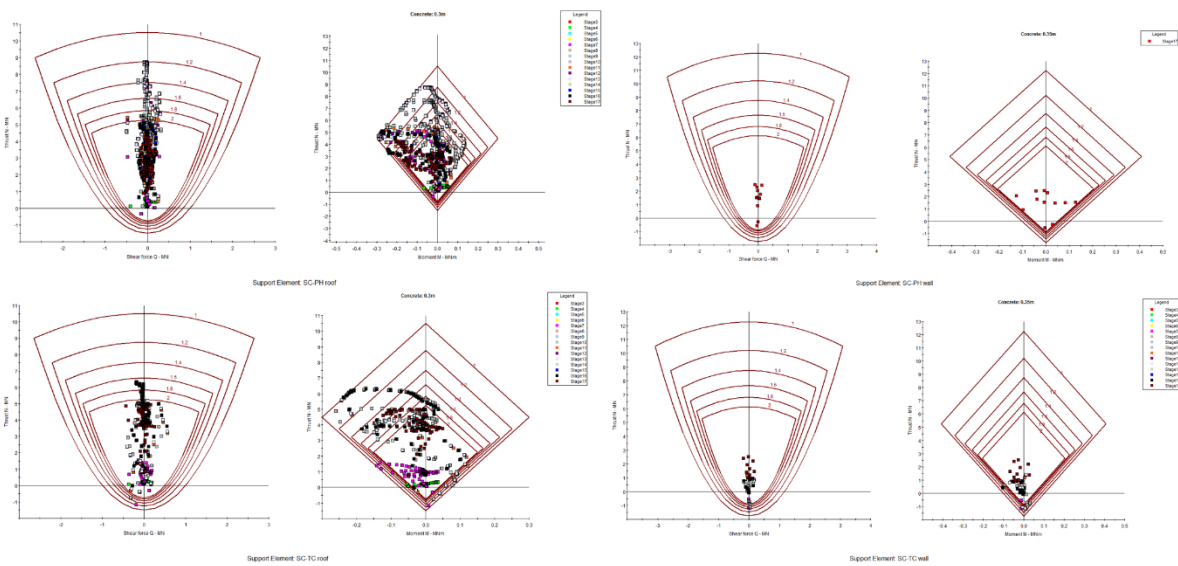
Figure 8.14: Support Capacity curve after Full Dynamic Analysis

The deformation of the cavern and the shift of the wall can be seen in
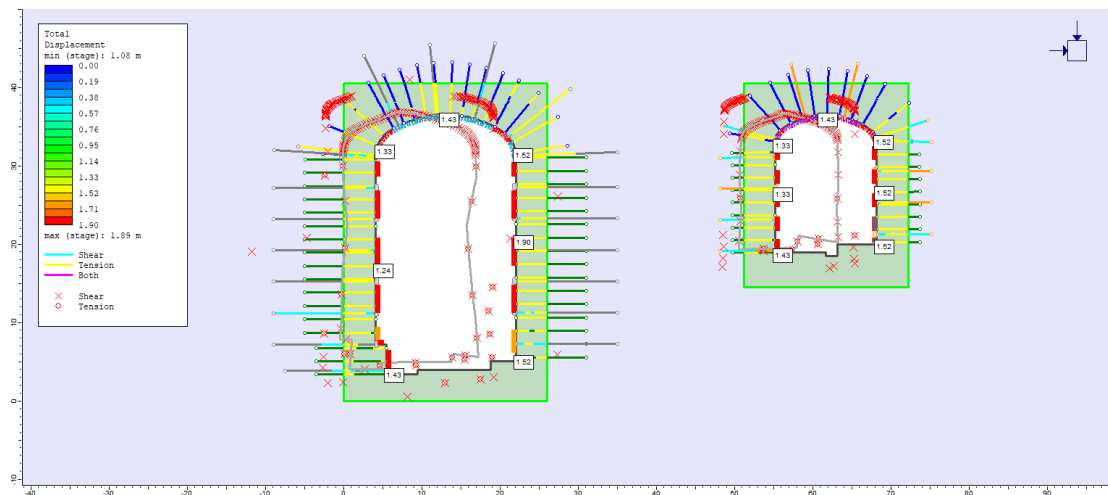
Figure 8.15: Full Dynamic model with shift of the contour wall The probable deformation with the intensity of earthquake is 1.43m with the applied strong ground motion.
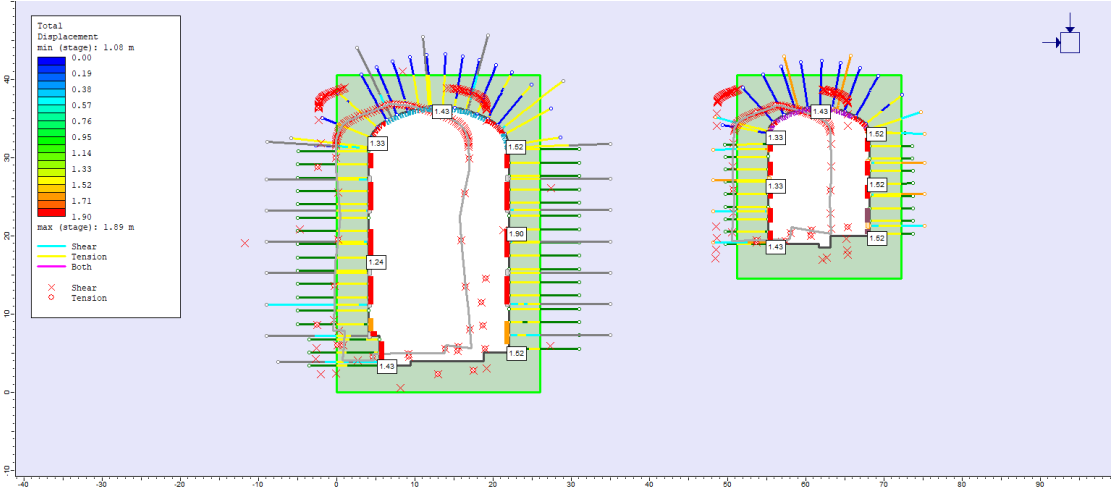
Figure 8.15: Full Dynamic model with shift of the contour wall

Table 8.2: Deformation and yield due to dynamic loading at different stages of cavern excavation

	Static Condition				Pseudo Dynamic				Simplified Dynamic				Full Dynamic			
Stage	Deformation (mm)	yielded finite element	yielded bolt	yielded liner	Deformation (mm)	yielded finite element	yielded bolt	yielded liner	Deformation (mm)	yielded finite element	yielded bolt	yielded liner	Deformation (mm)	yielded finite element	yielded bolt	yielded liner
1	120	1203	0	0	190	1170	0	0	190	1170	0	0	170	160	0	0
2	130	1261	37	10	200	1235	37	14	200	1235	37	14	170	158	29	4
3	130	1373	76	14	200	1301	74	47	200	1301	74	17	170	165	87	8
4	120	1665	129	19	200	1511	174	27	200	1511	174	27	270	197	171	35
5	120	1629	154	22	220	1693	301	30	210	1651	239	30	1052	191	382	51

110

9. COMPARISION AND DISCUSSION
9.1. Powerhouse Design and layout

The construction of the powerhouse underground is always a challenge in terms of location, orientation, shape and size of the cavern. The proposed design of the powerhouse and transformer cavern for Tamakoshi V HEP with augen gneiss with parting of schists. In this paper, the powerhouse and transformer cavern were evaluated based on the existing design principles and criteria of many researchers and scientists (Section 3.1). The powerhouse and transformer cavern are located at a depth of 186.84 m and 176. 36 m, which have good rock cover, and the effect of weathering is also very low according to the rock mass evaluation (Section 4.2.2.6). The powerhouse and transformer cavern are located 200 m from the public road, so the construction material can be transported to the site more easily through the exploratory tunnel constructed near the powerhouse. The possibility of a new site is quite difficult in light of the land acquisition that has already occurred. Changing the location could change the desired power generation, which is not desired in this study. For this reason, the orientation will be discussed further. The shape of the caverns is a curved roof with smooth transitions between the roof and the wall, which prevents the formation of cracks in case of protruding corners.

The rosette plot in Figure 4.5 shows the original and alternative alignments with the joint set and tectonic direction. The original alignment has an unfavourable orientation with the dominant main joint sloping steeply toward high walls, and the angle between the cavern alignment and the tectonic is 100°. The alternative orientation is oriented at an angle close to the bisection of the two dominant main joints J1 and Jf with a minimum angle of 15°-25°, as recommended by (Nilsen & Palmström, 2000). The alternative orientation is more favourable in terms of avoiding structurally induced instabilities (Section 3.1.2). The angle between the alternative orientation and tectonic stress is 20°, which could contribute to horizontal principal stresses. Skewing of stresses in the cross-section of the cavern due to topographic effects can lead to a concentration of stresses in the part of the roof facing the valley side, leaving the other side of the roof stress-free and increasing the failure of the block camber, so that special care should be taken.

9.2.   Stability assessment of the Powerhouse cavern
9.2.1.   Stress Distribution

Using empirical and analytical methods, it is relatively difficult to make accurate calculations of stress distribution. The irregular cavern shape and the angle between the principal stresses and the horizontal and vertical

axes are the main reasons for such difficulties. Therefore, these results should only be indicative and should not reflect the exact values of the stress magnitudes. The topographical influence on the stresses can be clearly seen in the results of the numerical models, which is not possible with analytical and empirical methods. The Kirsch equation does not take into account the shape of the outcrop and underestimates the stress values in the ceiling of the cavern. The properties of the rock mass, which affect the radial distribution of the secondary stresses, are also not taken into account in Kirsch's solution. The empirical methods proposed by (Hoek & Brown, 1980) provide stress values that are in better agreement with the disturbed zone for both the powerhouse and transformer orientations, but lower than the values for the undisturbed zone. The disturbed zone has a lower Young's modulus than the rest of the rock mass, so some of the stress is transmitted radially into the less disturbed rock mass. The outcrop shapes used in the empirical method are generalized.

9.2.2. Stability assessment

There are two different instability problems that can occur in the Tamakoshi V powerhouse and transformer cavern HEP. They are wedge/block falls and plastic deformations however, rockburst analysis has also been done altogether. The wedge/block fall events were analyzed using the input parameters from the geological mapping. The background and results of the instabilities are quantified. The stability of the wedges and blocks is verified by numerical modeling using Unwedge 5.0. In case of plastic deformations, available geological data are used to quantify the deformations in the powerhouse and transformer cavern. Different methods such as empirical, semi-empirical, analytical and numerical modeling with RS2 and RS3 are used to evaluate the plastic deformation.

Referring to the results of empirical methods, From the Q-system, the deformation that was estimated at the roof was 0.0739 m and the along the wall was 0.131 m, it is decided to apply available semi-empirical and analytical methods to quantify strain in the powerhouse and transformer cavern. The methods of (Hoek & Marinos, 2000) and (Panthi & Shrestha, 2018) were used to calculate the plastic strain along the cavern length and resulted in strains up to 0.18 % and 0.90 % without support, respectively, confirming the few stability problems. This tunnel instability is evidenced by the use of Convergence confinement method, which shows a similar extent of deformation when an intermediate stress scenario is used. The vertical stress condition overestimates the deformation and therefore suggests that it is not very useful for weak rock conditions. CCM is the most developed method as it takes into account the effects of the working face. The longitudinal deformation profiles generated provide information on how far

from the working face the deformation of the tunnel is significant. The use of numerical models has enhanced the visualization of the instabilities observed in the tunnel. The models provided results comparable to those obtained by other methods. Both elastic and plastic analysis were performed in the numerical model. It should be noted that only the numerical model and CCM are able to evaluate the structural system. The critical sections mentioned above were particularly studied, and it was clearly seen that these sections had significantly higher deformations and most of the supports used yielded and were therefore inadequate. Therefore, the author recommends that these sections need to be strengthened with higher support measures.

9.3. Comparison of impact of static loading and dynamic loading

The stress situation in the rock is influenced by both tectonic activity and the geologic setting. This influence is even more pronounced in the Himalayan region, where tectonic movements are active, leading to periodic dynamic earthquakes. As a result of earthquakes, there is a permanent reduction in the stress state, especially in areas of weakness and shear zones (Basnet & Panthi, 2019). On the other hand, if the rock is solid, homogeneous, and of good quality, the risk of stress reduction under dynamic loading is minimal, and stress accumulation may occur in certain cases. Apart from the change in stress state, stability problems may also occur during an earthquake, such as loosening of rocks in poor rock formations, failure of several supports, and increase in deformation from a few centimeters to several meters (Palmstrom & Stille, 2010). Therefore, it is important to perform dynamic analysis in addition to static analysis to study the change in stress state, failure of supports, and change in deformation in a seismically active region such as the Himalayas.

The stability of the powerhouse and transformer cavern of Tamakoshi V HEP was evaluated under static loading (see Section 7.2) and dynamic loading (see Section 8) using the numerical model in RS2 and RS3. Figure 9.1 and Figure 9.2 show the deformation along the cavern perimeter under static and dynamic loading for the powerhouse and transformer cavern, respectively. As shown in Figure 7.18, Figure 9.1 and Figure 9.2, the deformation of the roof (A) of the powerhouse cavern is 0.12 m under static loading, 0.22 m under psuedo-static and simplified dynamic loading, and 1.43 m under full dynamic loading. For the transformer cavern, the deformation in the roof (A) is 0.09 m under static loading, 0.18 m under pseudostatic and simplified dynamic loading, and 1.43 m under full dynamic loading. This increase could be the reason for the increased failure of bolts and lining elements during the dynamic analysis. The total displacement is

0.1 m to 1.2 m, which could be due to the weak and critical rock mass with the disturbed zone. The stress increase is 0.3 MPa in the caverns. However, discontinuities such as zones of weakness and shear in the rock dampen the stress state during an earthquake.
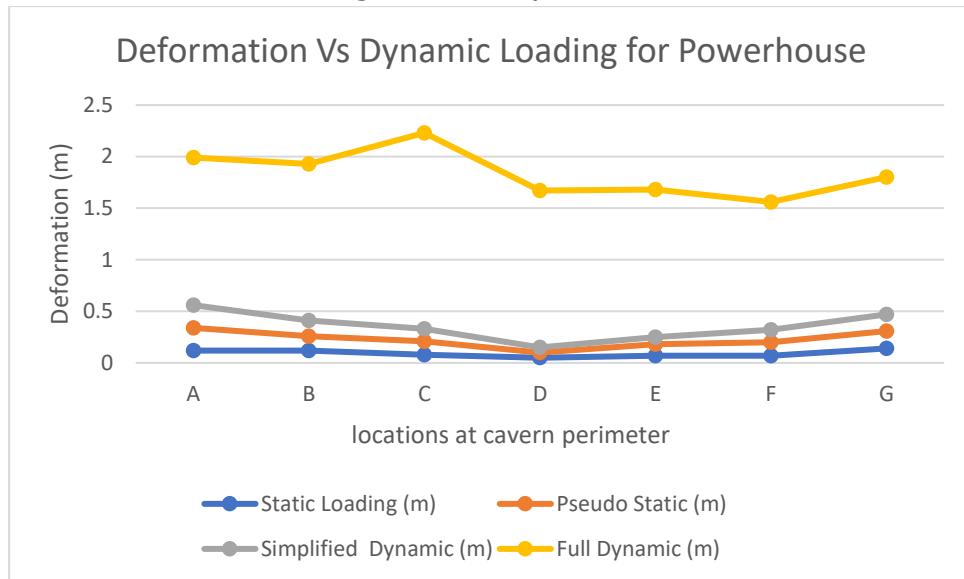
Figure 9.1: Deformations at different point of the powerhouse cavern under dynamic loading
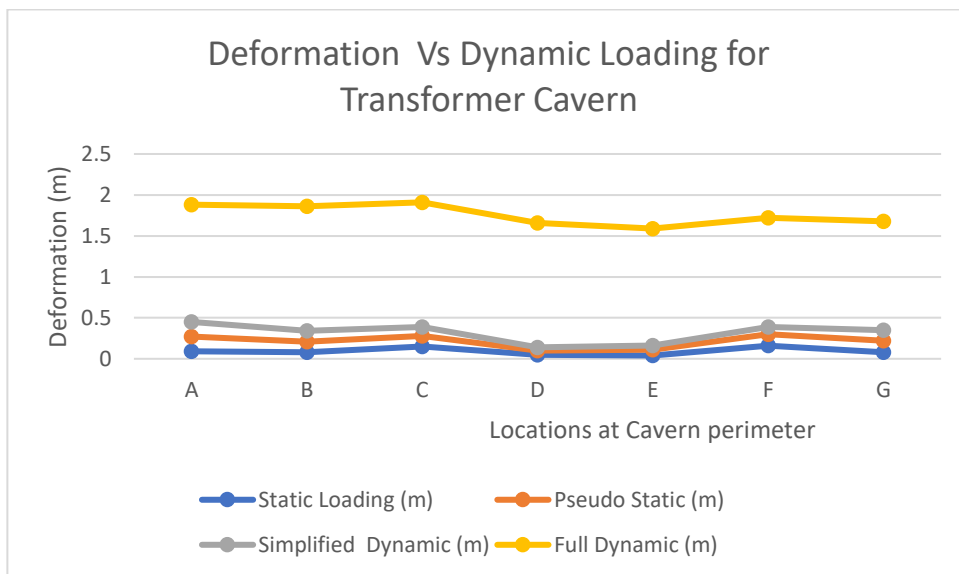
Figure 9.2: Deformation at different point of transformer cavern under dynamic loading

10. CONCLUSION AND RECOMMENDATION
10.1. Conclusion

The presence of highly schistose, fractured, weak rock masses and active tectonic stresses creates several stability problems in the construction of underground openings in the Himalayan geology. The most common problems are block/wedge falls and plastic deformation/squeezing at considerable depth and weak rock masses. Tamakoshi V HEP was selected for stability assessment where block/wedge falls and plastic deformation were analysed along with seismic loading. The main cause of instability is the poor condition of the rock in the powerhouse and transformer cavern. Considering the location and importance of the power plant complex, a safe and cost-effective design is a must, which includes the placement, alignment, and overall stability of the caverns.

Analysis of Tamakoshi V HEP identified minor block/wedge failures on the roof and wall of the powerhouse and transformer cavern. The rock quality is very weak with a Q value of 0.833. The wedge/block failure analysis was performed numerically using the UnWedge 5.0 programme. Similarly, the rock burst analysis was performed using the Kirsch relation and the method of Hoek and Brown. Plastic deformation analysis is performed using 5 different methods, namely empirical methods such as (Singh et al., 1992), (Goel et al., 1995) and Q-system (Grimstad & Barton, 1993a), semi-empirical methods such as (Hoek & Marinos, 2000) and (Panthi & Shrestha, 2018) and analytical methods such as Convergence Confinement Method (CCM). Static and dynamic analysis and numerical modelling using RS2 and RS3. Rock support was estimated using empirical and numerical methods. All of these methods require good estimates of in-situ stress and rock properties. Therefore, the estimation of input parameters is an important task for the analysis. The main conclusions from this work are presented below:

- ❖ Estimating rock mass parameters was one of the major challenges during the analysis. They were estimated and cross-checked based on available geological reports, literature, and discussions with the supervisor to
- ❖ Wedge/block fall has been carried out based on geological mapping data in the roof and wall of the caverns. The analysis UnWedge 5.0. In UnWedge, the analysis was performed using both deterministic and probabilistic approaches with support optimization.
- ❖ Q-system and empirical formulas, both suggest bolt length of 6 m bolt for the roof and 10 m bolt for the wall. Similar lengths of bolts for the roof and the wall are provided in Numerical model but with different spacing, and further recommended

❖ Force acting on the subsurface rock support during a seismic event. The evaluation of support pressure, conducted using an empirical, semi-empirical, and analytical approach to support pressure and a numerical model evaluation of the induced internal forces in a permanent support system.

❖ It was found that support systems in weak rock mass environments are subjected to high seismic loads with increasing depth.

❖ The deformation behaviour of a support system is not always useful to compare support systems.

❖ RS2 and RS3 were used for the deformation analysis of the powerhouse and transformer cavern. The results of the numerical simulations can be compared to some extent with the results of other analyses. This proves that these softwares' FEM can be used in the design of caverns in weak rock.

❖ The use of disturbed zone intensifies the criticality of the analysis making the support estimation more intensive.

10.2. Recommendation

The recommendations for the proper procedure for analysis of deformations in a cavern are affected by the limitations in this study.

▪ Stress measurement at the site is essential for verification of the estimated value from various analysis methods.

▪ Underground excavations in seismically active areas need to be assessed for stability. The capacity to survive a dynamic earthquake should also be taken into consideration, rather than just optimizing designs for static conditions.

▪ Ground water effect has not been considered in entire study. Therefore, effect of water can be seen during evaluation of stability in the powerhouse and transformer caverns.

▪ Monitoring of cavern behavior like deformation, inflow/leakage, block fall, failure in support during construction and operational period should always be prioritized so that effectiveness of support can be determined.

▪ Field observations and laboratory test are very important for accurate estimation of rock mass properties since these input parameters are the most important factors for analysis.

▪ Under the "design, as you go" philosophy, where assumed parameters and predictions are adjusted in conjunction with available information and actual rock conditions as construction progresses, the deformation of the test tunnel near the powerhouse should be monitored. Numerical modelling should also be used in the

powerhouse cavern. Any necessary changes to the construction sequence and support means should be made on this basis and after consultation with an experienced engineering geologist.

REFERENCES

Aydan, Ö., Akagi, T., & Kawamoto, T. (1993). The squeezing potential of rocks around tunnels; theory and prediction. *Rock Mechanics and Rock Engineering*, *26*(2), 137–163.

Barla, G., Borri-Brunetto, M., Devin, P., & Zaninetti, A. (1995). *Validation of a distinct element model for toppling rock slopes*. 8th ISRM Congress.

Barton, N. (2002). Some new Q-value correlations to assist in site characterisation and tunnel design. *International Journal of Rock Mechanics and Mining Sciences*, *39*(2), 185–216.

Barton, N., Lien, R., & Lunde, J. (1974). *Analysis of Rock Mass Quality and Support Practice in Tunneling: And a Guide for Estimating Support Requirements*. Norwegian Geotechnical Institute Oslo.

Basnet, C. B., & Panthi, K. K. (2017). 3D in-Situ Stress Model of Upper Tamakoshi Hydroelectric Project Area. *Hydro Nepal: Journal of Water, Energy and Environment*, *21*, 34–41. https://doi.org/10.3126/hn.v21i0.17819

Basnet, C. B., & Panthi, K. K. (2018). Analysis of unlined pressure shafts and tunnels of selected Norwegian hydropower projects. *Journal of Rock Mechanics and Geotechnical Engineering*, *10*(3), 486–512.

Basnet, C. B., & Panthi, K. K. (2019). Evaluation on the Minimum Principal Stress State and Potential Hydraulic Jacking from the Shotcrete-Lined Pressure Tunnel: A Case from Nepal. *Rock Mechanics and Rock Engineering*, *52*(7), 2377–2399. https://doi.org/10.1007/s00603-019-1734-z

Bieniawski, Z. (n.d.). *T.(1976): Rock mass classification in rock engineering*. 97–106.

Bieniawski, Z. T. (1989). *Engineering rock mass classifications: A complete manual for engineers and geologists in mining, civil, and petroleum engineering*. John Wiley & Sons.

Brady, B. H. G., & Brown, E. T. (2007). Rock mechanics and mining engineering. In *Rock Mechanics for underground mining* (pp. 1–16). Springer.

Cai, M., & Kaiser, P. (2006). Visualization of rock mass classification systems. *Geotechnical and Geological Engineering*, *24*(4), 1089–1102. https://doi.org/10.1007/s10706-005-7464-x

Cai, M., Kaiser, P. K., Tasaka, Y., & Minami, M. (2007). Determination of residual strength parameters of jointed rock masses using the GSI system. *International Journal of Rock Mechanics and Mining Sciences*, *44*(2), 247–265. https://doi.org/10.1016/j.ijrmms.2006.07.005

Cai, M., Kaiser, P., Uno, H., Tasaka, Y., & Minami, M. (2004). Estimation of rock mass deformation modulus and strength of jointed hard rock masses using the GSI system. *International Journal of Rock Mechanics and Mining Sciences*, *41*(1), 3–19.

Carranza-Torres, C., & Fairhurst, C. (1999). The elasto-plastic response of underground excavations in rock masses that satisfy the Hoek–Brown failure criterion. *International Journal of Rock Mechanics and Mining Sciences*, *36*(6), 777–809.

Carranza-Torres, C., & Fairhurst, C. (2000). Application of the Convergence-Confinement method of tunnel design to rock masses that satisfy the Hoek-Brown failure criterion. *Tunnelling and Underground Space Technology*, *15*(2), 187–213. https://doi.org/10.1016/S0886-7798(00)00046-8

Chandra, S., Nilsen, B., & Lu, M. (2010). Predicting excavation methods and rock support: A case study from the Himalayan region of India. *Bulletin of Engineering Geology and the Environment*, *69*(2), 257–266.

Chauhan, K. (2020). *Planning and Rock Engineering Design of the Underground Structures of the Tamakoshi V Hydroelectric Project*.

Duncan Fama, M. (1993). *Numerical modeling of yield zones in weak rock*.

Eberhardt, E. (2012). The hoek–brown failure criterion. In *The ISRM Suggested Methods for Rock Characterization, Testing and Monitoring: 2007-2014* (pp. 233–240). Springer.

Edvardsson, S., & Broch, E. (n.d.). *UNDERGROUND POWERHOUSES AND HIGH PRESSURE TUNNELS*. 2.

Edvardsson, S., & Broch, E. (2002). Underground powerhouses and high pressure tunnels. Hydropower Development No. 14, Dept. *Hydraulic and Environmental Engineering, NTNU. Trondheim*.

Edvardsson, S., & Broch, E. (2003). *Underground powerhouses and high pressure tunnels* (Issue BOOK). Norwegian University of Science and Technology, dpt of Hydraulic and ….

Gattinoni, P., Pizzarotti, E. M., & Scesi, L. (2014). *Engineering geology for underground works*. Springer.

Goel, R. K., Jethwa, J. L., & Paithankar, A. G. (1995). Indian experiences with Q and RMR systems. *Tunnelling and Underground Space Technology*, *10*(1), 97–109.

Goel, R. K., Jethwa, J. L., & Paithankar, A. G. (1996). Correlation between Barton's Q and Bieniawski's RMR—A new approach. *International Journal of Rock Mechanics and Mining Sciences & Geomechanics Abstracts*, *33*(2), 179–181. https://doi.org/10.1016/0148-9062(95)00057-7

Goodman, R. E. (1989). *Introduction to rock mechanics* (Vol. 2). Wiley New York.

Grimstad, E. d. (1993). *Updating the Q-system for NMT*. Proceedings of the International Symposium on Sprayed Concrete-Modern use of wet mix sprayed concrete for underground support, Fagemes, Oslo, Norwegian Concrete Association, 1993.

Grimstad, E., & Barton, N. (1993a). Updating of the Q system for NMT-Intl symposium on sprayed concrete-Modern use of wet mix sprayed concrete for underground support. *Fagernes Technol*, *22*, 377–387.

Grimstad, E., & Barton, N. (1993b). Updating of the Q system for NMT-Intl symposium on sprayed concrete-Modern use of wet mix sprayed concrete for underground support. *Fagernes Technol*, *22*, 377–387.

Hammett, R., & Hoek, E. (1981). Design of large underground caverns for hydroelectric projects with particular reference to structurally controlled failure mechanisms. *Recent Developments in Geotechnical Engineering for Hydro Projects.(Edited by Kulhawy FH)*, 192–206.

Henriksen, A., & Selmer-Olsen, A. R. (1970). Automatic methods for determining nitrate and nitrite in water and soil extracts. *Analyst*, *95*(1130), 514–518.

Hoek, E. (1994). *Strength of rock and rock masse*.

Hoek, E. (2007). Rock mass properties. *Practical Rock Engineering*, *7*.

Hoek, E., & Brown, E. T. (1980). Empirical strength criterion for rock masses. *Journal of the Geotechnical Engineering Division*, *106*(9), 1013–1035.

Hoek, E., & Brown, E. T. (1997). Practical estimates of rock mass strength. *International Journal of Rock Mechanics and Mining Sciences*, *34*(8), 1165–1186.

Hoek, E., & Brown, E. T. (2019). The Hoek–Brown failure criterion and GSI – 2018 edition. *Journal of Rock Mechanics and Geotechnical Engineering*, *11*(3), 445–463. https://doi.org/10.1016/j.jrmge.2018.08.001

Hoek, E., Carranza-Torres, C., & Corkum, B. (2002). Hoek-Brown failure criterion-2002 edition. *Proceedings of NARMS-Tac*, *1*(1), 267–273.

Hoek, E., & Diederichs, M. S. (2006). Empirical estimation of rock mass modulus. *International Journal of Rock Mechanics and Mining Sciences*, *43*(2), 203–215. https://doi.org/10.1016/j.ijrmms.2005.06.005

Hoek, E., Kaiser, P., & Bawden, W. (1995). Support of underground excavation in hard rock: Rotterdam. *AA Balkema*, 84–97.

Hoek, E., & Marinos, P. (2000). Predicting tunnel squeezing problems in weak heterogeneous rock masses. *Tunnels and Tunnelling International*, *32*(11), 45–51.

Hoek, E., & Marinos, P. (2007a). A brief history of the development of the Hoek-Brown failure criterion. *Soils and Rocks*, *2*(2), 2–13.

Hoek, E., & Marinos, P. (2007b). A brief history of the development of the Hoek-Brown failure criterion. *Soils and Rocks*, *2*(2), 2–13.

Hoek, E., Marinos, P., & Benissi, M. (1998). Applicability of the geological strength index (GSI) classification for very weak and sheared rock masses. The case of the Athens Schist Formation. *Bulletin of Engineering Geology and the Environment*, *57*(2), 151–160. https://doi.org/10.1007/s100640050031

Hoek, E., & Moy, D. (1993). Design of large powerhouse caverns in weak rock. In *Surface and Underground Project Case Histories* (pp. 85–110). Elsevier.

Hudson, J. A., & Harrison, J. P. (1997). *Engineering Rock Mechanics: An Int roduction to th e Principl es*. Perg am on, Oxford.

Hudson, N. W. (1993). *A study of the reasons for success or failure of soil conservation projects*. FAO.

Hutchinson, D. J., & Diederichs, M. S. (1996). *Cablebolting in underground mines*.

Karlsrud, K., & Kveldsvik, V. (2002). Control of water leakage when tunneling under urban areas in the Oslo region. *Norwegian Tunneling Society, Pub*, *12*.

KC, P. K., & Panthi, K. K. (2011). Engineering Geological Design of Underground Works for Upper Madi Hydroelectric Project. *Hydro Nepal: Journal of Water, Energy and Environment*, *9*, 27–34.

Li, C. C. (2017). Principles of rockbolting design. *Journal of Rock Mechanics and Geotechnical Engineering*, *9*(3), 396–414. https://doi.org/10.1016/j.jrmge.2017.04.002

Marinos, V., Marinos, P., & Hoek, E. (2005). The geological strength index: Applications and limitations. *Bulletin of Engineering Geology and the Environment*, *64*(1), 55–65.

Martin, P. (1999). Public policies, regional inequalities and growth. *Journal of Public Economics*, *73*(1), 85–105.

McCutchen, W. (1982). *Some elements of a theory for in-situ stress. Technical note: Int J Rock Mech Min Sci, V19, N4, Aug 1982, P201–203*. *19*(6), 129.

Myrvang, A. (2001). Rock Mechanics. *Norway University of Technology (NTNU), Trondheim (in Norwegian)*.

NGI. (2013). *Using the Q-system—Rock mass classification and support design*.

Nilsen, B., & Broch, E. (2009). Engineering Geology of Rocks, Basic Level Compendium. *Department of Geology and Mineral Resources, NTNU*, 76.

Nilsen, B., & Palmström, A. (2000). *Engineering Geology and Rock Engineering: Handbook*. Norwegian Group for Rock Mechanics.

Nilsen, B., & Thidemann, A. (1993). *Rock engineering*. Norwegian Institute of Technology, Division of Hydraulic Engineering.

Nobuo, T., Sawada, K., Shigefuji, M., Bijukchhen, S. M., Ichiyanagi, M., Sasatani, T., Dhakal, Y. P., Rajaure, S., & Dhital, M. R. (2015). Shallow underground structure of strong ground motion observation sites in the Kathmandu valley. *NEPAL GEOLOGICAL SOCIETY*, 50.

Palmstrom, A., & Broch, E. (2006). Use and misuse of rock mass classification systems with particular reference to the Q-system. *Tunnelling and Underground Space Technology*, *21*(6), 575–593. https://doi.org/10.1016/j.tust.2005.10.005

Palmstrom, A., & Singh, R. (2001). *The deformation modulus of rock masses 퇴 comparisons between in situ tests and indirect estimates*. 17.

Palmstrom, A., & Stille, H. (2010). *Rock engineering*.

Panet, M. (1996). Two case histories of tunnels through squeezing rocks. *Rock Mechanics and Rock Engineering*, *29*(3), 155–164.

Panthi, K. K. (2006). *Analysis of engineering geological uncertainties related to tunnelling in Himalayan rock mass conditions*.

Panthi, K. K. (2013). Predicting tunnel squeezing: A discussion based on two tunnel projects. *Hydro Nepal: Journal of Water, Energy and Environment*, *12*, 20–25.

Panthi, K. K., & Basnet, C. B. (2016). Review on the major failure cases of unlined pressure shafts/tunnels of Norwegian hydropower projects. *Hydro Nepal: Journal of Water, Energy and Environment*, *18*, 6–15.

Panthi, K. K., & Nilsen, B. (2007). Predicted versus actual rock mass conditions: A review of four tunnel projects in Nepal Himalaya. *Tunnelling and Underground Space Technology*, *22*(2), 173–184. https://doi.org/10.1016/j.tust.2006.04.005

Panthi, K. K., & Shrestha, P. K. (2018). Estimating tunnel strain in the weak and schistose rock mass influenced by stress anisotropy: An evaluation based on three tunnel cases from Nepal. *Rock Mechanics and Rock Engineering*, *51*(6), 1823–1838.

Power, M. S., Rosidi, D., & Kaneshiro, J. Y. (1998). *SEISMIC VULNERABILITY OF TUNNELS AND UNDERGROUND STRUCTURES REVISITED*.

Rahman, M. M., & Bai, L. (2018). Probabilistic seismic hazard assessment of Nepal using multiple seismic source models. *Earth and Planetary Physics*, *2*(4), 327–341.

Rathore, A. (2016). *Stability assessment of the underground powerhouse cavern for the Sach Khas hydroelectric project in Himachal, India*.

Sakurai, S., & Takeuchi, K. (1983). Back analysis of measured displacements of tunnels. *Rock Mechanics and Rock Engineering*, *16*(3), 173–180.

Saurer, E., Marcher, T., & John, M. (2013). *Decisive design basis and parameters for power plant caverns*. 1858–1864.

Saurer, E., Marcher, T., & Lesnik, M. (2011). *Grid space optimization of jet grouting columns*. 1055–1060.

Schelling, D. (1992). The tectonostratigraphy and structure of the eastern Nepal Himalaya. *Tectonics*, *11*(5), 925–943.

Selmer-Olsen, R. (1977). ExamPles of the behaviour of shotcrete linings underground. *Shotcrete for Ground Support. ACI Publ. SP-S4*.

Shang, J., Hencher, S., & West, L. (2016). Tensile Strength of Geological Discontinuities Including Incipient Bedding, Rock Joints and Mineral Veins. *Rock Mechanics and Rock Engineering*, *49*. https://doi.org/10.1007/s00603-016-1041-x

Shrestha, G. L. (2006). *Stress induced problems in Himalayan tunnels with special reference to squeezing*.

Shrestha, P. K., & Panthi, K. K. (2014). Analysis of the plastic deformation behavior of schist and schistose mica gneiss at Khimti headrace tunnel, Nepal. *Bulletin of Engineering Geology and the Environment*, *73*(3), 759–773.

Shrestha, S. (2014). *Probabilistic Seismic hazard Analysis of Kathmandu City, Nepal*. *2*(1), 10.

Singh, B., Jethwa, J. L., Dube, A. K., & Singh, B. (1992). *Correlation between Observed Support Pressure and Rock Mass Quality*. *7*(1), 16.

Sulem, J., Panet, M., & Guenot, A. (1987). *An analytical solution for time-dependent displacements in a circular tunnel*. *24*(3), 155–164.

Tshering, T. (2011). *The Impact of Earthquakes on Tunnels in different Rock Mass Quality Q-: A numerical analysis*.

Udpa, L., Sun, Y., Lord, W., & Shin, Y. (1989). Mesh and Boundary Considerations in the Numerical Modeling of Large 3-D

Electromagnetic NDT Geometries. In *Review of Progress in Quantitative Nondestructive Evaluation* (pp. 793–800). Springer.

Vestad, M. L. (2014). *Analysis of the deformation behavior at the underground caverns of Neelum Jhelum HPP, Pakistan*. Institutt for geologi og bergteknikk.

Vlachopoulos, N., & Diederichs, M. S. (2009). Improved Longitudinal Displacement Profiles for Convergence Confinement Analysis of Deep Tunnels. *Rock Mechanics and Rock Engineering*, *42*(2), 131–146. https://doi.org/10.1007/s00603-009-0176-4

Wood, J. A. (1972). Fragments of terra rock in the Apollo 12 soil samples and a structural model of the moon. *Icarus*, *16*(3), 462–501.

Yun, K. K., Choi, S., Ha, T., Hossain, M. S., & Han, S. (2020). Comparison of long-term strength development of steel fiber shotcrete with cast concrete based on accelerator type. *Materials*, *13*(24), 5599.

Zhao, J. (2000). Applicability of Mohr–Coulomb and Hoek–Brown strength criteria to the dynamic strength of brittle rock. *International Journal of Rock Mechanics and Mining Sciences*, *37*(7), 1115–1121.

APPENDICIES

A.1 Determination of m_i (Hoek and Marinos, 2000)

Rock type	Class	Group	Texture			
			Coarse	Medium	Fine	Very fine
SEDIMENTARY	Clastic		Conglomerates (21 ± 3) Breccias (19 ± 5)	Sandstones 17 ± 4	Siltstones 7 ± 2 Greywackes (18 ± 3)	Claystones 4 ± 2 Shales (6 ± 2) Marls (7 ± 2)
	Non-Clastic	Carbonates	Crystalline Limestone (12 ± 3)	Sparitic Limestones (10 ± 2)	Micritic Limestones (9 ± 2)	Dolomites (9 ± 3)
		Evaporites		Gypsum 8 ± 2	Anhydrite 12 ± 2	
		Organic				Chalk 7 ± 2
METAMORPHIC	Non Foliated		Marble 9 ± 3	Hornfels (19 ± 4) Metasandstone (19 ± 3)	Quartzites 20 ± 3	
	Slightly foliated		Migmatite (29 ± 3)	Amphibolites 26 ± 6	Gneiss 28 ± 5	
	Foliated*			Schists 12 ± 3	Phyllites (7 ± 3)	Slates 7 ± 4
IGNEOUS	Plutonic	Light	Granite 32 ± 3 Diorite 25 ± 5 Granodiorite (29 ± 3)			
		Dark	Gabbro 27 ± 3 Norite 20 ± 5	Dolerite (16 ± 5)		
	Hypabyssal		Porphyries (20 ± 5)		Diabase (15 ± 5)	Peridotite (25 ± 5)
	Volcanic	Lava		Rhyolite (25 ± 5) Andesite 25 ± 5	Dacite (25 ± 3) Basalt (25 ± 5)	
		Pyroclastic	Agglomerate (19 ± 3)	Breccia (19 ± 5)	Tuff (13 ± 5)	

A2. GSI determination (Hoek and Marinos, 2000)
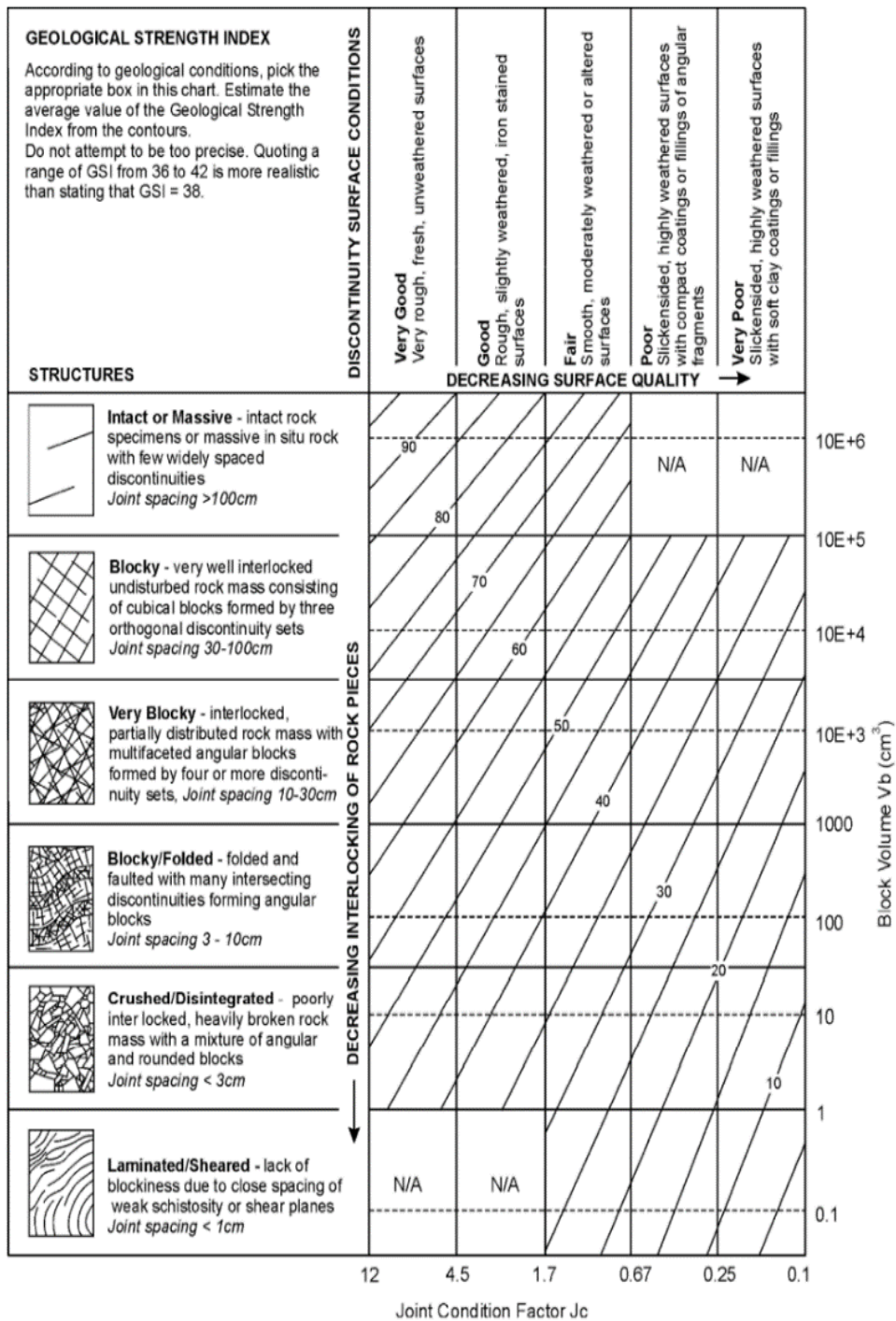
A.3 Value of disturbance factor based on Hoek et al. (2002a)

Appearance of rock mass	Description of rock mass	Suggested value of D
	Excellent quality controlled blasting or excavation by Tunnel Boring Machine results in minimal disturbance to the confined rock mass surrounding a tunnel.	$D = 0$
	Mechanical or hand excavation in poor quality rock masses (no blasting) results in minimal disturbance to the surrounding rock mass.	$D = 0$
	Where squeezing problems result in significant floor heave, disturbance can be severe unless a temporary invert, as shown in the photograph, is placed.	$D = 0.5$ No invert
	Very poor quality blasting in a hard rock tunnel results in severe local damage, extending 2 or 3 m, in the surrounding rock mass.	$D = 0.8$
	Small scale blasting in civil engineering slopes results in modest rock mass damage, particularly if controlled blasting is used as shown on the left hand side of the photograph. However, stress relief results in some disturbance.	$D = 0.7$ Good blasting $D = 1.0$ Poor blasting
	Very large open pit mine slopes suffer significant disturbance due to heavy production blasting and also due to stress relief from overburden removal.	$D = 1.0$ Production blasting
	In some softer rocks excavation can be carried out by ripping and dozing and the degree of damage to the slopes is less.	$D = 0.7$ Mechanical excavation

A.4   Residual GSI as suggested by Cai et al. (2007)
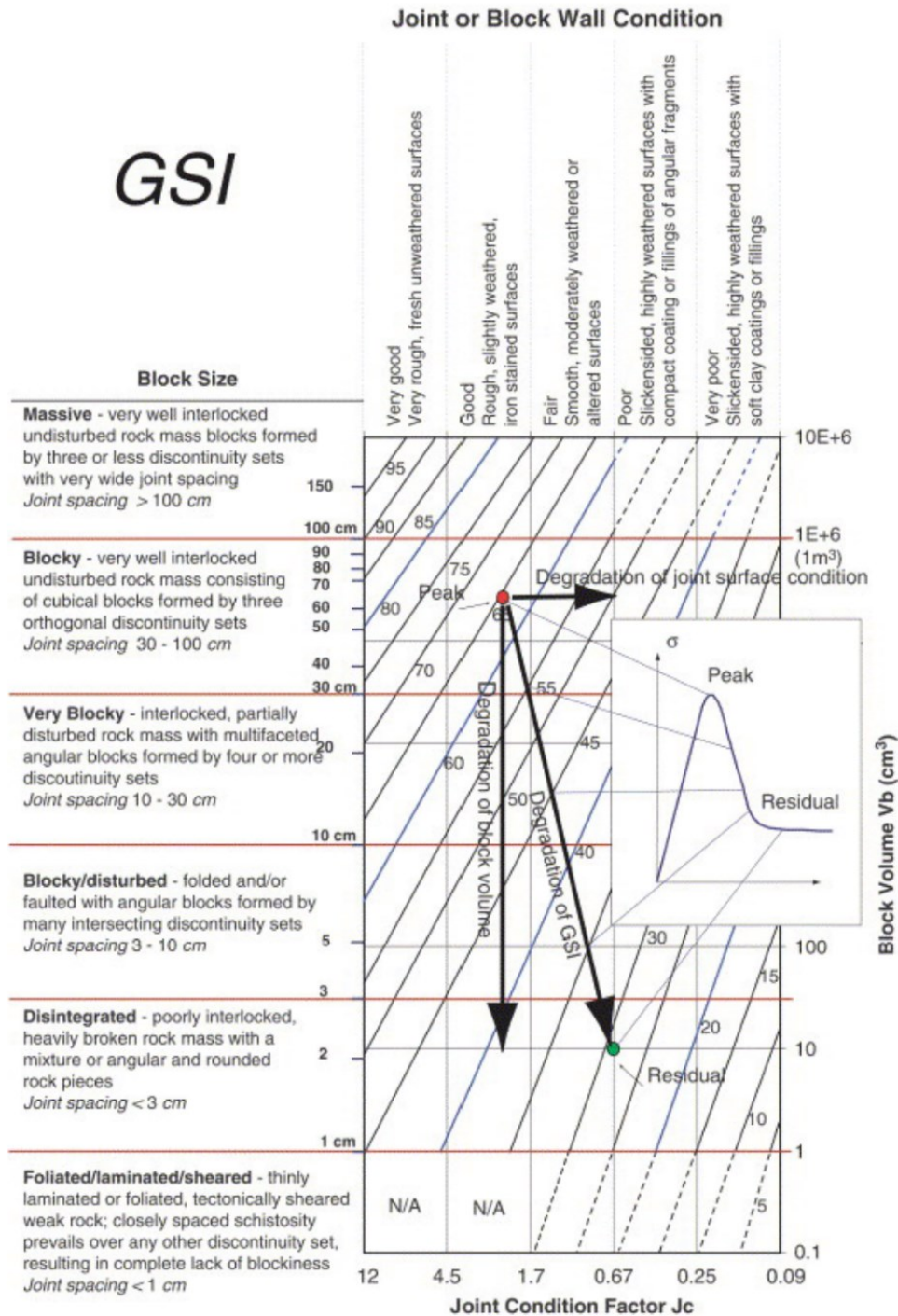
A.5 Ratings for input parameters in Q-system based on Barton (2002)

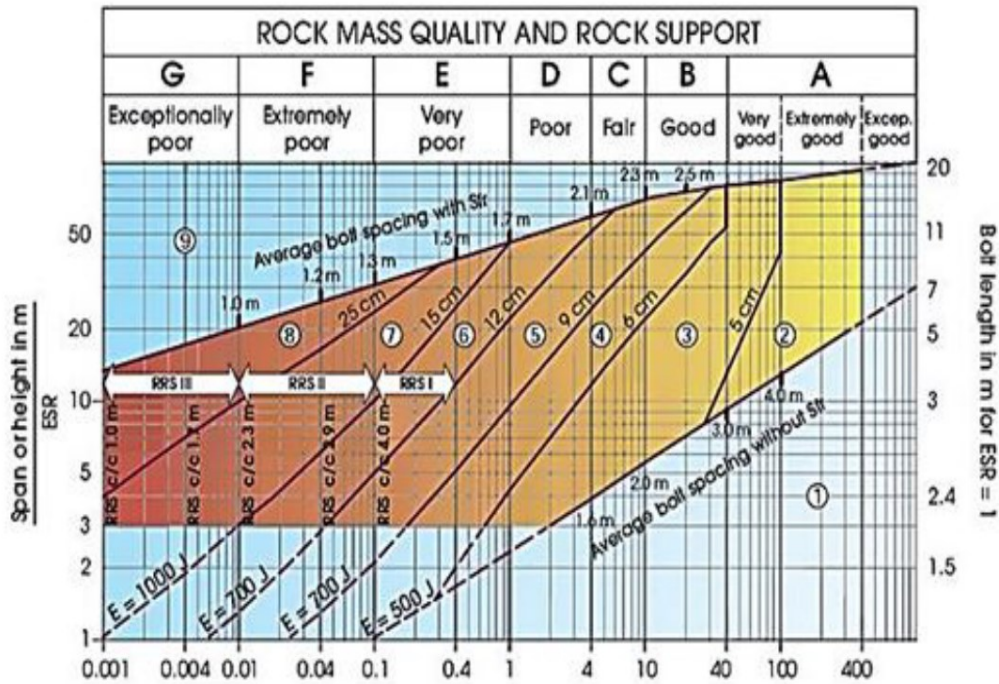| RQD (Rock quality designation, %)		J_n (Joint set number)	
Very poor	0 - 25	Massive, no or few joints	0.5 - 1
Poor	25 - 50	One joint set	2
Fair	50 – 75	One joint set + random joints	3
Good	75 – 90	Two joint sets	4
Excellent	90 - 100	Two joint sets + random	6
Notes:		Three joint sets	9
(i) where RQD is reported or measured as ≤		Three joint sets + random	12
10 (including 0), a nominal value of 10 is used to evaluate Q.		Four or more joint sets, heavily jointed, sugar cube etc	15
(ii) RQD intervals of 5 i.e. 100, 95, 90 etc.,		Crushed rock, earthlike	20
are successfully accurate.		*Note:* For tunnel intersections, use (3 x J_n) and for portals use (2 x J_n)	

J_r (Joint roughness number)

(a) Rock wall contact		(b) Rock wall contact before 10 cm shear	
Discontinuous joints	4	Rough or irregular, undulating	1.5
Rough or irregular, undulating	3	Smooth, undulating	1
Smooth, undulating	2	Slickensided, undulating	0.5
Slickensided, undulating	1.5		

© No rock wall contact when sheared	
Zone containing clay minerals thick enough to prevent rock wall contact	1
Sandy, gravely or crushed zone thick enough to prevent rock wall contact	1

Notes: (i) Description refers to small-scale features and intermediate scale features, in that order (ii) Add 1.0 if the mean spacing of the relevant joint set is greater than 3 m. (iii) Jr = 0.5 can be used for planner, slickenside joints having lineations, provided these are oriented for minimum strength. (iv) Jr and Ja classification is applied to the joint set that is least favorable for stability both from the point of view of orientation and shear resistance, $\tau \approx \sigma_n . \tan^{-1} (J_r/J_a)$

J_a (Joint alteration number)

(a) Rock wall contact (no mineral fillings, only coatings)	ϕ_r (appr.)	J_a
Tightly healed, hard, non-softening, impermeable filling i.e., quartz/epidote	-	0.75
Unaltered joint walls, surface staining only	25 - 35	1
Slightly altered joint walls, non-softening mineral coatings, sandy particles, clay free disintegrated rock ,etc.	25 - 30	2
Silty or sandy clay coatings, small clay fractions (non-softening)	20 - 25	3
Softening or low friction clay mineral coatings, i.e., kaolinite or mica. Also chlorite, talk, gypsum, graphite etc., and small quantities of swelling clay	8 - 16	4
(b) Rock wall contact before 10 cm shear (thin mineral fillings)		
Sandy particles, clay free disintegrated rock etc.	25 - 30	4
Strongly over-consolidated non-softening clay mineral fillings (continuous, but < 5mm thickness)	16 - 24	6

Medium or low over-consolidated non-softening clay mineral fillings (continuous, but < 5mm thickness)	12 - 16	8
Swelling clay fillings, i.e., montmorillonite (continuous, but < 5mm thick)	6 - 12	8 - 12
(c) No rock wall contact when sheared (thick mineral fillings)		
Zones or bands of disintegrated or crushed rock and clay	6 - 24	6, 8 - 12
Zones or bands of silty or sandy clay, small clay fraction (non-softening)	-	5
Thick, continuous zones or bands of clay	6 - 24	13 - 20

J_w **(Joint water reduction factor)**	Approx. P (bars)	J_w
Dry excavations or minor inflow, i.e., < 5 l/min locally	< 1	1
Medium inflow or pressure, occasional outwash of joint fillings	1 – 2.5	0.66
Large inflow or high pressure in competent rock with unfilled joints	2.5 - 10	0.5
Large inflow or high pressure, considerable outwash of joint fillings	2.5 - 10	0.33
Exceptionally high inflow or pressure at blasting, decaying with time	> 10	0.2 – 0.1
Exceptionally high inflow or pressure continuing without noticeable decay with time	> 10	0.2 – 0.1

Notes: (i) The last four factors are crude estimates. Increase J_w if drainage measures are installed. (ii) Special problems caused by ice formation are not considered. (iii) For general characterization of rock masses distance from excavation influences. The use of J_w = 1, 0.66, 0.5, 0.33, etc. as depth increases from say 0-5, 5-25, 25-250 to >250m is recommended, assuming that RQD/J_n is low enough (0.5-25) for good hydraulic connectivity.

SRF (Stress Reduction Factor)

(a) Weakness zones intersecting excavation, which may cause loosening of rock mass	SRF
Multiple occurrence of weakness zones containing clay or chemically disintegrated rock, very loose surrounding rock at any depth	10
Single weakness zone containing clay or chemically disintegrated rock (depth ≤ 50m)	5
Single weakness zone containing clay or chemically disintegrated rock (depth > 50m)	2.5
Multiple shear zones in competent rocks (clay free), loose surrounding rock at any depth	7.5
Single shear zone in competent rocks (clay free), (depth of excavation ≤ 50m)	5
Single shear zone in competent rocks (clay free), (depth of excavation > 50m)	2.5
Loose, open joints, heavily jointed or sugar cube etc. at any depth	5

Note: Reduce these values of SRF by 25 – 50 % if the relevant shear zones only influence but do not intersect the excavation.

(b) Competent rock, rock stress problems	σ_c / σ_1	σ_1 / σ_c	SRF
Low stress, near surface, open joints	> 200	< 0.01	2.5
Medium stress, favorable stress condition	200 - 10	0.01 – 0.3	1
High stress, very tight structures. Usually favorable to stability, may be unfavorable for wall stability	10 - 5	0.3 – 0.4	0.5 - 2
Moderate slabbing after > 1 hour in massive rock	5 - 3	0.5 – 0.65	5 - 50
Slabbing and rock burst after a few minutes of excavation	3 - 2	0.65 - 1	50 - 200
Heavy rock burst and immediate dynamic deformations	< 2	> 1	200 – 400

Notes: (i) For strongly anisotropic virgin stress field (if measured): when $5 \leq \sigma_1 / \sigma_3 \leq 10$, reduce σ_c to $0.75 \sigma_c$ and when $\sigma_1 / \sigma_3 > 10$, reduce σ_c to $0.5 \sigma_c$. (ii) For general characterization of rock mass, overburden from excavation influences. The use of SRF 5, 2.5, 1 and 0.5 is recommended as depth increases from say 0-5, 5-25, 25-250 to > 250m respectively.

© *Squeezing rock: plastic flow of incompetent rock under the influence of high rock pressure*	σ_1 / σ_c	SRF
Mild squeezing rock pressure	1 - 5	5 - 10
Heavy squeezing rock pressure	> 5	10 - 20

(d) Swelling rock: chemical swelling activity depending on pressure of water		SRF
Mild swelling rock pressure		5 - 10
Heavy swelling rock pressure		10 - 15

ROCK MASS QUALITY AND ROCK SUPPORT

$$\text{Rock mass quality } Q = \frac{RQD}{J_n} \times \frac{J_r}{J_a} \times \frac{J_w}{SRF}$$

Support categories

① Unsupported or spot bolting
② Spot bolting, **SB**
③ Systematic bolting, fibre reinforced sprayed concrete, 5-6 cm, **B+Sfr**
④ Fibre reinforced sprayed concrete and bolting, 6-9 cm, **Sfr (E500)+B**
⑤ Fibre reinforced sprayed concrete and bolting, 9-12 cm, **Sfr (E700)+B**
⑥ Fibre reinforced sprayed concrete and bolting, 12-15 cm + reinforced ribs of sprayed concrete and bolting, **Sfr (E700)+RRS I +B**
⑦ Fibre reinforced sprayed concrete >15 cm + reinforced ribs of sprayed concrete and bolting, **Sfr (E1000)+RRS II+B**
⑧ Cast concrete lining, **CCA** or **Sfr (E1000)+RRS III+B**
⑨ Special evaluation

Bolts spacing is mainly based on Ø20 mm

E = Energy absorbtion in fibre reinforced sprayed concrete

ESR = Excavation Support Ratio

Areas with dashed lines have no empirical data

RRS - spacing related to Q-value

Si30/6 Ø16 - Ø20 (span 10m)
D40/6+2 Ø16-20 (span 20m)

Si35/6 Ø16-20 (span 5m)
D45/6+2 Ø16-20 (span 10m)
D55/6+4 Ø20 (span 20m)

D40/6+4 Ø16-20 (span 5 m)
D55/6+4 Ø20 (span 10 m)
D70/6+6 Ø20 (span 20 m)

Si30/6 = Single layer of 6 rebars,
30 cm thickness of sprayed concrete

D = Double layer of rebars

Ø16 = Rebar diameter is 16 mm

c/c = RSS spacing, centre - centre

d

APPENDIX B.
B1. RELATIONSHIP BETWEEN RMR AND BARTON

Relationship between Q-Value and RMR(Panthi (2006)						
RMR= 9xlnQ +44(Bieniawaski, 1989) RMR = 15xlogQ +50 (Barton, 1995)						
Descriptions		Ranges of Q-Values		Range of RMR-Values		
Rock Class	Quality descriptions	Minimum	Maximum	Minimum		Maximum
Class 1	very good to excellent	100	1000	85		100
Class 2	Good	10	100	65		85
Class 3	Fair to good	4	10	56		65
Class 4	Poor	1	4	44		56
Class 5	Very poor	0.1	1	35		44
Class 6	Extremely poor	0.01	0.1	20		35
Class 7	Exceptionally poor	0.001	0.01	5		20

B2. DETAILED CALCULATIONS AND RESULTS

a. Hoek and Marinos (2000) Calculations

1. Prediction by Hoek and Marinos without support pressure

Component	Rock Type	Overburden Depth (m)	Vertical Stress p_0 [Mpa]	Rock mass Strength σcm [MPa] by Panthi (2006)			Prediction by Hoek and Marinos (2000) Strain % without support pressure			
				Min	Max	Average	Min	Max	Average	Prediction
Powerhouse Cavern	Augen Gneiss	186.239	5.0	4.18	5.32	4.74	0.14	0.32	0.16	few stability problems
Transformer cavern	Augen Gneiss	176.345	4.8	4.18	5.32	4.74	0.15	0.32	0.16	few stability problems

2. Prediction by Hoek and Marinos with support pressure. The combined support pressure was calculated by the CCM (SCC).

Component	Rock Type	Overburden Depth (m)	Support Pressure p_s [MPa]	Vertical Stress p_0 [Mpa]	Rock mass Strength σcm [MPa] by Panthi (2006)			Prediction by Hoek and Marinos (2000) Strain % with support pressure			
					Min	Max	Average	Min	Max	Average	Prediction
Powerhouse Cavern	Augen Gneiss	186.239	0.15	5.0	4.18	5.32	4.74	0.04	0.02	0.03	few stability problems
Transformer cavern	Augen Gneiss	176.345	0.15	4.8	4.18	5.32	4.74	0.02	0.01	0.02	few stability problems

3. Size of the plastic zone, and strain (%) converted to deformation in mm

Component	Rock Type	Overburden Depth (m)	Vertical Stress p_0 [Mpa]	Equivalent Diameter (m)	Diameter plastic zone by Hoek and Marinos (2000) [m]			Deformation in mm based on Strain (%) with support		
					Min	Max	Average	Min	Max	Average
Powerhouse Cavern	Augen Gneiss	186.239	5.0	13.34	18.15	15.93	16.96	36.68	31.35	34.38
Transformer cavern	Augen Gneiss	176.345	4.8	8.24	17.60	15.46	16.45	20.34	12.79	15.97

b. CCM Method

CONVERGENCE CONFINEMENT METHOD

Data Required				
Chainage(m)				
OverBurden	186.84			
Dimension(wXh)	18mx33.14m			
R(m)	13.34	k	0.42	
	186.84			
H(m)		σ_v (MPa)	5.00	
σ_0 (MPa)	4.80	σ_h (MPa)	4.60	
v	0.25			
L(m)	1.00			
Q	0.833			
Ei(Gpa)	34.24			
Erm(Gpa)	3.77			
Disturbance Factor	0.5			
Friction Angle	49.12			

m_i	26.00
GSI	41.00
mb	1.02
s	1.93E-04
a	0.50
σ_{ci} (MPa)	43.00
S_0	1.10E-01
P_i^{cr} (MPa)	2.73E-02
p_i^{cr} (MPa)	1.1867
$C(\alpha_0)$	0.66
P_{rm} (GPa)	2.54
G_{rm} (GPa)	1.02
Ψ (degree)	12.28
K_Ψ	1.54

For Bolts	
bolt provided	yes
l (m)	8.00
d_b (mm)	25.00
E_b (Gpa)	300.00
Q_b (m/MN)	0.14
T_{bf} (MN)	0.30
sc (m)	1.00
sl (m)	1.00
Ps_{max} (Mpa)	0.30
k_s (Mpa/m)	5.07
u_{rbmax} (mm)	59.20

For Shotcrete	
Installed	yes
σ_{cc}(Mpa)	35.00
v_c	0.20
t_c (mm)	300.00
E_c (GPa)	30.00
P_s^{max} (MPa)	0.78
K_s (MPa/m)	53.58
u_r^{max} (mm)	14.53

For Lattice girder		
Steel properties		
lattice girder provided	no	

Combination of Supports	
Ks(MPa/m)	58.65
urmax(mm)	14.53
Psmax(Mpa)	0.852

1. Longitudinal Displacement Profile

u_r^0 (mm)=			18.209	
sn	**x/R**	**x**	**u_r/u_r^m**	**ur**
1	-4.00	-53.36	0.002	0.11
2	-2.91	-38.81	0.010	0.55
3	-1.82	-24.25	0.045	2.50
4	-0.73	-9.70	0.160	8.95
5	0.36	4.85	0.398	22.26
6	1.45	19.40	0.669	37.40
7	2.55	33.96	0.852	47.61
8	3.64	48.51	0.941	52.57
9	4.73	63.06	0.977	54.62
10	5.82	77.61	0.991	55.41
11	6.91	92.17	0.997	55.71
12	8.00	106.72	0.999	55.82

2. Construction of GRC

SN	_p_i	P_i	R_{pl}	u_r
1.00	0.00	1.87E-04	18.067	55.89
2.00	0.11	2.66E-03	16.750	43.97
3.00	0.22	5.12E-03	16.091	38.85
4.00	0.32	7.59E-03	15.599	35.39
5.00	0.43	1.01E-02	15.193	32.78
6.00	0.54	1.25E-02	14.844	30.71
7.00	0.65	1.50E-02	14.535	29.01
8.00	0.76	1.75E-02	14.255	27.60
9.00	0.86	1.99E-02	14.000	26.40
10.00	0.97	2.24E-02	13.765	25.37
11.00	1.08	2.49E-02	13.545	24.49
12.00	1.19	2.73E-02	13.340	23.73
13.00	1.19	2.73E-02	elastic	23.73
14.00	4.80	1.10E-01	elastic	0.00

3. Construction of SCC

ur	ps
18.21	0.000
32.73	0.852
90.84	0.852

Tunnel Closure	
a	1.94
u_r^D	0.70
u_r^D/a (%)	0.01%

For FOS,	
P_s^{max}	0.85
P_s^d	0.15
FOS	5.68

APPENDIX C.
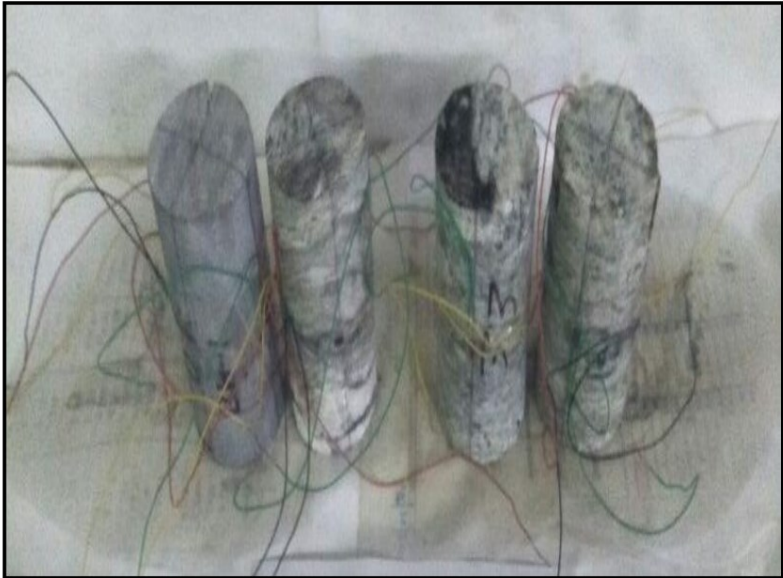### a. Lab test Samples

Figure 12-18:   View of Crushed Rock Core Samples after Triaxial Test

Figure 12-19:   a View of Crushed Rock Core Samples after Triaxial Test

Figure 12-10: View Rock Core Sample before Modulus of Elasticity & Poisson's Ratio

Figure 12-11: View of Crushed Rock Core Sample after Modulus of Elasticity & Poisson's Ratio

BOREHOLE NO. HB – 2', BOX NO. 1 OF 13, FROM 0.0 TO 5.0m

BOREHOLE NO. HB – 2', BOX NO. 2 OF 13, FROM 5.0 TO 10.0m

BOREHOLE NO. HB – 2', BOX NO. 3 OF 13, FROM 10.0 TO 15.0m

BOREHOLE NO. HB – 2', BOX NO. 4 OF 13, FROM 15.0 TO 20.0m

BOREHOLE NO. HB – 2', BOX NO. 5 OF 13, FROM 20.0 TO 25.0m

BOREHOLE NO. HB – 2', BOX NO. 6 OF 13, FROM 25.0 TO 30.0m

APPENDICIES
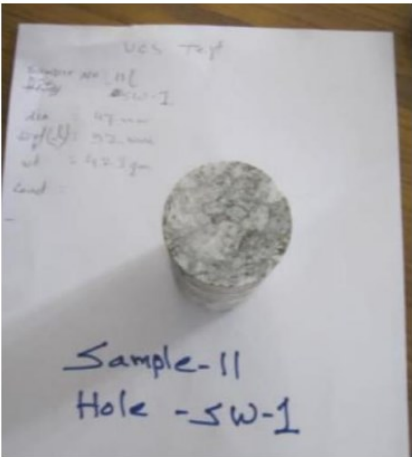
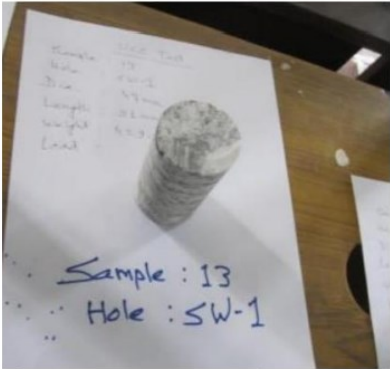
Figure 12-22: Sample No.11 Pre and Post UCS Test
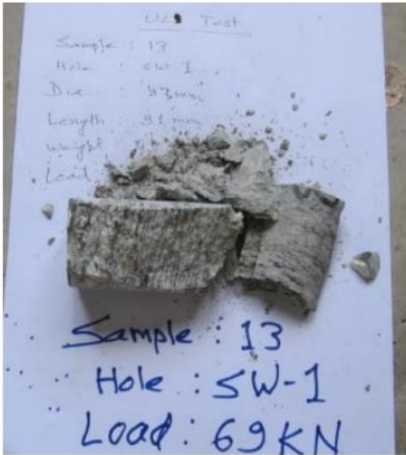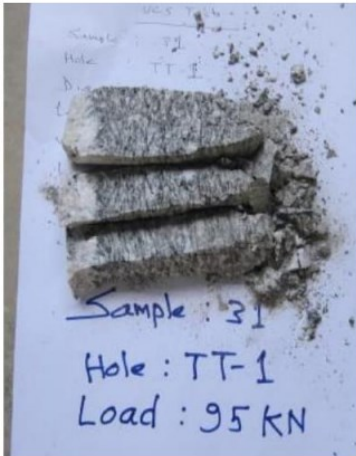

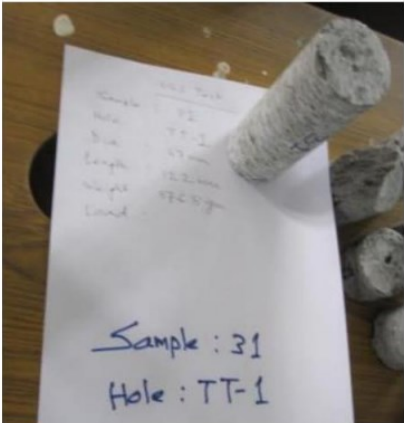**Figure 12-23:** Sample No.13 Pre and Post UCS Test

Figure 12-24: Sample No. 31 Pre and Post UCS Test

139

Material Properties

rock mass

Material Color	
Initial Element Loading	Field Stress Only
Unit Weight	0.027 MN/m3
Elastic Type	Isotropic
Poisson's Ratio	0.25
Young's Modulus	5852.9 MPa
Use Residual Young's Modulus	Yes
Residual Young's Modulus	1935.2 MPa
Failure Criterion	Generalized Hoek-Brown
Material Type	Plastic
Compressive Strength	43 MPa
mb Parameter	3.16121
s Parameter	0.001422
a Parameter	0.510622
GSI Parameter	41
mi Parameter	26
D Parameter	0
Residual mb Parameter	1.72256
Residual s Parameter	0.000215
Residual a Parameter	0.533437
Residual GSI Parameter	24
Residual mi Parameter	26
Residual D Parameter	0
Dilation Parameter	0
Tensile Cutoff Type	0
Material Behaviour	Drained
Porosity Value	0.5
Static Water Mode	Dry

disturbed zone

Material Color	
Initial Element Loading	Field Stress Only
Unit Weight	0.027 MN/m3
Elastic Type	Isotropic
Poisson's Ratio	0.25
Young's Modulus	2802.9 MPa
Use Residual Young's Modulus	Yes
Residual Young's Modulus	849.1 MPa
Failure Criterion	Generalized Hoek-Brown
Material Type	Plastic
Compressive Strength	43 MPa
mb Parameter	1.56608
s Parameter	0.000383
a Parameter	0.510622
GSI Parameter	41
mi Parameter	26
D Parameter	0.5
Residual mb Parameter	0.393616
Residual s Parameter	8.0219e-06
Residual a Parameter	0.574676
Residual GSI Parameter	12
Residual mi Parameter	26
Residual D Parameter	0.5
Dilation Parameter	0.05
Tensile Cutoff Type	0
Material Behaviour	Drained
Porosity Value	0.5
Static Water Mode	Dry

Liner Properties

Liner: SC-PH roof

Color	
Liner Type	Reinforced Concrete
Equivalent Young's modulus	31250 MPa
Equivalent thickness	0.3 m
Poisson ratio	0
Concrete Properties	
Thickness	0.3 m
Young's modulus	30000 MPa
Poisson ratio	0.2
Compressive strength	35 MPa
Tensile strength	5 MPa

Liner: SC-TC roof

Color	
Liner Type	Reinforced Concrete
Equivalent Young's modulus	31250 MPa
Equivalent thickness	0.3 m
Poisson ratio	0
Concrete Properties	
Thickness	0.3 m
Young's modulus	30000 MPa
Poisson ratio	0.2
Compressive strength	35 MPa
Tensile strength	5 MPa

Liner: SC-PH wall

Color	
Liner Type	Reinforced Concrete
Equivalent Young's modulus	31250 MPa
Equivalent thickness	0.35 m
Poisson ratio	0
Concrete Properties	
Thickness	0.35 m
Young's modulus	30000 MPa
Poisson ratio	0.2
Compressive strength	35 MPa
Tensile strength	5 MPa

Liner: SC-TC wall

Plastic model with multiple stages Modify v1 — Thursday, June 30, 2022

Color	
Liner Type	Reinforced Concrete
Equivalent Young's modulus	31250 MPa
Equivalent thickness	0.35 m
Poisson ratio	0
Concrete Properties	
Thickness	0.35 m
Young's modulus	30000 MPa
Poisson ratio	0.2
Compressive strength	35 MPa
Tensile strength	5 MPa

APPENDICIES

Bolt Properties

roof

Bolt Color	■ (blue)
Bolt Type	Fully Bonded
Bolt Diameter	30 mm
Bolt Modulus,E	300000 MPa
Tensile Capacity	0.3 MN
Residual Tensile Capacity	0 MN
Out-of-Plane Spacing	1 m
Pre-Tensioning Force	0 MN
Constant Pre-tensioning Force in Install Stage	Yes
Joint Shear	Yes

wall

Bolt Color	■ (green)
Bolt Type	Fully Bonded
Bolt Diameter	30 mm
Bolt Modulus,E	300000 MPa
Tensile Capacity	0.3 MN
Residual Tensile Capacity	0 MN
Out-of-Plane Spacing	1 m
Pre-Tensioning Force	0 MN
Constant Pre-tensioning Force in Install Stage	Yes
Joint Shear	Yes

CT PH

Bolt Color	■ (gray)
Bolt Type	Plain Strand Cable
Borehole Diameter	48 mm
Cable Diameter	32 mm
Cable Modulus,E	300000 MPa
Cable Peak	0.3 MN
Out-of-Plane Spacing	1 m
Water Cement Ratio	0.35
Joint Shear	Yes
Face Plates	Attached

CT TC

Plastic model with multiple stages Modify v1   Thursday, June 30, 2022

Bolt Color	■ (orange)
Bolt Type	Plain Strand Cable
Borehole Diameter	48 mm
Cable Diameter	32 mm
Cable Modulus,E	300000 MPa
Cable Peak	0.3 MN
Out-of-Plane Spacing	1 m
Water Cement Ratio	0.35
Joint Shear	Yes
Face Plates	Attached